

**EFFECT OF ELECTROMAGNETIC FIELD IN
MACHINING PROCESS**

XUAN YUE

**NATIONAL UNIVERSITY OF
SINGAPORE**

2007



**EFFECT OF ELECTROMAGNETIC FIELD IN
MACHINING PROCESS**

XUAN YUE

(B.ENG., Tianjin Univ., P.R. China)

**A THESIS SUBMITTED FOR THE DEGREE OF
MASTER OF ENGINEERING
DEPARTMENT OF MECHANICAL ENGINEERING
NATIONAL UNIVERSITY OF SINGAPORE**

2007

ACKNOWLEDGEMENTS

Throughout these 2 years of Research experience, the author would not have been able to achieve the desired results without the help of many people. The author would like to take this opportunity to express her sincere gratitude to the following who had guided her:

- **Supervisor A/Prof Chew Chye Heng** for his priceless knowledge and patient guidance during the entire project. His care and concern for student welfare is deeply appreciated and serves as an immense encouragement for the author in his future endeavors.
- **Lab Officer Mr. Cheng** for his selfless sacrifice in providing vital support during all stages of the experimental set-up.
- **Dynamics Laboratory Technical Staff Mr. Ahmad Bin Kasa, Ms Amy Chee and Ms Priscilla Lee** for their valued support and tolerance, providing an environment conducive to conduct the experiments.
- **Workshop 2 Technician Mr. Au** for providing his expertise and time in setting up and conducting the experiments.

TABLE OF CONTENTS

<u>TOPIC</u>	<u>PAGE</u>
ACKNOWLEDGEMENTS	I
TABLE OF CONTENTS	II
SUMMARY	VI
LIST OF TABLES	VIII
LIST OF FIGURES	IX
LIST OF SYMBOLS	XI
CHAPTER 1 INTRODUCTION	1
1.1 Tool Wear	3
1.2 Wear Characteristic Equation	6
1.3 Cemented Carbide	11
1.4 Cutting Forces in Turning	12
1.5 Forces in End Milling	14
1.6 Application of Magnetic Field and Electric Field	15
1.7 Effect of Magnetic Fields on Humans and Exposure Limits	18
CHAPTER 2 LITERATURE REVIEW	20
2.1 Effect of Magnetic Field	20
2.2 Effect of Current	23
2.3 Magneto-elastic Effect Review on Conducting Material	27
2.4 Magneto-elastic Effect review on Ferromagnetic Material	29

CHAPTER 3 REVIEW OF ELECTROMAGNETICS	34
3.1 Maxwell's Equation	34
3.2 Electromagnetic Constitutive Relations	35
3.2.1 Stationary media	36
3.2.2 Moving Media	37
3.3 Electromagnetic Boundary Conditions	38
3.4 Quasi-static Approximation	39
3.5 Magnetically Induced Currents	41
3.5.1 Introduction	41
3.5.2 Basic Equations for Eddy Current	41
3.5.3 Anisotropic Media and Skin Depth	43
3.6 Potential methods for Magnetic Field	45
3.7 Ferromagnetism	46
3.7.1 Ferromagnetic Domains	47
3.7.2 Soft and Hard Ferromagnetic Materials	48
3.8 Magnetic Force for Non-ferromagnetic and Ferromagnetic Material	50
3.9 Magnetic Field Distribution Case Study	51
 CHAPTER 4 MAGNETO-MECHANICAL PROBLEM	 54
4.1 Introduction	54
4.2 Fundamental of Magneto-Elasticity	55
4.3 Magneto-Elastic Conducting Plate Model	58
4.4 A Plate Theory for Ferro-Elastic Materials	60
4.5 System Dynamics in the Feed Direction	61

4.6 System Dynamics in the Cutting Direction	63
CHAPTER 5 EXPERIMENTAL SETUP	65
5.1 Experimental Setup for Turning Process	65
5.2 Experimental setup of Milling Process	70
5.3 Electromagnets Details	76
5.4 Procedure of Experiments	77
5.5 Measurement of Magnetic Field	78
CHAPTER 6 EXPERIMENT ANALYSIS AND NUMERICAL SIMULATION FOR TURNING	79
6.1 Effect of Magnetic Field on Wear	79
6.2 Variation of Force Due to Magnetization	82
6.3 Diffusion Wear and Force	84
6.4 Magnetization, Lenz's law Effect on Cutting Force	85
6.5 Magneto-elastic Interaction, Vibration and Tool Wear	87
6.6 Magnetic Pole Effect on Wear	89
6.7 Azimuthal Induction Currents and Electromagnet Model	91
6.8 Computer Simulations and Discussion	93
CHAPTER 7 EXPERIMENT ANALYSIS AND MODELLING FOR MILLING	99
7.1 Effect of Magnetic Field on Wear	99
7.2 Variation of Force Due to Magnetization	101

7.3 Quasi-Static and In-plane Induction Current	104
7.4 Eddy Current effect on Aluminum Oxide Sliding Contact	105
7.5 Eddy Current Effect on (TiAl)N Growth	107
7.6 Thermal Effect of Eddy Current	109
7.7 Polarity Effect of Induced Eddy Current	110
7.8 Computer Simulations and Discussion	111
CHAPTER 8 CONCLUSION	114
BIBLIOGRAPHY	117
APPENDICES	121
APPENDIX A	121
APPENDIX B	122

SUMMARY

In metal cutting practice, productivity and cost of machining are highly correlated to tool life due to the opportunity cost of machine down time during the replacement or resetting of tool inserts. Thus a small portion of tool insert life increase will contribute to a large increase of productivity and a reduction of product cost. A variety of machining solutions has been introduced over the years. In more recent attempts to increase tool life of inserts, a possible non-machining solution has been explored involving the use of magnetic fields. In this project, the effects of magnetic field on the tool life of a cutting insert during turning and milling operations will be studied in greater detail.

In this project, two commercial electromagnets were employed both in turning and milling machining processes. In the turning case, the electromagnets were fixed at the bottom and top of the tool holder, which enable the distribution of magnetic field on the tool. On the contrary, in milling process, the electromagnets were placed at the base of the workpiece.

Furthermore, under two different magnet orientations, North-North and North-South magnet orientation, parameters such as tool wear, surface finish and force experienced during cutting were then measured under each condition. Improvements in tool life, reduction in force experienced and slight improvements in surface finish were observed when the tool steel was being cut. This improvement is especially significant with regards to tool wear in which up to 44.5% improvement was observed when a constant magnetic field was applied. This project aims to investigate the effects of varying magnetic field strengths and

changing polarities on the tool wear of the tool inserts used in turning. As such, only the magnetic field strengths and the orientation of the magnets are varied on the work piece, while the other cutting parameters are kept constant. A control experiment was also done where no magnetic field is applied at all.

To predict the magnetic field distribution and corresponding magnetic force, a series of models were established by COMSOL using finite element method. The models includes: single electromagnet, tool holder with workpiece under different magnets setup in turning process, and induced eddy current on the rotating working for turning; workpiece with N-N and N-S electromagnets setup and rotating plate model. The predicted magnetic field distribution was in good agreement with the measured values.

The attempted explanation is in the light of magnetization force and force due to the induced eddy current. The aluminum film was also analyzed on the tool workpiece contact surface, which took into account the thermal effect. The simulation results showed reasonable effect on the reduction of the cutting force and significant reduction in the tool wear of the inserts with the application of magnetic fields. Trends can also be seen where increasing the field strengths correspond to better tool life.

LIST OF TABLES

Table 5-1 Experimental Instruments	67
Table 5-2 Turning workpiece Properties	68
Table 5-3 Cutting conditions in turning case	69
Table 5-4 Material properties for Tool Insert	72
Table 5-5 Material properties for ASSAB 718	73
Table 5-6 Milling Machining Conditions	75
Table 5-7 Electromagnet parameters	76
Table 6-1 Points values of magnetization	96

LIST OF FIGURES

Figure 1.1 Flank wear of a turning insert	6
Figure 1.2 Wear characteristic curve of flank wear	9
Figure 1.3 Wear characteristic curve of crater wear	10
Figure 1.4 Stress distribution on the tool face in the vicinity of the cutting edge	11
Figure 1.5 Cutting forces in turning process	14
Figure 1.6 Forces in end milling on the feed plane	15
Figure 1.7 Axial and radial magnetic fields in a thick solenoid as a function of the ratio of radial length to inner radius a_1	17
Figure 1.8 Cross section of electromagnet and magnetic flux density distribution on the surface	18
Figure 2.1 Vibration of ferromagnetic mass between poles of electromagnet	28
Figure 2.2 Morisue's cantilever beam	31
Figure 3.1 Boundary between two materials with different permeabilities	38
Figure 3.2 Skin depth vs. frequency	44
Figure 3.3 Hysteresis loop	49
Figure 4.1 Deformation of two dimensional plate with magnetic field	60
Figure 4.2 Cantilever beam model in the feed direction	62
Figure 4.3 Cantilever beam model in the cutting direction	63
Figure 5.1 Computer controlled turning machine	66
Figure 5.2 Turning Experimental Setup including electromagnets and Dynamometer	67
Figure 5.3 The application of the electromagnets on the tool holder with the Inserts	70
Figure 5.4 Makino Milling Machine	71
Figure 5.5 Fresh insert	72
Figure 5.6 Insert attached to holder in Milling	72

Figure 5.7 Electromagnets setup on workpiece in milling	75
Figure 5.8 Top Surface	78
Figure 5.9 Measured magnetic field flux density points	78
Figure 6.1 Tool wears with and without electromagnets under the N-N setup	80
Figure 6.2 Tool wears with and without electromagnets under the N-S setup	81
Figure 6.3 Radial forces against time with N-N setup	82
Figure 6.4 Axial forces against time with varied power supply	83
Figure 6.5 Tangential forces against time with N-N setup	83
Figure 6.6 Close loop relation	87
Figure 6.7 Tool wear reduction with N-N and N-S magnetic fields	90
Figure 6.8 Single cylindrical electromagnet	93
Figure 6.9 Model of electromagnets, tool holder and workpiece (N-N)	95
Figure 6.10 Model of electromagnets, tool holder and workpiece (N-S)	95
Figure 6.11 Eddy current on the unrolled workpiece	96
Figure 7.1 Tool wears with and without electromagnets under the N-N setup	100
Figure 7.2 Tool wears with and without electromagnets under the N-S setup	101
Figure 7.3 Forces against voltage supply on the 21 st pass with N-N setup	102
Figure 7.4 Forces against voltage supply on the 21 st pass with N-S setup	103
Figure 7.5 Model of electromagnets sticking to the workpiece with N-N setup	111
Figure 7.6 Model of electromagnets sticking to the workpiece with N-S setup	112
Figure 7.7 Eddy current on the rotating disk	112

LIST OF SYMBOLS

T	Absolute temperature
ΔE	Activation energy
Q_p	Activation energy for oxidation
φ	Activation energy of diffusion
H	Asperity hardness
F_a	Axial force in turning
D	Bending stiffness constant
λ	Boltzmann's constant
H_c	Coercive field
C_1, C_2	Constants in simplified wear characteristic equation
A_1, A_2, B_1	Constants in wear characteristic equation
J	Current density
T	Current vector potential
V	Cutting velocity
C_i	Damping coefficient associated with contact interaction
d_c	Depth of cut
u	Displacement
w	Displacement vector
μ_d	Dynamic Friction coefficient
t_{ij}	Elastic stress tensor
q	Electric charge density
σ	Electric conductivity
D	Electric displacement field

E	Electric field
ε	Electric permittivity
η	Electric susceptibility
Ψ	Electric vector potential
U	Energy per unit volume
F_i	Exciting force due to tool wear
J^e	Externally generated current density
f	Feed/rev
s	Film thickness
F	Force
F_x	Force in x direction in milling
F_y	Force in y direction in milling
ω	Frequency
F_f	Friction force
G	Gauss
R	Gas constant
Z	Holm's probability
I	Identity matrix
g	Initial gap
δ_{ij}	Kronecher Delta
λ, γ	Lame's elastic constants
L	Length
H	Magnetic field flux intensity
B	Magnetic flux density

P_m	Magnetic pressure
χ	Magnetic susceptibility
A	Magnetic vector potential
M	Magnetization density
Δm	Mass of oxygen per unit area
ρ	Mass per unit volume
s_{\max}	Maximum film thickness
$V_{B\max}$	Maximum flank wear
I	Moment of inertia
ω_0	Natural frequency
h_c	Nominal uncut thickness
σ_f	Normal stress due to friction force
σ_t	Normal stress on the contact surface
n ₂	Outward normal unit vector
K_p	Parabolic rate constant
ϵ_0	Permittivity of vacuum
μ_0	Permeability of vacuum
τ	Period between two consecutive cuts at the same locations
ν	Poisson's ratio
J_0	Polar moment of inertia
P	Polarization density
V_{loop}	Potential difference
F_R	Radial force in milling

F_r	Radial force in turning
A_r	Real area of contact
μ_r	Relative magnetic permeability
B_r	Remnant field
ϕ	Scalar potential
σ	Second-order tensors of electric conductivity
τ_f	Shear stress due to friction force
δ	Skin depth
dL	Sliding distance
K_i	Stiffness associated with the contact interaction
ρ_s	Surface charge density
\mathbf{J}_s	Surface current density
F_c	Tangential cutting force in turning
F_t	Tangential force in milling
θ	Temperature of the chip surface
T	Tesla
F_t	Thrust force
T	Time
δ_t	Time dependent skin depth
A	Transverse area
w	Transverse plate displacement
$\mathbf{e}_1, \mathbf{e}_2, \mathbf{e}_3$	Unit vector
\mathbf{e}_θ	Unit vector in the azimuthal direction cylinder coordinate

v	Velocity
V_B	Width of flank wear
dW	Wear volume
E	Young's modulus

CHAPTER 1

INTRODUCTION

Metal cutting is one of the most common manufacturing processes to produce the final shape of products, and its technology continues to advance in parallel with developments in materials, computers, and sensors. A blank is converted into a final product by cutting extra material away by turning, drilling, milling, broaching, boring, and grinding operations conducted on Computer Numerically controlled machine tools. Machining processes constitute a significant share of the total manufacturing costs and hence improving the efficiency of these processes can contribute to a significant reduction in manufacturing cost.

Tool wear is one of the important factors that determines the product cost and productivity. On one hand, proper tool type and cutting conditions should be selected such as cutting speed, feed rate and depth of cut. This will make the most use of the tool. On the other hand, machine tool downtime due to broken and worn tools is one of the main limitations to productivity.

Machine tools are regularly required to work to an accuracy of 0.02 mm and often to 0.002 mm. The permissible amounts of elastic flexure of the main frame and its subsidiary units must be small to achieve this degree of accuracy. The machine as a structure cannot be designed by normal stressing methods where load carrying capacity is the criterion, but must be designed to have negligible deflection and provide generous bearing surfaces so as to diminish wear.

Machinability is made up of a combination of five criteria: wear resistance, specific cutting pressure, chip breaking, built-up edge formation and tool coating character. The most significant variables indicating machinability are tool life and the quality of surface finish produced. Conditions of the material which determine machinability are composition, heat treatment and microstructure. The measurable mechanical properties of hardness, tensile strength and ductility give some indication of expected machining properties.

Some significant facts relating to machinability are given below:

- Hardness.
- Microstructure.
- Composition
- Free machining properties, such as inclusion of weaker insoluble material considerably increase the metal removal rates and resulting surface finish.

In metal machining, vibration occurs in the machine, tool or workpiece. It affects surface finish, accuracy, and adversely affects the life of carbide or ceramic tipped tools. The machine supports the tool and the workpiece in a controlled relationship so that structure or frame provides a basis for connection between spindles and sliding objects. Necessary adjustment is made before machining to insure the minimum distortion and vibration under load and processing. Machine tool vibration plays an important role in determining hindering productivity during machining. Excessive vibrations accelerate tool wear and chipping, causes poor surface finish, and may damage the spindle bearings.

1.1 Tool Wear

A basic knowledge of tool wear mechanism is helpful to analyze and control tool wear development. When cutting metals, a tool is driven asymmetrically into the work material to remove a thin layer (the chip) from a thick body (the workpiece). The chip formation occurs as the work material is sheared in the region of the shear plane extending from the tool edge to the position where the upper surface of the chip leaves the work surface. In this process, the whole volume of metal removed is subjected to extensive plastic deformation. The wear pattern at the tool/chip interface is significantly determined by the movement of the chip across the rake face and around the tool edge. Tool wear is the product of a combination of load factors on the cutting edge. The life of the cutting edge is decided by several loads, which engage to change the geometry of the edge. The main load factors, including mechanical, thermal, chemical and abrasive, interact between tool, workpiece material and cutting conditions. Clearly, whenever the tool is engaged in a cutting operation, tool wear will develop in one or more areas on and near the cutting edge. The major mechanisms of tool wear include [1]:

- I. Abrasion in which hard regions of the workpiece are dragged over the tool and cut, plow or groove local regions of the tool. The cutting edge's ability to resist abrasion is largely connected to the tool hardness.
- II. Diffusion wear is mostly affected by the chemical load during the cutting process. The chemical properties of the tool material and the affinity of the tool material to the workpiece material will decide the development of the

diffusion wear mechanism. The metallurgical relationship between the materials will determine the amount of wear mechanism.

- III. Adhesion and diffusion in which work material tends to stick to the tool and components of the tool material diffuse into the work material. Adhesion wear occurs mainly at low machining temperatures on the chip face of the tool. This mechanism often leads to the formation of a built-up edge between the chip and the edge. The built-up edge can be sheared off and commence build-up again or cause the edge to break away in small pieces or fracture.
- IV. The extreme case of large scale plastic deformation of the tool edge which can happen at very high temperatures.

Besides the classification in the light of generating mechanism, tool wear can also be considered in two catalogs: gradual wear and chipping. Chipping is the sudden removal of cutting tool material. Severe Chipping (micro-chipping) often leads to hazardous tool break. The gradual wear usually refers to flank wear and crater wear, which increases gradually as the machining operation proceeds. Various tool wear types are summarized in table A-1 (see appendix A).

Among all of these wear types, there are two of these wears that are the main concern and act as the criteria to evaluate the tool wear break stage.

- Flank wear takes place on the flanks of the cutting edge, mainly from the abrasive wear mechanism. On the clearance sides, leading, trailing and nose

radius are subjected to the workpiece moving past during and after chip formation. This is usually the most normal type of wear and maintaining safe progressive flank wear is often the main concern in metal machining. Excessive flank wear will lead to poor surface finish, inaccuracy and increasing friction as the edge changes shape.

- Crater wear on the chip face can be due to abrasive and diffusion wear mechanisms. The crater is formed through tool material being removed from the chip face either by the hard particle grinding action or at the hottest part of the chip face through the diffusive action between the chip and tool material. Hardness, hot hardness and minimum affinity between materials minimize the tendency for crater wear. Excessive crater wear changes the geometry of the edge and can deteriorate chip formation, change cutting force directions and also weaken the edge.

Of the two major types of tool wear, flank wear and crater wear, the measurement of flank wear is of great concern since the amount of flank wear is often used in determining the tool life. In addition, the mechanism of wear development can be more accurately modeled for flank wear than for crater wear. In our experiment including turning and milling, the flank wear is the most obvious wear and dominates through the whole cutting process. Thus we define some basic parameters and show the details in Fig. 1.1.

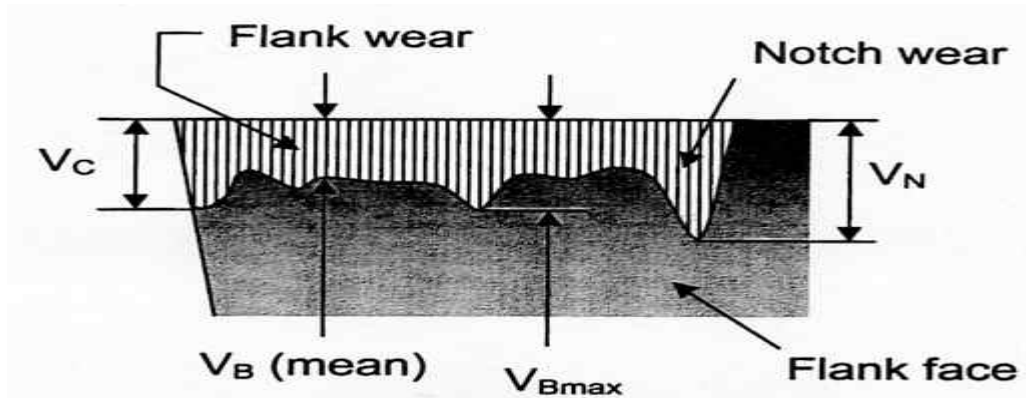


Figure 1.1 Flank wear of a turning insert [1]

- a. V_B is the mean width of flank wear;
- b. V_{Bmax} is the maximum flank wear;
- c. V_c is the maximum wear at nose radius;
- d. V_N is the notch wear.

V_B and V_{Bmax} can be measured by optical microscope and are commonly used as the level of the tool in the manufacturing community.

1.2 Wear Characteristic Equation

Since the F.W. Taylor proposed the classic tool life equation $VT^n = C$, where T is the tool life, V is the cutting speed and n and C are constants, numerous researchers have studied the tool wear and tool life characteristics.

Wear due to adhesion and abrasion appears to play the major role in the continuous dry cutting of steels with tungsten carbide tools without a built-up edge. It is further considered that the adhesion type of wear mechanism would be rate determining, while the abrasion due to hard particles in the matrix of steel such as carbide, silica

(SiO₂) and corundum (Al₂O₃) may be complementary because temperatures and normal stresses on the tool face are extremely high and mutual diffusion of constituents between the steel and the tool is well known to take place in the practical range of cutting conditions for tungsten carbide tools.

Usui et al. [3] presented an Archard type of equation for adhesive wear:

$$dW = A_r \frac{c}{b} Z dL \quad (1.1)$$

where dW is the wear volume for sliding distance dL , A_r the real area of contact, c the height of the postulated plate-like wear particle, b the mean spacing of the asperities and Z the probability of producing a wear particle per asperity encounter (Holm's probability). Regarding A_r in Eq. (1) as the area for unit apparent area of contact, we may write Eq. (1) as

$$dW = \frac{\sigma_t}{H} \frac{c}{b} Z dL \quad (1.2)$$

where H is the asperity hardness and σ_t is the normal stress on the contact surface. c/b in the above equation may be regarded as being approximately constant owing to the existence of the size effect. Since the asperity hardness H depends more strongly on the bulk properties of the softer of the pair of mating surfaces than on those of the asperity itself, it may depend on the diffused layer, temperature, strain and strain rate on the chip surface in contact. Neglecting variation in the strain and the strain rate in the practical range of cutting conditions for carbide tools, we may simply assume the following equation by analogy with the rate process, since material strength and diffusion are similarly affected by temperature:

$$H = A_1 \exp\left(\frac{A_2}{\theta}\right) \quad (1.3)$$

where A_1 and A_2 are constants and θ is the temperature of the chip surface. The probability Z may be considered as that for yielding a weld which is strong enough to produce a wear particle when an asperity encounter takes place. Since such weld formation is a kind of thermally activated rate process, the probability Z will be expressed by the following equation, if the interlocking time and the flash temperature rise during the encounter are regarded as being almost constant within a given range of cutting conditions:

$$Z = B_1 \exp\left(-\frac{\Delta E}{\lambda\theta}\right) \quad (1.4)$$

where B_1 is a constant, λ is Boltzmann's constant, ΔE is the activation energy and θ is the temperature of the chip surface. Substituting Eq. (3) and (4) into Eq. (2) and regarding c/b as constant, we obtain

$$\frac{dW}{\sigma_c dL} = C_1 \exp\left(-\frac{\Delta E + \lambda A_2}{\lambda\theta}\right) \quad (1.5)$$

where C_1 is a constant. Although $\Delta E + \lambda A_2$ in the above equation depends on the structure and the element concentration of the diffused layer on the contact surface, we may regard it as being approximately constant if the variety of cutting conditions is limited. We then arrive at the equation

$$\frac{dW}{\sigma_c dL} = C_1 \exp\left(-\frac{C_2}{\theta}\right) \quad (1.6)$$

Furthermore, the comparison between flank wear and crater wear shown in Fig. 1.2 and Fig. 1.3 was also made. It is interesting that the data points, which were all

obtained for flank wear in Fig. 1.2, lie on the characteristic line obtained for crater wear Fig. 1.3 when the temperature is increased. This means that the wear characteristic is the same, no matter which type of wear is being considered. So in our experiment, in consider of the dry cutting environment and high cutting speed, the high temperature is unavoidable. Thus flank wear is the main standard to evaluate the tool life.

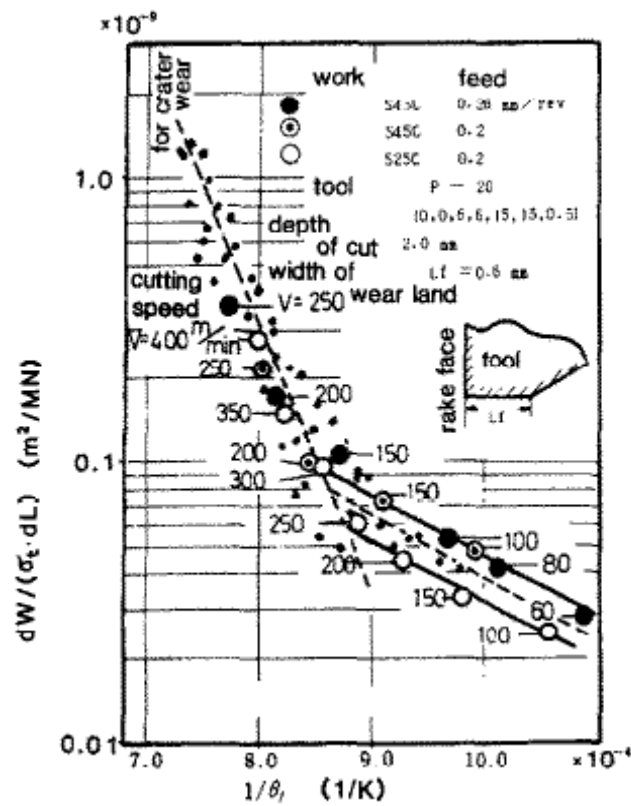


Fig. 1.2 Wear characteristic curve of flank wear [3]

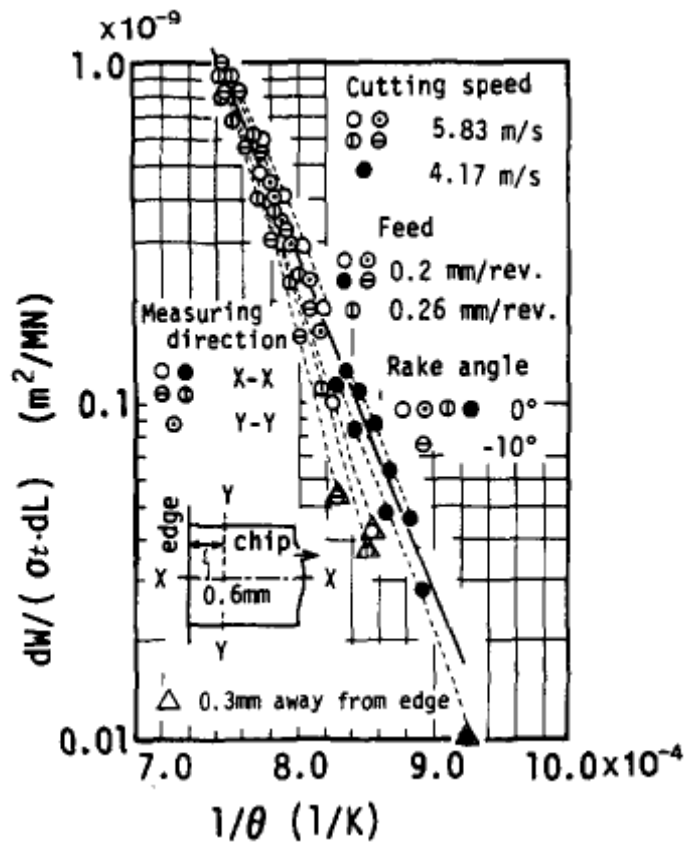


Fig. 1.3 Wear characteristic curve of crater wear [3]

The contact between the flank wear and the machined surface appears to be elastic except in the vicinity of the cutting edge. In steady cutting with negligible vibration, it is considered that the elastically recovered machined surface just behind the cutting edge (the recovery is about 2 pm) is depressed slightly during the cutting by the flank wear of which the shape is similar to the recovered surface, and this slight depression is enough to give the stresses τ_f and σ_f elastically. Figure 1.4 shows a sketch of the stress distribution around the cutting edge; the cutting edge roundness is exaggerated. If the material is assumed to be rigid and perfectly plastic, the boundary condition at

point B in Fig. 1.4 requires $\tau_f = \sigma_f$ at point B when τ_f is the principal shear stress there.

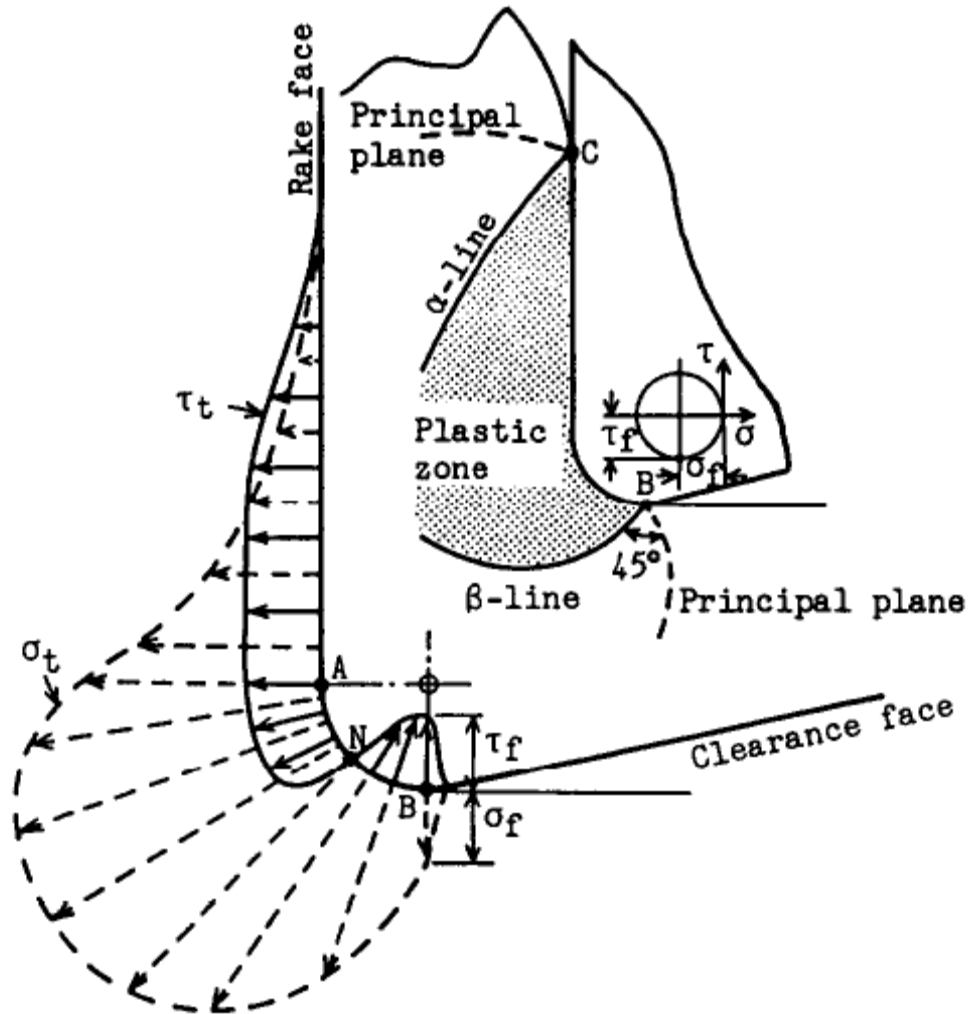


Fig. 1.4 Stress distribution on the tool face in the vicinity of the cutting edge [3]

1.3 Cemented Carbide

Cemented carbide is a tool-material made up of hard carbide particles, cemented together by a binder. It has an advantageous combination of properties for metal cutting and along with high speed steel, has dominated metal cutting performance at higher cutting speeds. Cemented carbide is a metallurgical product, made primarily

from a number of different carbides in a binder. These carbides are very hard and those of tungsten carbide, titanium carbide, tantalum carbide, niobium carbide are the main ones. The binder is mostly cobalt. In addition, the carbides are soluble in each other and can form cemented carbide without a separate metal binder. The hard particles vary in size, between 1-10 microns and usually make up between 60-95 percent in volume portion of the material.

The coating layer of titanium carbides is only a few microns thick and largely changes the performance of the tool insert. The effect of the coating continues long after it has partly worn off, resulting in the reduction of insert wear when machining steel. Coated grades have been developed and found wide acceptance in metal machining. The main coating materials are titanium carbide, titanium nitride, and aluminum oxide-ceramic and titanium carbonitride. Titanium carbide and aluminum oxide are very hard materials with extra wear resistance and are chemically inert, providing a chemical and heat barrier between tool and chip.

1.4 Cutting Forces in Turning

Forces in a machine tool are caused by a variety of static, dynamic and thermal stresses. The cutting force is closely related to the tool wear and can also act as the main feedback of wear level during machining process. It is necessary to evaluate and analyze the interrelationship of cutting forces. Figure 1.5 shows the basic forces in turning process, which consist of the tangential cutting force F_c , the axial force F_a , and the radial force F_r . The tangential cutting force is due to rotational relative

motion between the tool tip and the workpiece. This is normally the largest cutting force component and acts in the direction of cutting velocity V . The feed force F_a is generated by the longitudinal feeding motion of the tool with respect to the workpiece. The magnitude of feed force, in general, ranges between 30% and 60% of tangential force. The radial force, is the least significant of all cutting force components and is produced by the thrusting action of the tool tip against the work material. The large feed force F_a is indicative of a large chip tool contact area on the rake face. Since the feed force is a measurement of the drag which the chip exerts as it flows away from the cutting edge across the rake face. The radial force F_r is produced by the approach angle of the tool and it is the force needed to hold the tool against the workpiece in the axial direction. It usually has zero velocity. These three forces can be resolved to determine the total resultant force F . Their relationship becomes especially important when deflection of tool with large overhang or a slender workpiece is a factor as regards to accuracy and vibration tendencies. As can be expected, the size relationship between the force components varies considerably with the type of machining operation. The tangential force often dominates in milling and turning operations. The radial force is of particular interest in boring operations and the axial force in drilling.

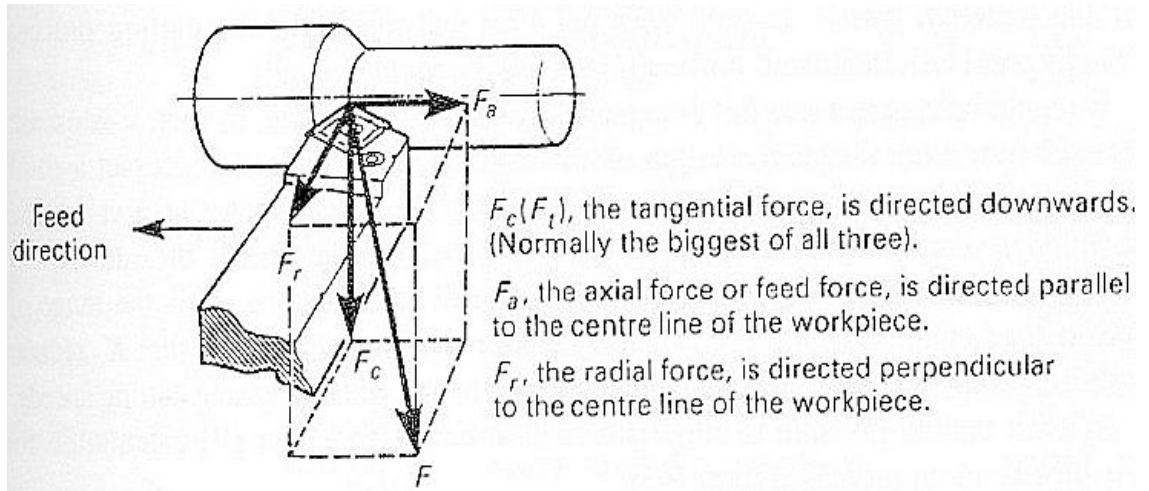


Fig 1.5 Cutting forces in turning process

Vibration tendency is one consequence of the cutting force. As for the deflection of the tool or workpiece, those can be affected by vibrations in the cutting process due to varying working allowance or material conditions as well as the formation of built-up edges.

1.5 Forces in End Milling

The milling process uses a cutter with several teeth which rotates at high speed, and moves slowly across the workpiece. An end mill typically has four cutting edges, and commonly used milling cutters are extremely fine grained (TiAl)N particles bonded to a tough cemented carbide core. End mills do not have cutting teeth across all the end so that there exists 'dead' area in the centre.

Figure 1.6 shows the components of the forces exerted by the workpiece on a cutting tooth, which act in a plane perpendicular to the cutter axis. The axial load on the cutter will be treated separately.

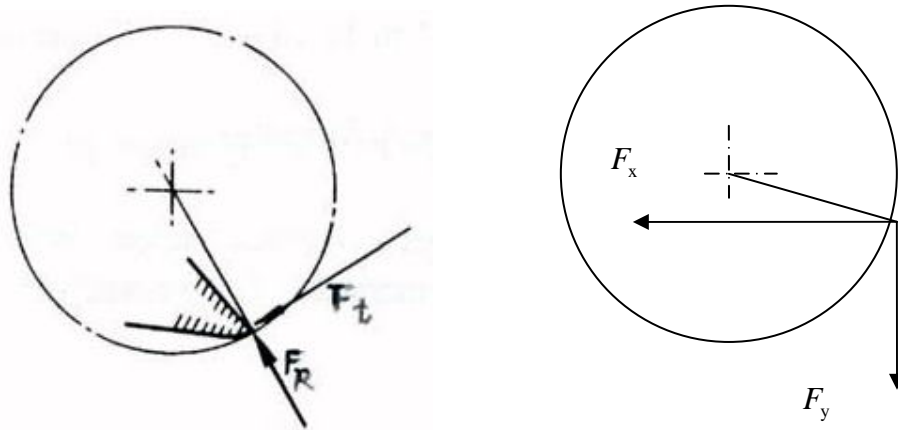


Fig. 1.6 Forces in end milling on the feed plane

F_t is the tangential force which determines the torque on the cutter; the tangential force F_t can be regarded as the rubbing force between the workpiece and the tooth. The value of F_t will depend upon the chip area being cut and on the specific cutting pressure. However, it is difficult to measure the F_t and F_R directly. So we compromise to measure the force in three fix directions: x direction (feed direction), y direction(normal to the feed direction and on the surface plane) and z direction(perpendicular to milling surface).

1.6 Application of Magnetic Field and Electric Field

It is important to have an understanding of how the electromagnet works and how it affects the magnetic field in the cutting area, and in turn the interaction between

cutting tool and workpiece. It is known from elementary physics that the motion of a conductor in a steady magnetic field can create an electric field or voltage that can induce the flow of current in the conductor. The induced electric field and the magnetic field will produce electromotive force that impedes the motion with the opposite velocity force direction.

When a conducting structure moves in a magnetic field, eddy current is generated in the structure, and the interaction of the induced eddy current with the applied magnetic fields generates electromagnetic damping.

The magnetic field and body forces for a finite length solenoid can be calculated by numerical methods. As an example, the magnetic field for a solenoid of length equal to 4 times the inner radius and outer to inner radius ratio of 3 is given here in Fig. 1.7, providing a roughly idea for the magnetic field circulation. For a constant current density, the magnetic field drops to zero almost linearly through the thickness. Also, the radial magnetic field at the quarter-plane is almost an order of magnitude smaller than the axial field. This model assumes that the axial field decreases linearly through the thickness and is zero at the outer radius in the central portion of the solenoid.

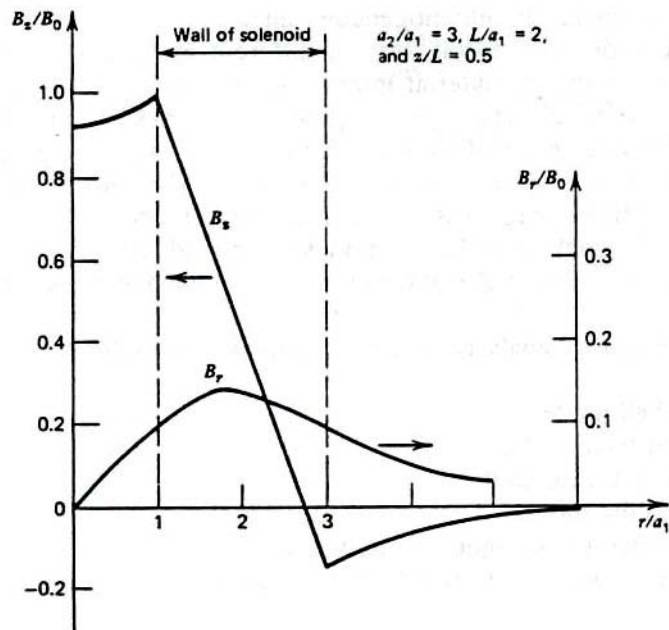
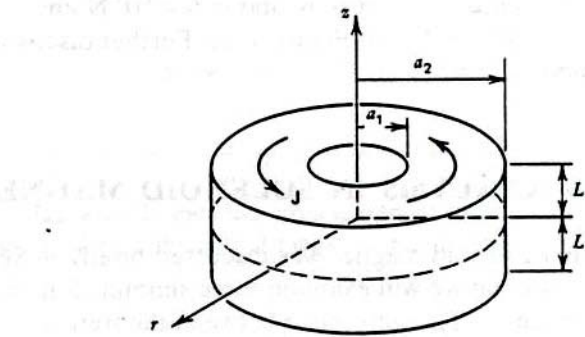


Fig. 1.7 Axial and radial magnetic fields in a thick solenoid as a function of the ratio of radial length to inner radius a_1

The commercial electromagnet we used is similar to this model and the cross section is shown in Fig. 1.8 with the magnetic flux density distribution on the surface along the radial of the cylinder.

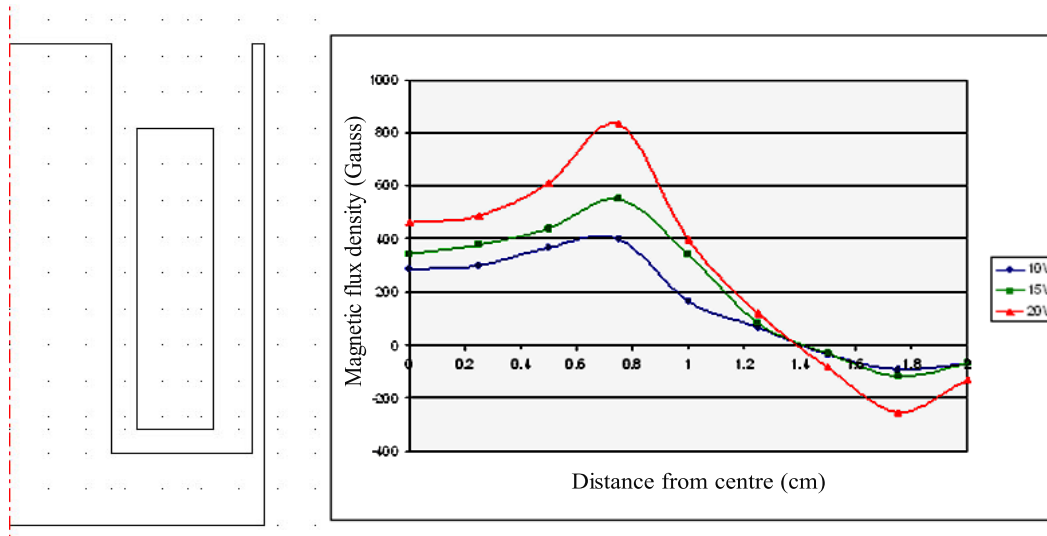


Fig 1.8 Cross section of electromagnet and magnetic flux density distribution on the surface

1.7 Effect of Magnetic Fields on Humans and Exposure Limits

For those who must work in magnetic environments, it is important that we should not be exposed to excessive magnetic field. There has been a long history of industrial exposure to low magnetic fields, say less than 0.02 Tesla (T), and low frequencies, 50-60Hz, without any observed effect on health.

There are three variables that must be considered when discussing limits of field exposure, which include magnitude, field gradient, and time rate of change. High dc magnetic fields have been observed to affect the chemical reaction rates of polymeric and biologically important molecules. DNA molecules have been reported to suffer a slight orientation in extremely high fields of more than 10T.

Alternating-current magnetic fields greater than 0.1T with a frequency range of 10-100Hz could evoke a visual response in the retina “magnet phosphene.” But it is not

known to be harmful. Some of the effects of inhomogeneous fields include effects on tissue growth and white blood cell formation.

In spite of some efforts to study the effects of magnetic fields on humans, the extent of risk to humans working in high-field environments has not been completely explored. Therefore, it is necessary to keep the magnetic field application as low as possible to achieve the expected effect in industries.

CHAPTER 2

LITERATURE REVIEW

2.1 Effect of Magnetic Field

The main topic of this thesis is on the effect of electromagnetic field in machining processes, such as turning and milling. The two small electromagnets we used have largely reduced the tool insert wear rate. In metal machining industry, tool life determines the productivity and cost of machining to some extent. Even a small increase in tool lifetime would greatly reduce the total machining cost by reducing the tool insert replacement frequency and saving the cost of new tool inserts.

The research concerning the magnetic effect on tool wear can be tracked back to 1966, when Bobrovskii [4] and Kanji and Pal [5] applied external electrical current in drilling process. They reported the increase of tool life without explicit explanation for this phenomenon. Similarly, Pal and Gupta [6] also did the drilling case by employing alternating magnetic signal on high speed steel tool against gray cast iron and SG iron workpiece. One experiment involved placing a solenoid to produce magnetic field both on the tool and the workpiece when drilling the gray iron. Another experiment changed the magnetic setup and a solenoid was placed on top of the tool block rather than the malleable iron workpiece and the magnetic field concentrated on the drilling tool. They indicated that magnetic field considerably reduces the wear rate and the gain percentage depends on the intensity of magnetization and cutting conditions. There were more details in experimental setup

and theoretical analysis deserved further study.

Muju and Ghosh [7] first employed magnetic field in the turning process and they revealed the ferromagnetic effect by differentiating friction materials pair in terms of ferro-material or nonferro-material. The three rubbing pairs included mild steel pins against brass, brass pins against mild steel and nickel pins against brass. The attempted explanation was such in the microscale that magnetic field enhanced dislocation velocity by a factor of four at room temperature and resulted in the increased rate of abrasive wear for magnetic body and decreased rate of wear for nonmagnetic body.

Three years later, Muju and Ghosh [8] further explained the phenomenon of diffusive wear and pointed out that external magnetic field enhanced the dislocation agglomeration and facilitated the generation of vacancies. And the enhancement in diffusivity was greater in ferromagnetic body, which would cause the negative hardness gradient. The above two papers omitted the thermal effect in dislocation which is also important in machining process.

Palumier et al. [9] discussed the effect of dc coil magnetic field on the wear of a ferromagnetic steel pin from the surface modifications point of view. They observed the formation of a hard passivated coating on sliding surface when the pin-on-disk contact environment is dry without lubricant. They contribute the increasing oxidation rate to the decrease of oxidation kinetic activation which is related to the

presence of magnetic field. However, there is no details to explain the principle how the magnetic field decrease the kinetic energy. They also reported the higher vacancy defect density in the sliding surface which in turn results in the stronger surface microhardness of steel.

They adopted the parabolic law assumption from Pal and Das and defined the mass of oxygen per unit area Δm as:

$$\Delta m = K_p t^{1/2} \quad (2.1)$$

where t is the experiment time and K_p is the parabolic rate constant

$$K_p = A \exp(-Q_p / RT) \quad (2.2)$$

where A is the Arrhenius constant, Q_p the activation energy for oxidation, R the gas constant and T the absolute temperature. The relationship is linear in a magnetic field, which supports the theory that the process of oxidation follows the Arrhenius equation. Then the oxidation activation energy can therefore be calculated from:

$$Q_p = \left(\ln A - \ln(\Delta m^2 / t) \right) RT \quad (2.3)$$

It is obvious that the applied magnetic field decreases the oxidation kinetic activation energy of steel and thus increases the oxidation.

By applying a large DC coil around the HSS cutting tool, Mansori, Pierron and Paulmier [10] continued to address the qualitative assessments of external magnetic field effect on turning process. They reported the same trend of increased tool durability and magnetic field by examining the crater wear at the outer edge. They also investigated the magnetic field effect on temperature and chip formation. The

magnetization indeed advanced the temperature rise especially after long time cutting. They also attributed the tool wear evolution to the finer chip adhesive to the rake as a third body lubricant. The magnetic field they applied is $4.8 \times 10^4 \text{ Am}^{-1}$. In considering the hazard of magnetic field to electric devices and human beings in industrial application, less magnetic field should be preferred.

2.2 Effect of Current

Rather than the application of magnetic field by coils, currents were also introduced directly into the experiments. Paulmier, Mansori and Zaidi[11] discussed the effect of electric current in 1997. They used power supply to produce electric current crossing the sliding contact between XC48/graphite pin-on-disc pair. They deduced the conclusion that the passage of 40A electric current tends to orient the graphite crystallites and leads to friction coefficient reduction. The electric current was produced by power supply and it is not applicable to the industry machining and the electric current is difficult to control.

Yamamoto [12, 13] observed that under boundary lubrication condition in a ball-on-disk machine, during sliding of steel pair in the presence of an additive-free mineral oil, the friction coefficient decreased but the ball wear increased when the disk was at a higher potential than the ball compared to the condition when no current passed. The decrease in friction coefficient was concluded to be due to the formation of a passivation layer on the surface of the disk. With continued sliding, damage to the passivation layer lead to increased friction coefficient. However, when the ball was at

higher potential than the disk, no decrease in friction coefficient was observed, and the ball wear was lower than that obtained when no current passed through the contact. Under mixed and hydrodynamic lubrication conditions, the friction coefficient increased irrespective of the direction of the current flow. It was postulated that the application of an electric field interfered with the lubricant film formation ability. In mixed lubrication regime, removal of the electrical field decreased the friction coefficient to a level lower than that observed when no current passed through the contact (Yamamoto et al. 1996).

The effect of an applied electric field on the running-in operation of a roller bearing was studied by Takeuchi [14]. In the mixed lubrication regime, when the bearing was anode the friction coefficient increased and also the bearing temperature increased and showed sign of seizure. The bearing surface was oxidized as would be expected, because of anodic reaction. However, when the bearing was cathode, the friction coefficient rapidly decreased and so did the bearing temperature. The lubricant used in this experiment was additive-free mineral oil.

The effect of an external electric field on the operation of an aluminium oxide-cast iron sliding contact joint was explored by Wistuba [15] in 1997. He compared the mating of this sliding contact joint operating in an external homogeneous electric field in the presence of polar lubricants. The focus is on the aluminium oxide layer, functioning in a joint with cast iron as an electric conductor and on the creation of boundary layers on sliding surfaces. The durability of these layers depends on the

applied electric field strength and polarization directions. The electric field changes the friction force in such a way that positive polarization of the sample decreases the friction force when the polarity is in the same direction of internal electric field. Lubrication of a dielectric-conductor type benefits the sliding mating of material, which leads to further decrease of friction forces. The greatest effectiveness of external electric field was achieved with $U = 0.2-0.4V$, positive polarity of the sample, unit pressure $q = 0.25 \text{ Mpa}$, sliding velocity $v = 0.5\text{m/s}$, dose 0.25 mg/cm^2 of base oil +5% of isooctyl trichloroacetate.

Gangopadhyay et al. [16] continued the ball-on-disk experiment and they reported that when the ball was cathode at room temperature, a small current(10 mA) reduced wear rate of the ball by about an order of magnitude. The ball wear rate remained low up to 100 mA current. However, increasing the current strength beyond 100 mA did not reduce the ball wear rate any further. In contrast, when the ball was anode the ball wear rate increased. When they raised the temperature to $100 \text{ }^{\circ}\text{C}$, the direction of the current flow influenced the ball wear rate in a similar fashion to that observed at room temperature. At 100 mA current, the ball wear rate decreased by about a factor of 3, less than that observed at room temperature.

In 2006, Gangopadhyay's group [17] investigated the wear control achieved by passage of an electric current in the presence of lubricant and extended the application to a face milling machining process. The decrease or increase of wear is decided by the anode or cathode to which the metal object connects. When the insert

is anode, the tool insert wear decreases compared with no current passes through. By contrast, the insert wear is higher when it is connected to the cathode than those with anode and without current. Compared with the former experiments conducted by Paulmier and some other researchers, the current used by Gangopadhyay is much lower, ranging from 0.2-0.5 A. However, the changing of current strength do not affect insert wear significantly.

Gangopadhyay et al. [16] also gave some explanation in terms of the surface film in the presence of lubricant, based on the experiment on the friction and wear behavior of a steel pair when an electric current was passed through the contact with fully formulated engine oils. The effect of friction coefficient was not much important because it only changed to a small degree but the wear was impacted significantly by 2–3 orders of magnitude, which is also affected by the direction and current strength of current flow. High wear was observed on the anode surface and low wear on the cathode surface. They attributed difference in wear rate of surfaces with and without current to the modification of the elemental composition of surface films formed at the contact.

The above results suggest that application of an electric field in a lubricated sliding contact initiates an electrochemical reaction where an oxidation reaction occurs at the anode and a reduction reaction at the cathode surface. In an additive-free lubricant, the oxidation reaction formed an oxide layer which controlled the wear and which is also partially responsible for the friction reduction.

Most of the above researchers applied the magnetic field by winding the tool or the workpiece. Others directly introduced the current by power supply. The effective magnetic intensity was high in the order of 10^4 A/m. Even in the pin-disk case, the loading forces were ten times less than those in metal cutting manufacture. In our turning experiment, two commercial electromagnets are introduced. The electric current intensity is about 0.2A and the magnetic intensity induced in the cutting area was 1500-3000 A/m. Under such low flux intensity, the tool wear also showed obvious improvement.

Our study of the interactive effect between magnetic field and eddy current, as well as the behavior of the couple in tool wear and cutting force required the analysis of the magnetic field distribution, the induced eddy current density because of the workpiece rotation, and the Lorentz force that may affect the vibration damping, which finally resulted in the improvement of tool wear.

2.3 Magnetoelastic Effect Review on Conducting Material

Ferromagnetic flexible structures are usually in the environment of strong magnetic field and magnetized. They are subjected to the strong magnetic forces arising from the coupling or mutual influence of the magnetization and magnetic field. Sometimes, the strong magnetic force leads to deformation of ferromagnetic structures.

One of the early papers on electromagnetic buckling of soft magnetic materials was Mozniker [18]. In this experiment, he placed a nonferromagnetic cantilever beam,

with a ferromagnetic solid on the end, between the poles of an electromagnet, as can be seen in Fig. 2.1. The equation of motion for the lowest transverse mode was given by

$$\frac{d^2u}{dx^2} + \omega_0^2 u - KB_0^2 \frac{gu}{(g^2 - u^2)^2} = 0 \quad (2.4)$$

where g is the initial gap(equal distance from each pole) between the magnet and the beam and B_0 is the magnetic field produced by the electromagnet. The linearized equation has a vibratory solution whose frequency decreases with current:

$$\omega^2 = \omega_0^2 \left(1 - \frac{KB_0^2}{g^3 \omega_0^2} \right) \quad (2.5)$$

This equation indicates the decrease in natural frequency with magnetic field by a simple model. For a rod in a transverse magnetic field, Moon [19] observed experimentally that motion parallel to the field suffers a decrease in natural frequency, while vibration transverse to the field appears to increase the frequency of the lowest bending mode of a cantilevered rod.

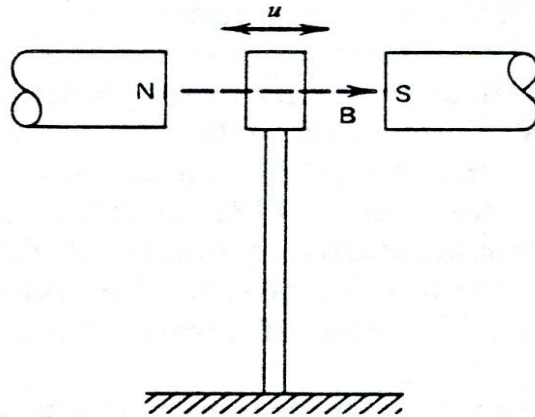


Fig. 2.1 Vibration of ferromagnetic mass between poles of electromagnet

Based on numerical calculations Wallerstein and Peach [20] concluded that the actual field at the surface of the undeformed plate in a normal magnetic field was 86% higher than the applied field \mathbf{B}_0 , where the infinite plate theory admits no change in the normal field due to the plate. Peach also pointed out that for a finite plate, the flux near the edge is concentrated, thus raising the average flux across the plate above the external field.

The coupling effect between electromagnetic field and mechanical response of a conducting structure was explored by Lee et al [21], by finite element method. A numerical model for fully coupled analysis of magnetically induced vibrations of the conducting plates in transient magnetic fields was developed and was in good agreement with the data in their electromagnetic induction experiments. The mechanical responses are considerably damped due to the magneto-elastic interactions. And the maximum displacement at the tip of the beam from the coupled analysis is about 40% smaller than that from the uncoupled case. Besides that, the peak current densities are reduced due to the field-structure interactions and the damping effect is more prominent in the tip element than in the base element of the cantilevered plate. Although the peak current density is considerably reduced, the eddy current does not decay monotonically after reaching the peak.

2.4 Magnetoelastic Effect review on Ferromagnetic Material

For ferromagnetic structures an applied DC magnetic field may change the effective stiffness. An application of this idea has been applied to an ultrasonic generator by

Birr, Koryu Ishii and Combs [22]. A transformer core is excited by a dc pulses and the dynamic equivalent macroscopic transverse stiffness of a laminated iron core system varies in a wide range in a relatively low magnetic flux bias ranging from 100-180 gauss. The experiments showed that the effective stiffness of the core is a function of the magnetic bias. The resonant frequency of the system is dominated by the dc magnetic bias on the core and not by the circuit. If no magnetic field was applied to the core, the circuit was so lossy that no oscillations were observed. Whenever the dc magnetic bias is increased, the oscillations frequency increases. Thus the magnetic bias controls the effective dynamics stiffness of the core system, thereby controlling the vibration frequency. The stiffer is the core system, the higher the vibration frequency. A elastic wave equation describes the relationship between the vibration frequency $\Delta\omega$ and the change of magnetic field ΔH :

$$\Delta\omega = \frac{\chi}{8\delta l} \sqrt{\frac{E}{\rho}} \left[\frac{\partial}{\partial \sigma_n} \left(\frac{\delta l}{l} \right) - \frac{1}{E} \right] \frac{(\Delta H)^2}{\Delta \left(\frac{\delta l}{l} \right)} \quad (2.6)$$

Where χ is the magnetic susceptibility, E is the Young's modulus, ρ is the density of the material, $\delta l/l$ is the strain, and σ_n is the stress.

The coupling effect between eddy current and deformation of structure also plays an important role for ferromagnetic materials about their dynamic behavior in magnetic field. This coupling effect of structure under transient field has been investigated by some researchers [23-25]. Morisue [23] explored the interaction of a copper rectangular beam with crossed time-changing and steady uniform magnetic fields, as shown in Fig. 2.2.

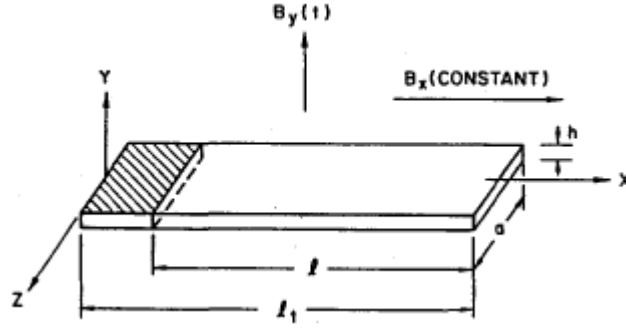


Fig 2.2 Morisue's cantilever beam

The time-changing magnetic field $B_y(t)$ is perpendicular to the beam, while the steady field B_x is parallel to it. Because of the time-changing field in y direction, eddy current is produced in paths parallel to the z direction and interacts with the constant magnetic field in x direction, then Lorentz force will cause lateral beam deflection in y direction. The deflection also causes the magnetic field in x direction changes and additional eddy currents will oppose the former induced current, resulting an reduced eddy current.

Takagi et al [24] described computational analysis and an experiment of plate deflection in magnetic field. A thin elastic isotropic homogenous plate with electrical conductivity σ and magnetic permeability μ is employed with the distribution of magnetic field. With the assumption that the deflection is small and a plate is thin enough compared with skin depth, they derived the governing equation of eddy current analysis considering the coupling effect:

$$\frac{\partial^2 T}{\partial x^2} + \frac{\partial^2 T}{\partial y^2} = \sigma \frac{\partial}{\partial t} (B_{oz} + B_{ez}) - \sigma C \quad (2.7)$$

$$C = B_{ox} \frac{\partial^2 w}{\partial x \partial t} + B_{oy} \frac{\partial^2 w}{\partial y \partial t} - \frac{\partial B_{oy}}{\partial z} \frac{\partial w}{\partial t} \quad (2.8)$$

$$B_{ez} = \frac{\mu_0 h}{4\pi} \iint_s \frac{\frac{\partial T}{\partial x}(x-x') + \frac{\partial T}{\partial y}(y-y')}{\left[(x-x')^2 + (y-y')^2 \right]^{3/2}} dx' dy' \quad (2.9)$$

where w is lateral displacement, \mathbf{T} is the current vector potential, B_{ez} is the magnetic flux density in the beam induced by the eddy current. Based on the eddy current analysis, the Lorentz's force induced deflection can be expressed as:

$$D \left(\frac{\partial^4 w}{\partial x^4} + \frac{\partial^4 w}{\partial x^2 \partial y^2} + \frac{\partial^4 w}{\partial y^4} \right) + \rho h \frac{\partial^2 w}{\partial t^2} = h B_y j_x - h B_x j_y \quad (2.10)$$

here D , h and ρ are bending rigidity, plate thickness and mass density, respectively.

Takagi and Tani [25] further improved the calculation method by introducing modal magnetic damping method, which can analysis eddy current and plate bending coupling effect separately. The equivalent magnetic viscous damping coefficient was obtained from the condition that dissipated energy due to magnetic damping is equal to joule heating caused by induced current. However the magnetic field they used is pulse signal and the plate is only 0.0003m thick with 0.04x0.115m, width and length.

Zhou and Zheng [26] established a series of governing equations for soft ferromagnetic thin plate structures' magnetoelastic interaction in complex magnetic fields. The theoretical model can describe the magnetoelastic instability and the increase of natural frequency of ferromagnetic plates in an in-plane magnetic field. The magnetic body force was formulated by $\mathbf{f} = \mathbf{M} \cdot \nabla \mathbf{B}$ due to the magnetization of the ferromagnetic materials.

By introducing the theoretical model and general expression of magnetic force that has been arisen from magnetoelastic interaction proposed by Zhou and Zheng [2.23], Wang and Lee [27] described the dynamic stability of a soft ferromagnetic beam-plate in a transverse magnetic field. The equations about magnetoelastic interaction and magnetic damping were derived. Taking into account of magnetic damping effect induced by eddy current, Lorentz volume force play a important role in the ferromagnetic beam-plate. They contributed the forces to two parts: equivalent magnetic force acting on the ferromagnetic plate and body force vector from Lorentz's force $\mathbf{f} = \mathbf{J} \times \mathbf{B}$.

CHAPTER 3

REVIEW OF ELECTROMAGNETICS

3.1 Maxwell's Equation

Maxwell's equations are the fundamentals of electromagnetics. The problem of electromagnets application in machining process, the multiple effects including vibration control in a macroscopic scale, and the magnetic field circulation can be obtained by solving Maxwell's equations subject to certain boundary conditions, stating the relationship between the fundamental electromagnetic quantities. For general Maxwell's four differential equations and one additional equation of continuity can be written as

$$\nabla \times \mathbf{H} = \mathbf{J} + \frac{\partial \mathbf{D}}{\partial t} \quad (3.1)$$

$$\nabla \times \mathbf{E} + \frac{\partial \mathbf{B}}{\partial t} = 0 \quad (3.2)$$

$$\nabla \cdot \mathbf{B} = 0 \quad (3.3)$$

$$\nabla \cdot \mathbf{D} = q \quad (3.4)$$

$$\nabla \cdot \mathbf{J} + \frac{\partial q}{\partial t} = 0 \quad (3.5)$$

where q is the charge density (C/m^3), \mathbf{J} is the current density (A/m^2), \mathbf{B} is the flux density, \mathbf{H} is the flux intensity and \mathbf{D} is the electric flux. These five equations are not all independent.

When studying the effect of magnetic forces on the deformation, stresses, motion, and stability of solid bodies, the full set of Maxwell's equations leads to hyperbolic

differential equations for the field variables with propagating wave solutions. Such wave-type solutions are important in the study of waveguides, antennas, and electromagnetic wave propagation and scattering problems. However, for those problems with much lower frequencies (less than 10^7 Hz), the wavelengths associated with such wave solutions are much longer than conventional structures of interest. By dropping the displacement current $\partial\mathbf{D}/\partial t$, the equations take on the characteristics of either a diffusion equation or elliptic equation. The neglect of $\partial\mathbf{D}/\partial t$ in ampere's law is also considered as the quasi-static approximation, which will be explained in the later part.

3.2 Electromagnetic Constitutive Relations

It is obvious that equations (3.1) to (3.5) are not sufficient to determine all the field parameters since there are more variables than equations. Additional equations are introduced which are called constitutive relations, describing the macroscopic properties of material.

$$\mathbf{D} = \varepsilon_0 \mathbf{E} + \mathbf{P} \quad (3.6)$$

$$\mathbf{B} = \mu_0 (\mathbf{H} + \mathbf{M}) \quad (3.7)$$

$$\mathbf{J} = \sigma \mathbf{E} \quad (3.8)$$

where ε_0 is the permittivity of vacuum, μ_0 is the permeability of vacuum, and σ is the conductivity; \mathbf{P} is the polarization density and \mathbf{M} is magnetization density.

3.2.1 Stationary media

For a stationary rigid body where \mathbf{E} and \mathbf{B} are considered to be independent, constitutive equations of the following form is prescribed in terms of two field vectors:

$$\mathbf{P} = \mathbf{P}(\mathbf{E}, \mathbf{B}) \quad (3.9)$$

$$\mathbf{M} = \mathbf{M}(\mathbf{E}, \mathbf{B}) \quad (3.10)$$

$$\mathbf{J} = \mathbf{J}(\mathbf{E}, \mathbf{B}) \quad (3.11)$$

In the classical linear theory of isotropic rigid, stationary, electromagnetic materials these equations take the form

$$\mathbf{D} = \varepsilon_0(1 + \eta)\mathbf{E} = \varepsilon\mathbf{E} \quad (3.12)$$

$$\mathbf{B} = \mu_0(1 + \chi)\mathbf{H} = \mu\mathbf{H} \quad (3.13)$$

$$\mathbf{J} = \sigma\mathbf{E} \quad (3.14)$$

where the constant η is called the electric susceptibility and χ is the magnetic susceptibility. These constants as well as electric conductivity σ can have a strong dependence on the temperature. At low temperature, as low as 0-20K, many materials become superconducting, that is $\sigma \rightarrow \infty$. In this state, steady closed currents can persist indefinitely. Thus voltage drops across superconducting circuits become zero for steady currents. However, for time-varying currents, an electric force is required to change the momentum of the electrons, which is proportional to \mathbf{J} . Thus Ohm's law is replaced by a relation with a parameter of λ in the form:

$$\mathbf{E} = \mu_0\lambda^2\dot{\mathbf{J}} \quad (3.15)$$

3.2.2 Moving Media

Faraday's law of induction explains the motion of a conductor in a steady magnetic field creating an electric field or voltage that can induce the flow of current in the conductor. And the electromotive force is proportional to the changing rate of the magnetic flux through the close loop. Thus the electric field in a moving frame of reference \mathbf{E}' relative to that in a stationary frame \mathbf{E} differs by a term proportional to the velocity and the magnetic field flux density. It is one of the principle interactions between mechanics and electromagnetics, and is expressed mathematically by the relation

$$\mathbf{E}' = \mathbf{E} + \mathbf{v} \times \mathbf{B} \quad (3.16)$$

Similar relations hold for other electromagnetic variables, but are not important in quasistatic magnetic problems as equation (3.13). These additional relations are list below:

$$\mathbf{D}' = \mathbf{D} + \mathbf{v} \times \frac{\mathbf{H}}{c^2} \quad (3.17)$$

$$\mathbf{P}' = \mathbf{P} + \mathbf{v} \times \mathbf{M} \quad (3.18)$$

$$\mathbf{H}' = \mathbf{H} - \mathbf{v} \times \mathbf{D} \quad (3.19)$$

$$\mathbf{B}' = \mathbf{B} - \mathbf{v} \times \frac{\mathbf{E}}{c^2} \quad (3.20)$$

$$\mathbf{M}' = \mathbf{M} - \mathbf{v} \times \mathbf{P} \quad (3.21)$$

$$\mathbf{J}' = \mathbf{J} - q\mathbf{v} \quad (3.22)$$

where $c^2 = 1/(\mu_0 \epsilon_0)$ is the square of the speed of light in vacuum. These equations are valid for velocities small compared with the speed of light.

3.3 Electromagnetic Boundary Conditions

Understanding the behavior of electromagnetic fields at the interface between different materials is very important in the study of structures in magnetic fields. Because drastic changes of field can occur at a boundary, deformation or movement of a surface provides a primary coupling between the magnetic field and the deformation of the structure.

Electromagnetic boundary conditions are best understood by applying the Maxwell's equations to an infinitesimal volume containing two media, with normal unit vector \mathbf{n}_2 directs from material 2 to material 1 in Fig. 3.1.

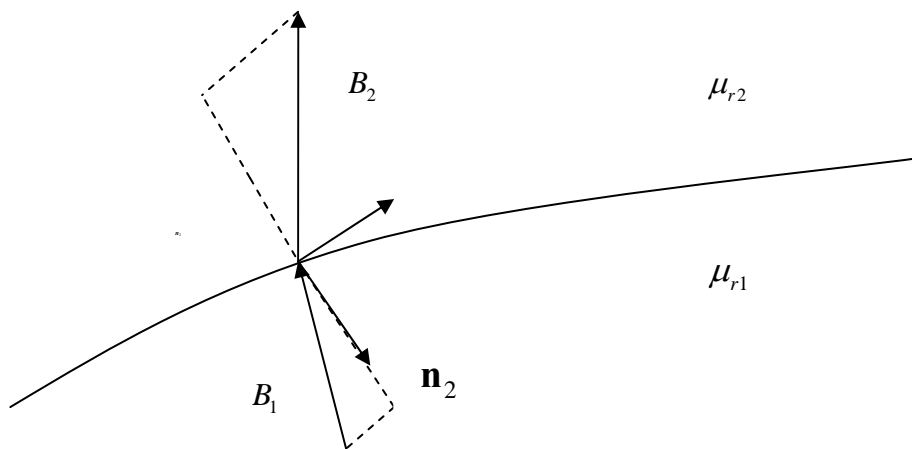


Fig. 3.1 Boundary between two materials with different permeabilities

The electric and magnetic fields are assumed to have different values and directions on either side of the interface. In addition, a surface charge density ρ_s (C/m^2) and surface current density \mathbf{J}_s (A/m) are flowing on the interface.

The associated boundary conditions are listed below:

$$\mathbf{n}_2 \times (\mathbf{E}_1 - \mathbf{E}_2) = 0 \quad (3.23)$$

$$\mathbf{n}_2 \times (\mathbf{D}_1 - \mathbf{D}_2) = \rho_s \quad (3.21)$$

$$\mathbf{n}_2 \times (\mathbf{H}_1 - \mathbf{H}_2) = \mathbf{J}_s \quad (3.22)$$

$$\mathbf{n}_2 \times (\mathbf{B}_1 - \mathbf{B}_2) = 0 \quad (3.23)$$

There are two of these conditions are independent, consisting of one of the first and the fourth equations and one of another two equations. After substituting a consequence about the interface condition for the current density is:

$$\mathbf{n}_2 \cdot (\mathbf{J}_1 - \mathbf{J}_2) = -\frac{\partial \rho_s}{\partial t} \quad (3.24)$$

3.4 Quasi-static Approximation

The equations used to determine the induction of eddy currents in conductors are a limiting form of Maxwell's equations. The quasi-static approximate theory neglects the electric displacement currents $\partial \mathbf{D} / \partial t$. This assumption is based on two arguments. First, examine the conservation of charge equation (3.5). For a linear material, one can write \mathbf{J} in terms of \mathbf{D} using Eqs. (3.6-3.8) and then use the relation between charge density and \mathbf{D} , $q = \nabla \cdot \mathbf{D}$, to obtain an equation for the charge density

$$\frac{\partial q}{\partial t} + \frac{\sigma}{\varepsilon} q = 0 \quad (3.25)$$

This equation has a solution proportional to $\exp[-(\sigma / \varepsilon)t]$, so that any net charge will decay exponentially in a characteristic time, $\tau = \varepsilon / \sigma$ (for aluminum $\tau < 10^{-18}$). Thus the almost-instantaneous decay of charge in good conductors leads one to write

$$\nabla \cdot \mathbf{J} = 0 \quad (3.26)$$

This suggests that the current density has a vector potential

$$\mathbf{J} = \nabla \times \mathbf{H} \quad (3.27)$$

which differs from Maxwell's equation by the absence of $\partial \mathbf{D} / \partial t$.

In the second argument, one writes Maxwell's equations for time harmonic field of frequency ω . The equation for the magnetic field \mathbf{B} in a linear isotropic conductor becomes

$$\nabla^2 \mathbf{B} = i\mu\sigma\omega \left(1 + \frac{i\omega\epsilon}{\sigma} \right) \mathbf{B} \quad (3.28)$$

It is clear that ω can be as high as 10^8 and the second term on the right hand will be very small. Under the assumption that $\omega\epsilon / \sigma \ll 1$, the non-harmonic form will become

$$\nabla^2 \mathbf{B} = \mu\sigma \frac{\partial \mathbf{B}}{\partial t} \quad (3.29)$$

This can also be derived directly from Maxwell's equations by dropping the displacement current $\partial \mathbf{D} / \partial t$.

The assumption of zero charge changes the form of Maxwell's equation from a wave equation to a diffusion equation. This has important mathematical consequences with regards to finding analytical or numerical solutions. The neglect of free volume charge density does not mean that net charge cannot reside in a good conductor; quite the contrary since a good conducting body in an electric field will experience regions of positive and negative charge density. And the charge will reside on the surface of the conductor.

3.5 Magnetically Induced Currents

3.5.1 Introduction

The problem for calculating the induced currents, forces, and temperature field resulting from the interaction of the pulsed or time-varying magnetic fields and electrically conducting solids can be cataloged into two groups [28]:

- (1) for which the deformation or motion of the solid does not appreciably affect the induced currents
- (2) those the interaction between the induced currents and deformation is strong enough to require the simultaneous solution of both current and deformation fields.

In the first set of problems, one treats the conducting solid as rigid when seeking the solution for the induced currents. These calculated currents and magnetic field are then used to find the magnetic forces and the resulting deformation or motion of the solid. Such problems are called hierarchically coupled.

3.5.2 Basic Equations for Eddy Current

A general expression of eddy current induced because of the conductor motion in a magnetic field is

$$\mathbf{J} = \sigma(\mathbf{E} + \mathbf{v} \times \mathbf{B}) + q\mathbf{v} \quad (3.30)$$

Thus a moving conductor with velocity \mathbf{v} and electric conductivity σ in a stationary magnetic field will have induced current even if the initial electric field $\mathbf{E}=\mathbf{0}$ or charge $q=0$. For most of practical problem, we have $q \cong 0$ in good

conductors. Also, in time-dependent field problems where currents are induced, $|\mathbf{E}| \sim |\mathbf{v}||\mathbf{B}|$, so that for velocities much less than the speed of light $\mathbf{B}' \cong \mathbf{B}$. Similarly, for non-polarizable materials, we have $\mathbf{P}' = 0$ and the magnetization $\mathbf{M}' = \mathbf{M}$ for $v^2/c^2 \ll 1$. Therefore, the electric field will be the only variable that differs significantly and the main concern of calculation.

The quasistatic equations of Faraday and Ampere are first-order linear partial differential equations in \mathbf{E} , \mathbf{B} , \mathbf{J} and \mathbf{H} . They are

$$\nabla \times \mathbf{E} + \frac{\partial \mathbf{B}}{\partial t} = 0 \quad (3.31)$$

$$\nabla \times \mathbf{H} - \mathbf{J} = 0 \quad (3.32)$$

These equations are often reduced to a second-order partial differential equation by using constitutive equations for $\mathbf{B}(\mathbf{H})$ and $\mathbf{J}(\mathbf{E}, \mathbf{B}, \mathbf{v})$. The classic treatment of the subject assumes a linear ferromagnetic material and Ohm's law for linear isotropic material,

$$\mathbf{B} = \mu \mathbf{H} \quad (3.33)$$

$$\mathbf{J} = \sigma (\mathbf{E} + \mathbf{v} \times \mathbf{B}) \quad (3.34)$$

While wave propagation is a distinctive feature of time-dependent electromagnetic fields in dielectric media or free space, in good electrical conductors, time-dependent magnetic fields exhibit diffusive behavior. The general equation for a moving conductor is given by

$$\frac{1}{\sigma \mu} \nabla^2 \mathbf{B} + \nabla \times (\mathbf{v} \times \mathbf{B}) = \frac{\partial \mathbf{B}}{\partial t} \quad (3.35)$$

When the velocity of the conductor is constant, $\nabla \mathbf{v} = 0$, the equations for \mathbf{B} take

the form

$$\frac{1}{\mu\sigma}\nabla^2\mathbf{B}=\left(\frac{\partial}{\partial t}+\mathbf{v}\cdot\nabla\right)\mathbf{B}\quad (3.36)$$

For a constrained rigid conductor, $\mathbf{v}=\mathbf{0}$ and the magnetic field and current density can be simplified as:

$$\nabla^2\mathbf{B}=\mu\sigma\frac{\partial\mathbf{B}}{\partial t}\quad (3.37)$$

$$\nabla^2\mathbf{J}=\mu\sigma\frac{\partial\mathbf{J}}{\partial t}\quad (3.38)$$

The basic set of equations consists of the quasistatic form of Maxwell's equations, which describe the evolution of the electric and magnetic fields, and a constitutive relation (Ohm's law) for the current density \mathbf{J} (\mathbf{E} , \mathbf{B} , \mathbf{v}). In ferromagnetic conductors one needs an additional constitutive relation \mathbf{B} (\mathbf{H}).

3.5.3 Anisotropic Media and Skin Depth

A more general relation is required in anisotropic media, such as in a superconducting fiber composite material operating in the normal regime; that is

$$\mathbf{J}=\boldsymbol{\sigma}\cdot(\mathbf{E}+\mathbf{v}\times\mathbf{B})\quad (3.39)$$

where $\boldsymbol{\sigma}$ is second-order tensors. According to the theory of second-order tensors, a set of orthogonal directions can be found in the material such that the above equation can be written in the form

$$\mathbf{J}=\sigma_1E_1\mathbf{e}_1+\sigma_2E_2\mathbf{e}_2+\sigma_3E_3\mathbf{e}_3\quad (3.40)$$

where \mathbf{e}_1 , \mathbf{e}_2 , and \mathbf{e}_3 are orthogonal unit vectors and σ_i are the principal conductivity coefficients in these directions. In Cartesian coordinates, each of the

components of \mathbf{B} , \mathbf{E} , or \mathbf{J} satisfies a diffusion equation.

For time harmonic problems with frequency ω , there is a common characteristic length or skin depth for all the fields $\delta = (2 / \mu \sigma \omega)^{1/2}$. For bodies whose smallest dimension $L \gg \delta$, all the time-varying fields and currents will be composed to a layer in the solid of the order of the skin depth. The conductor effectively shields the interior from the applied field by the induction of eddy currents whose own magnetic field opposes the applied field in the interior of the conductor. Values of the skin depth for various conductors and frequencies are show in Fig. 3.2.

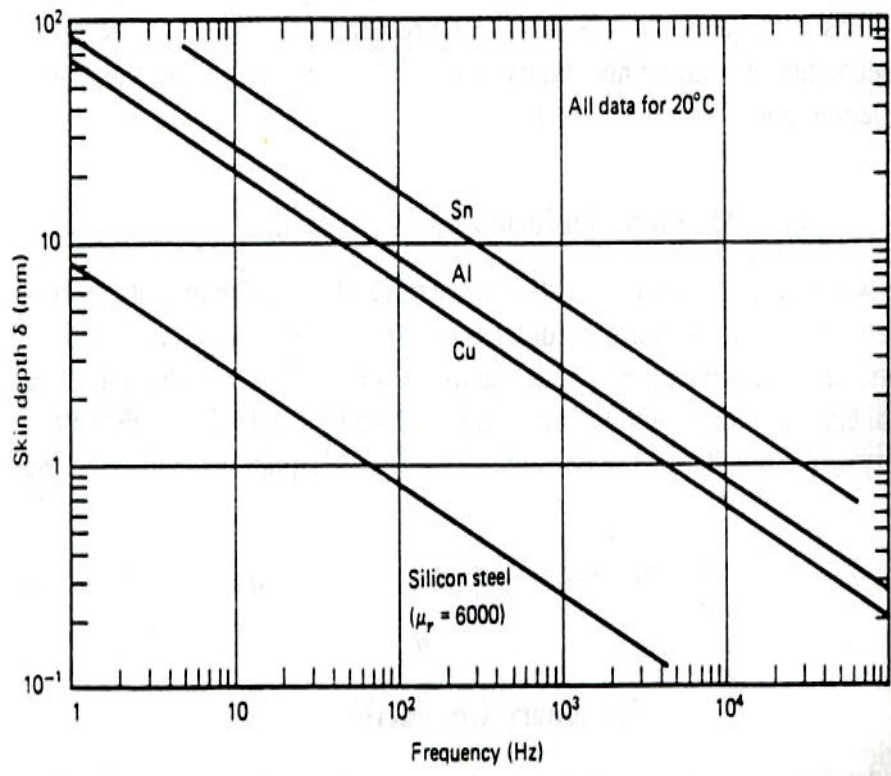


Fig. 3.2 Skin depth vs. frequency [28]

For transient applied fields, a time dependent skin depth is obtained

$$\delta_t = \left(\frac{4t}{\mu\sigma} \right)^{1/2} \quad (3.41)$$

which grows in time. If the thickness of a conducting plate is h , the time for a magnetic field to diffuse through the plate after a sudden change can be estimated

$$t_0 = \frac{1}{4} \mu\sigma h^2 \quad (3.42)$$

3.6 Potential methods for Magnetic Field

In order to better solve the differential Maxwell's Equations, potential methods is employed by involving a single partial equation for a vector potential function, which is suitable for two dimensional and three dimensional problems.

There are two vector potential methods for solving eddy-current problems. One is based on the conservation of flux by defining the magnetic vector potential \mathbf{A} :

$$\mathbf{B} = \nabla \times \mathbf{A} \quad (3.40)$$

and the other on the conservation of charge, in terms of electric vector potential $\boldsymbol{\psi}$,

$$\mathbf{J} = \nabla \times \boldsymbol{\psi} \quad (3.41)$$

Bring the potential into Faraday's law, the equation can be expressed as

$$\nabla \times \left(\mathbf{E} + \frac{\partial \mathbf{A}}{\partial t} \right) = 0 \quad (3.42)$$

This implies that the electric field can be expressed through a scalar potential ϕ ,

$$\mathbf{E} = -\frac{\partial \mathbf{A}}{\partial t} - \nabla \phi \quad (3.43)$$

Where ϕ is the scalar potential and $\nabla^2 \phi = 0$. To get a unique solution, the

magnetic vector potential \mathbf{A} is divergence-free,

$$\nabla \cdot \mathbf{A} = 0 \quad (3.44)$$

By assuming the linear ferromagnetic material, $\mathbf{B} = \mu\mathbf{H}$, the Ampere's law results in

$$\nabla^2 \mathbf{A} = -\mu\mathbf{J} \quad (3.45)$$

3.7 Ferromagnetism

The Curie temperature is a critical point to define the ferromagnetic material. The Curie point of a ferromagnetic material is the temperature at which it loses its characteristic ferromagnetic ability. At temperatures below the Curie point the material possess a spontaneous magnetization and the magnetic moments are partially aligned within magnetic domains. This is the result of complex quantum mechanical exchange interaction for which the magnetic energy keeps lower if the ionic magnetic moments are parallel and cooperatively aligned. As the temperature is increased from below the Curie point, thermal fluctuations increasingly destroy this alignment, until the net magnetization becomes zero at and above the Curie point. Above the Curie point, the material is purely paramagnetic.

At temperatures below the Curie point, an applied magnetic field has a paramagnetic effect on the magnetization, but the combination of paramagnetism with ferromagnetism leads to the magnetization following a hysteresis curve with the applied field strength.

3.7.1 Ferromagnetic Domains

The magnetization phenomenon can be explained in the microscale by the basic element of magnetic domain [29], in which the magnetic fields of atoms are grouped together and aligned. In an unmagnetized object, like an initial piece of metal all the magnetic domains are pointing in different directions. The magnetization vectors of the domains are arranged in such a way that their vectors sum is zero, so that there are closed magnetic flux paths within the material and no net observable magnetization.

Domains are spontaneously nucleated in all ferromagnetic materials in order to reduce the magnetostatic energy that would be associated with the leakage of magnetic flux in to the surrounding space. The presence of domain and behavior of the domain walls when subjected to applied fields is of fundamental importance in understanding the magnetic properties of ferromagnetic materials. When an external field is applied, the domains whose magnetization vectors are closest to the field direction grow at the expense of those which are less favorably oriented. Thus the process of magnetization is some of domains growth and displacement of domain walls, which are ultimately 'swept out' of the material.

3.7.2 Soft and Hard Ferromagnetic Materials

For nonferromagnetic isotropic materials we can relate \mathbf{M} and \mathbf{H} through a simple linear constitutive law with the magnetic susceptibility χ :

$$\mathbf{M} = \chi \mathbf{H} \quad (3.46)$$

For linear ferromagnetic materials, the relationship can also be expressed by Eq. (3.46) with the susceptibility $\chi \sim 10^4$ or higher. The principal metals in this category are iron, nickel, cobalt and their alloys.

The relation between \mathbf{M} and \mathbf{H} for general ferromagnetic material is not a single-valued function and depends on the history of \mathbf{H} . And the curve describing the relationship between magnetization \mathbf{M} and magnetic field \mathbf{H} is much similar to the hysteresis loop of \mathbf{B} vs. \mathbf{H} , as shown in Figure 3.3, in which B_r is the remnant field and H_c is the coercive field. In a magnetic material, \mathbf{B} and $\mu_0 \mathbf{H}$ differ by the magnetization \mathbf{M} , that is expressed as

$$\mathbf{B} = \mu_0 (\mathbf{H} + \mathbf{M}) \quad (3.47)$$

\mathbf{M} can be induced by external magnetic fields or in some materials can spontaneously exist in the absence of external fields.

During the magnetization process, the applied field moves the domain wall through the material against various microstructural and crystallographic obstacles. The magnitude of the field required to do this determines whether the material is classified as magnetically hard or soft. For soft ferromagnetic material, it is easily magnetized and would quickly become unmagnetized when its magnetic domains returned to a random order.

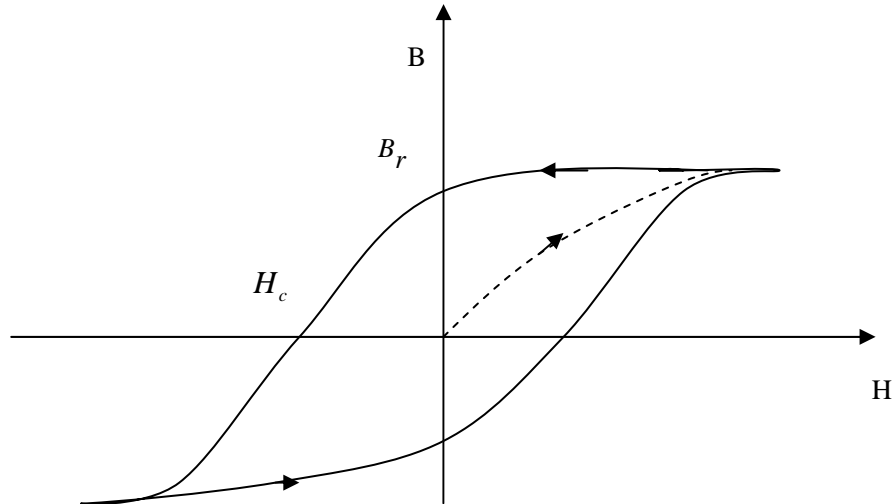


Fig 3.3 Hysteresis loop. (Dashed line: non-hysteretic material; solid lines for ferromaterials)

There are two idealized category of materials. For one, the hysteresis loop is small and one can write \mathbf{B} as a single-values function of \mathbf{H} such that $\mathbf{B}(\mathbf{H}) \rightarrow 0$ as $\mathbf{H} \rightarrow 0$. Such materials are defined as soft magnetic materials. A special case is the soft linear ferromagnetic material where

$$\mathbf{B} = \mu_0 \mu_r \mathbf{H} \quad (3.48)$$

Materials for which when B is close to B_r , as H reduced to zero, are called hard magnetic materials. The permanent magnetic materials are in this category.

3.8 Magnetic Force for Non-ferromagnetic and Ferromagnetic Material

When magnetization is not present in a conducting solid, the body force on an element with charge density q and current density \mathbf{J} is given

$$\mathbf{f} = q\mathbf{E} + \mathbf{J} \times \mathbf{B} \quad (3.49)$$

The current density \mathbf{J} depends on the motion velocity \mathbf{v} , and the electric and magnetic fields $\mathbf{J}' = \sigma \mathbf{E}'$. By the good conductor assumption, this relation becomes

$$\mathbf{J} = \sigma(\mathbf{E} + \mathbf{v} \times \mathbf{B}) \quad (3.50)$$

Also where the material is electrically anisotropic the electrical conductivity σ becomes a second-order tensor. The electric field \mathbf{E} can either be supplied by an external source, or induced in the conductor by a time varying magnetic field. The electric and magnetic fields relationship is by Faraday's law

$$\nabla \times \mathbf{E} + \frac{\partial \mathbf{B}}{\partial t} = 0 \quad (3.51)$$

We consider the conductor is a thin flat plate, where the current distribution across the plate thickness can be assumed to be uniform. Further we assume that the currents are either steady or quasi-steady. If a stability analysis of the plate were made, the effect of small out-of-plane deformations on the field would be made and bending stresses would become important. Since the current across the thickness h is uniform and we define

$$\mathbf{J} = \sigma \mathbf{E}. \quad (3.52)$$

For steady-state or low frequency currents we have a continuity condition

$$\nabla \cdot \mathbf{J} = 0 \quad (3.53)$$

The concomitant magnetic field to the current distribution is

$$\mathbf{B}_1(\mathbf{r}) = \frac{\mu_0}{4\pi} \int \frac{\mathbf{J}(\mathbf{r}') \times (\mathbf{r} - \mathbf{r}')}{|\mathbf{r} - \mathbf{r}'|^3} dV' \quad (3.54)$$

where \mathbf{J} is induced by time-varying field \mathbf{B}_0 .

The dynamic magnetic forces on nonferromagnetic conductors are calculated from the Lorentz forces $\mathbf{J} \times \mathbf{B}$ on the solid. However, if the solid can be magnetized, additional forces act on the solid. The distribution of the magnetization forces is not unique and depends on the chosen stress-strain-magnetization relation. The total force on the solid, however, is independent of the particular force model chosen and can be calculated from integration of the Maxwell stress vector on a surface S surrounding the magnetized body,

$$\mathbf{F} = \frac{1}{\mu_0} \int_S \mathbf{n} \cdot \left[\mathbf{B}\mathbf{B} - \frac{1}{2} B^2 \mathbf{I} \right] dA \quad (3.55)$$

where \mathbf{n} is the outward surface normal, \mathbf{I} the identity matrix, A the area.

3.9 Magnetic Field Distribution Case Study

One case study is explained here of a homogeneous, isotropic, nonmagnetic, conducting rod with circular cross section of radius a and infinite length in the cylindrical coordinate. The basic principle expected is that the motion of a conducting body in a magnetic field with no initial current is usually damped by the introduction of eddy currents. The total magnetic field can be written as a sum of the initial field \mathbf{B}_0 and the incremental field \mathbf{B}_1 due to deformation. The initial field inside and outside the rod is given [30] by

$$\mathbf{B}_0^- = \mu J_0 \frac{r}{2} \mathbf{e}_\theta \quad \mathbf{B}_0^+ = \frac{\mu_0 J_0 a^2}{2r} \mathbf{e}_\theta \quad (3.56)$$

where \mathbf{e}_θ is a unit vector in the azimuthal direction, J_0 the polar moment of inertia of the cross section of conductor, + means inside the rod and – the outside.

The perturbed magnetic field \mathbf{B}_1 satisfies Maxwell's equation where displacement currents have been neglected in terms of induced current density \mathbf{J}

$$\nabla \times \mathbf{B}_1^- = \mu_0 \mathbf{J} \quad (3.57)$$

Here we introduce the magnetic vector potential \mathbf{A} such that $\mathbf{B}_1^- = \nabla \times \mathbf{A}$. It follows from Maxwell's equation together with the gauge condition $\nabla \cdot \mathbf{A} = 0$, which \mathbf{A} must satisfy

$$\nabla^2 \mathbf{A} = -\mu_0 \mathbf{J} \quad (3.58)$$

Taking the curl of the vector potential \mathbf{A} we get the perturbed magnetic field distribution. For the inside region $0 < r \leq a$

$$B_{1r}^- = \left[i \left(k\alpha_1 - \frac{C_1'}{2} \right) I_1'(kr) + iC_1 I_2(kr) \right] e^{ikz} \cos \theta \quad (3.59)$$

$$B_{1\theta}^- = \left[-i \left(k\alpha_1 - \frac{C_1'}{2} \right) \frac{I_1(kr)}{kr} + iC_1 I_2(kr) \right] e^{ikz} \sin \theta \quad (3.60)$$

$$B_{1z}^- = - \left(k\alpha_1 + \frac{C_1}{2} \right) I_1(kr) e^{ikz} \cos \theta \quad (3.61)$$

where C_1 can be expressed in light of amplitude of displacement w_0 and modified first order I_1 , and wave number k , defined as $k = \pi / L$, L is the support length for coil :

$$C_1 = \frac{iJ_0 w_0 \mu_0}{I_1'(ka)} \quad (3.62)$$

And for the outside $a \leq r < \infty$,

$$B_{1r}^+ = ik\beta_1 K_1'(kr) e^{ikz} \cos \theta \quad (3.63)$$

$$B_{1\theta}^+ = -ik\beta_1 \frac{K_1(kr)}{kr} e^{ikz} \sin \theta \quad (3.64)$$

$$B_{1z}^+ = -k\beta_1 K_1(kr) e^{ikz} \cos \theta \quad (3.65)$$

where α_1, β_1 are constants to be determined from boundary conditions, K_1 is the modified second kind of first order

CHAPTER 4

MAGNETO-MECHANICAL PROBLEM

4.1 Introduction

When a structural component made of conductive material is placed in a transient magnetic field, its dynamic behaviour depends on both the mechanical and electromagnetic characteristics of the system. The electromagnetically induced motion of the structure due to the Lorentz force induces additional eddy current and further modifies the dynamic characteristics of the system.

One distinction between magneto-mechanical instabilities and conventional examples in the mechanical sciences is the fact that magnetic forces are of the body force type in comparison with surface loads such as end loads on columns. When the body deforms, the magnetic forces change, introducing a feedback loop between the structure and the circuit or source of the magnetic field. Of course, there also some uncoupled magneto-elastic problems where the deformation of the body does not measurably affect the magnitude or direction of the magnetic field. The body force on magnetized material can be represented by electromagnetic stresses acting on the surface of the body. These magnetic stresses are of the order of $\mu_0 M^2$, which for the best ferromagnetic material is around 10^2 N/cm^2 or less. Compared to the typical yield stress (greater than 10^4 N/cm^2) for ferromagnetic metals, the magnetic stress is insignificant unless it acts on a structure where small loads applied at one point produce large stresses elsewhere in the solid.

4.2 Fundamental of Magneto-Elasticity

If an electrically conducting elastic solid is subjected to a mechanical load while immersed in a varying magnetic field, the laws of Hooke and Maxwell will still determine the elastic field and the electro-magnetic field, respectively. The superposition of these two fields may however generate the new phenomenon of interaction between each other. It will be seen below that the electromagnetic field influences the elastic field by entering the elastic stress equations of motion as a body force of Lorentz's force, while the elastic field in its turn influences the electromagnetic field by modifying Ohm's law.

On one hand, Hook's law states that in an elastically isotropic solid the elastic stress tensor t_{ij} is linearly related to the elastic strain tensor e_{ij} according to the law

$$t_{ij} = 2\lambda e_{ij} + \gamma e \delta_{ij} \quad (4.1)$$

where λ and γ are Lamé's elastic constants and δ_{ij} is the Kronecher Delta and

defined as $\delta_{ij} = \begin{cases} 1 & i = j \\ 0 & i \neq j \end{cases}$. In terms of the elastic displacement w , another two

parameters are:

$$e_{ij} = \frac{1}{2}(w_{i,j} + w_{j,i}) \quad (4.2)$$

$$e = \nabla \cdot w \quad (4.3)$$

On the other hand, Maxwell equations which constitute the other part of magneto-elastic theory are

$$\nabla \times \mathbf{H} = \mathbf{J} + \frac{\partial \mathbf{D}}{\partial t} \quad \nabla \cdot \mathbf{B} = 0 \quad (4.4)$$

$$\nabla \times \mathbf{E} = -\frac{\partial \mathbf{B}}{\partial t} \quad \nabla \cdot \mathbf{D} = q \quad (4.5)$$

together with the relations

$$\mathbf{D} = \varepsilon \mathbf{E} \quad \mathbf{B} = \mu \mathbf{H} \quad (4.6)$$

here \mathbf{H} is the total magnetic field vector, including primary and induced parts, \mathbf{E} is electric field vector induced by the application of initial magnetic field and \mathbf{J} is the vector of the induced electric current density. The coefficients ε and μ are electric permittivity and magnetic permeability, respectively. q is the electric charge density. It is to be noted that the elastic field described by equations (4.1) and (4.2), and electromagnetic field determined by equations (4.4-4.6) do not contain directly any interaction term.

Now by taking into account of the interactive effect of magnetic field and mechanical deflection, the equation of motion for an electrically conducting elastic solid can be written as [31]

$$\rho \frac{\partial^2 w_i}{\partial t^2} = \frac{\partial t_{ik}}{\partial x_k} + (\mathbf{J} \times \mathbf{B})_i + q\mathbf{E} + \mathbf{F} \quad (4.7)$$

where ρ is the mass per unit volume of the elastic solid and \mathbf{F} is the body force per unit mass. The fact that the current density \mathbf{J} induced by the magnetic field \mathbf{B} retards the motion of the conductor, is expressed by the second term on the right-hand side of (4.7); the third term represents the force due to the existence of the charge density q in the electric field \mathbf{E} . It is thus seen that the occurrence of these two electric terms in the stress equation of motion causes an interaction with the elastic field. In a moving conductor the current is determined by the Ohm's law as

$$\mathbf{J} = \sigma \left(\mathbf{E} + \frac{\partial \mathbf{w}}{\partial t} \times \mathbf{B} \right) + q \frac{\partial \mathbf{w}}{\partial t} \quad (4.8)$$

where σ is the electrical conductivity. Here the w -dependent terms show that the current distribution is modified by the elastic deformations. Thus the interaction between the elastic field and the electromagnetic field is expressed through equations (4.7) and (4.8).

Equations from (4.1-4.8) form the basis of the magneto-elasticity and are to be solved with prescribed initial and boundary conditions which are both mechanical and magnetic. The differential equations (4.1-4.6) are all linear. Non-linearity enters into the theory through the interaction terms in (4.7) and (4.8). If the induced magnetic field is small, as is usually the case, in comparison with the applied primary field \mathbf{H}_0 we can put $\mathbf{H} = \mathbf{H}_0 + \mathbf{h}$ where squares and higher powers of \mathbf{h} as well as the products of \mathbf{h} and \mathbf{w} and be neglected. In this way the nonlinear terms in equations (4.7) and (4.8) can be linearised. Mathematical simplifications in solving special problems may also be obtained by neglecting the displacement current \mathbf{D} and the charge density q . The assumption of a perfect conductor simplifies the problems still further.

The stresses t_{ij} in equation (4.1) are due to the elastic deformations of the medium and are called Hooke's mechanical stresses. The application of the electromagnetic field also produces stresses in the medium and the corresponding stress tensor \bar{t}_{ij} is called Maxwell's electromagnetic stress. It is given in terms of electric and magnetic field by [31]

$$\bar{t}_{ij} = \varepsilon \left[E_i E_j - \frac{1}{2} E_k E_k \delta_{ij} \right] + \frac{1}{\mu} \left[B_i B_j - \frac{1}{2} B_k B_k \delta_{ij} \right] \quad (4.9)$$

The total stress T_{ij} is the sum of these two types of stresses, $T_{ij} = t_{ij} + \bar{t}_{ij}$. It is to be remembered that unlike Hooke's stresses, the Maxwell stresses can exist in vacuum; consequently in solving boundary value problems of magneto-elasticity, Maxwell stresses in vacuum are also to be taken into account.

4.3 Magneto-Elastic Conducting Plate Model

One example was developed by Pao and Yeh [32] using the static theory for a ferromagnetic plate in a static magnetic field. The resulting equation for bending of classic thin plate was found to be

$$D \left(\frac{\partial^4 w}{\partial x^4} + 2 \frac{\partial^4 w}{\partial x^2 \partial y^2} + \frac{\partial^4 w}{\partial y^4} \right) + \frac{[(\mathbf{B} \cdot \mathbf{n})^2]}{2\mu_0} = 0 \quad (4.10)$$

where w is the lateral plate deflection and the brackets $[]$ are defined by $[f] = f(\text{top}) - f(\text{bottom})$. D is the bending stiffness given in terms of the plate thickness h and the elastic constants E . In this model the effect of the body forces are replaced by magnetic tension on the top and bottom surfaces of the plate.

When the conductor is in the form of a conducting plate, we can also integrate the magnetic forces through the thickness. The equation of motion for the lateral motion of the plate w is given [28] by

$$D \nabla_1^4 w + \rho h \frac{\partial^2 w}{\partial t^2} = F + \mathbf{n} \cdot \nabla \times \mathbf{c} \quad (4.11)$$

where for nonferro-magnetic materials,

$$F = \int \mathbf{n} \cdot (\mathbf{J} \times \mathbf{B}) dz \quad (4.12)$$

$$\mathbf{c} = \int z \mathbf{n} \times (\mathbf{J} \times \mathbf{B}) dz \quad (4.13)$$

Here \mathbf{n} is the unit vector normal to the plate surface and D is the plate stiffness constant expressed in terms of Young's modulus E , the height h and the Poisson's ratio ν given by

$$D = \frac{Eh^3}{12(1-\nu)} \quad (4.14)$$

and the Laplacian $\nabla_1^2 = \left(\frac{\partial^2}{\partial x^2} \right) + \left(\frac{\partial^2}{\partial y^2} \right)$. The average membrane stresses in the plate must satisfy

$$\nabla \cdot \mathbf{t} + \int (\mathbf{J} \times \mathbf{B}) \cdot (\mathbf{I} - \mathbf{nn}) dz = \rho h \frac{\partial^2 \mathbf{u}}{\partial t^2} \quad (4.15)$$

Where \mathbf{I} is the identity matrix, \mathbf{t} is the stress tensor and \mathbf{u} is the average in-plane displacement vector.

The in-plane stresses t_{ij} satisfy the equations

$$\frac{\partial t_{xx}}{\partial x} + \frac{\partial t_{xy}}{\partial y} + J_y (B_z^0 + B_z^1) = \rho \frac{\partial^2 u_x}{\partial t^2} \quad (4.16)$$

$$\frac{\partial t_{xy}}{\partial x} + \frac{\partial t_{yy}}{\partial y} + J_x (B_z^0 + B_z^1) = \rho \frac{\partial^2 u_y}{\partial t^2} \quad (4.17)$$

where x, y are in the plane, and z has origin at plane mid-surface, u presents the displacement.

4.4 A Plate Theory for Ferro-Elastic Materials

Considering a two dimensional plate in which the stress in the x_2 direction and assuming $\partial/\partial y = 0$, as shown in Fig. 4.1, the field equations of stress take the form[28]

$$\frac{\partial t_{11}}{\partial x_1} + \frac{\partial t_{21}}{\partial x_2} + \frac{\chi}{\mu_r^2} \frac{\partial P_m}{\partial x_1} = 0 \quad (4.18)$$

$$\frac{\partial t_{12}}{\partial x_1} + \frac{\partial t_{22}}{\partial x_2} + \frac{\chi}{\mu_r^2} \frac{\partial P_m}{\partial x_2} = 0 \quad (4.19)$$

$$t_{12} = t_{21} \quad (4.20)$$

with the stress t_{ij} , the magnetic pressure P_m . The boundary conditions on the top and bottom surfaces of the plate become

$$t_{12} = 0 \quad (4.21)$$

$$t_{22} = \frac{\chi^2}{\mu_r^2} \frac{B_2^2}{2\mu_0} \quad (4.22)$$

where only magnetic forces are assumed to be acting.

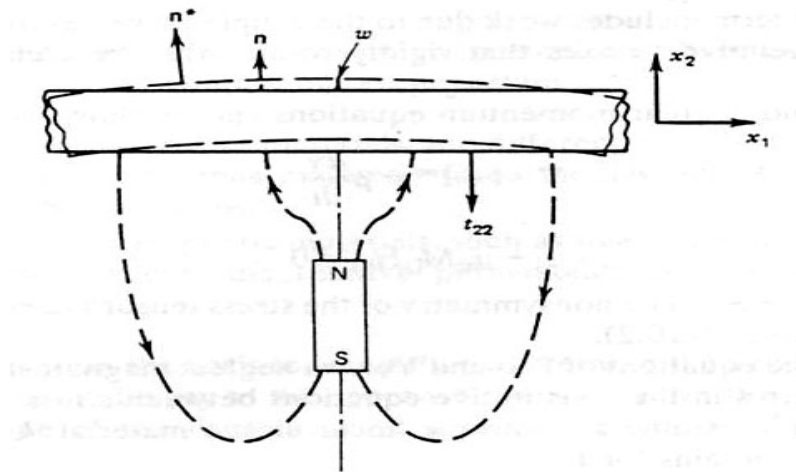


Fig. 4.1 Deformation of two dimensional plate with magnetic field

4.5 System Dynamics in the Feed Direction

To simplify the problem, the tool holder-cutting insert combination is modeled as a two dimensional cantilever beam with external forces acting on the end. The external forces include the cutting force, thrust force, friction force, and interaction between the tool flank and workpiece. The relationship between tool wear and displacement of the tool system is developed and discussed.

Model Development is shown in Fig. 4.2. By considering the one dimensional beam model for bending vibration in the z (feed) direction, the governing equation can be written as [27]:

$$EI \frac{\partial^4 z(x,t)}{\partial x^4} + \rho A \frac{\partial^2 z(x,t)}{\partial t^2} = 0 \quad (0 < x < L) \quad (4.23)$$

where E is Young's modulus, I is the moment of inertia, t is time, A is the transverse area and L is the length of the cantilever beam. The boundary conditions are described as:

1. At the clamped end, $x=0$

$$z(x,t) \Big|_{x=0} = 0 \quad \frac{\partial z(x,t)}{\partial x} \Big|_{x=0} = 0 \quad (4.24)$$

2. At the free end, the boundary conditions are

$$\frac{d^2 z(x,t)}{dx^2} \Big|_{x=L} = 0 \quad EI \frac{d^3 z(x,t)}{dx^3} \Big|_{x=L} = F_t(t) + F_i(t) \quad (4.25)$$

where $F_{t(t)} = k_{zq} [z(L,t) - z(L,t - \tau) + h_c]$ is the thrust force,

$F_i(t) = K_i z_i(t) + C_i \dot{z}_i(t)$ is the interactive force,

in which K_i and C_i are the stiffness and damping coefficients, respectively, associated with the contact surface.

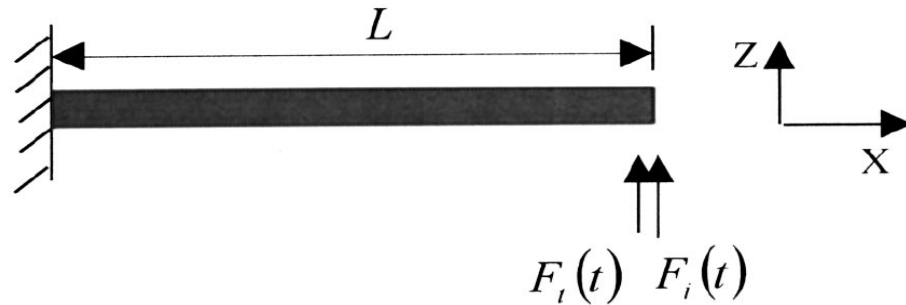


Figure 4.2 Cantilever beam model in the feed direction

We can obtain the equation for static deflection of a beam by suppressing the time dependence in Eq. (1). For this case the displacement $z(x)$ expression can be simplified as

$$EI \frac{\partial^4 z(x,t)}{\partial x^4} = 0 \quad (4.26)$$

with the same boundary condition. The displacement of this equation can be derived as

$$z = \frac{Fl^3}{3EI} \left[\frac{x^2}{l^2} \left(\frac{3}{2} - \frac{x}{2l} \right) \right] \quad (4.27)$$

And the deformation and angle at the right end, where the force is applied, are

$$z|_{x=l} = \frac{Fl^3}{3EI} \quad \theta = \frac{Fl^2}{2EI} \quad (4.28)$$

4.6 System Dynamics in the Cutting Direction

The more important part of cutting is the cutting direction motion, expressed in Fig. 4.3, which is dominated by friction force $F_{f(t)}$ and cutting force $F_{c(t)}$, and the corresponding governing equation is [27]

$$EI \frac{\partial^4 y(x,t)}{\partial x^4} + \rho A \frac{\partial^2 y(x,t)}{\partial t^2} = 0 \quad (0 < x < L) \quad (4.29)$$

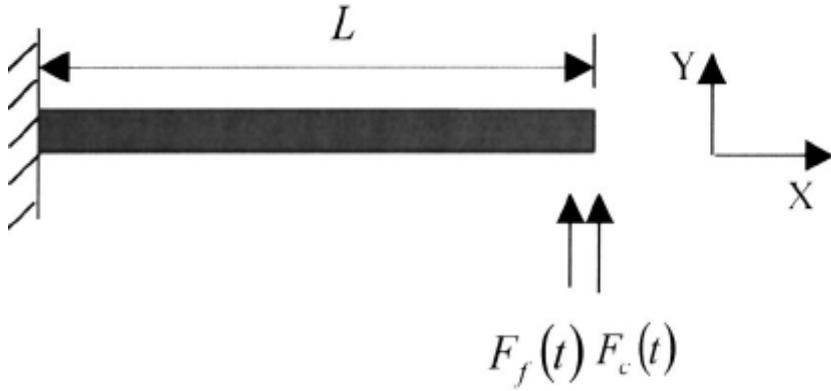


Figure 4.3 Cantilever beam model in the cutting direction

1. At the clamped end, $x=0$

$$y(0,t) = 0 \quad \left. \frac{\partial y(x,t)}{\partial x} \right|_{x=0} = 0 \quad (4.30)$$

2. At the free end, the boundary conditions are

$$\left. \frac{d^2 y(x,t)}{dx^2} \right|_{x=L} = 0 \quad EI \left. \frac{d^3 y(x,t)}{dx^3} \right|_{x=L} = F_c(t) + F_f(t) \quad (4.31)$$

where $F_{c(t)} = k_{yq} [z(L,t) - z(L,t - \tau) + h_c]$,

$$F_f(t) = \mu_d [F_i(t) + F_t(t)] = \mu_d \left\{ K_{zq} [z(L, t) - Z(L, t - \tau) + h_c] + F_i(t) \right\} ,$$

and μ_d is the dynamic friction coefficient, k_{zq} and k_{yq} are the directional gain in the thrust and cutting direction, respectively.

CHAPTER 5

EXPERIMENTAL SETUP

In this chapter, the experimental data on the performance of the electromagnetic effect is determined and compared with the computer models to be explained later. The performance data of the electromagnetic effect were based on two machining process, turning and milling. Even though the distribution of magnetic field in both processes is different, both the reduction of the tool wear rates in each case greatly supports the electromagnetic damping effect in metal machining process.

5.1 Experimental Setup for Turning Process

The turning machining was implemented on Okuma LH35-N lathe machine, as shown in Fig. 5.1. The cutting tool insert is (TiAl)N-coated cemented carbide against the mild steel ASSAB 760 workpiece. The tool inserts used were (TiAl)N-coated cemented carbide inserts from Sandvik Coromant and the series number is CNMG 12 04 08-QM 1005. The tool inserts are mounted on a tool holder. The tool holder is also from Sandvik, of which the series is DCLNR 2525M 12. The shafts are ordered in a single batch to ensure homogeneity in their material properties.



Fig. 5.1 Computer controlled turning machine

Besides the basic turning machine system, additional instruments have been set up to measure the tool wear, surface finish and magnetic field and record the cutting forces in three mutually perpendicular directions: radial, axial and tangential directions, respectively. All the measuring instruments are listed in Table 5-1 and the basic setup is shown in Fig. 5.2. To ensure the comparability of the experimental results and reduce the impact of inhomogeneous property of workpiece, a new workpiece and tool insert were used for each specific cutting condition.

Table 5-1 Experimental Instruments

Experimental Measuring Instrument For Turning

Kistler Type 9121.2 Piezoelectric Force Dynamometer

Kistler Multi Channel Charge Amplifier 5019A

Sony Instrumental Cassette Recorder, Type PC 208A

Taylor Hobson Surface Finish Instrumentation

Magna Gauss Meter

MT.16 Toolmakers Microscope

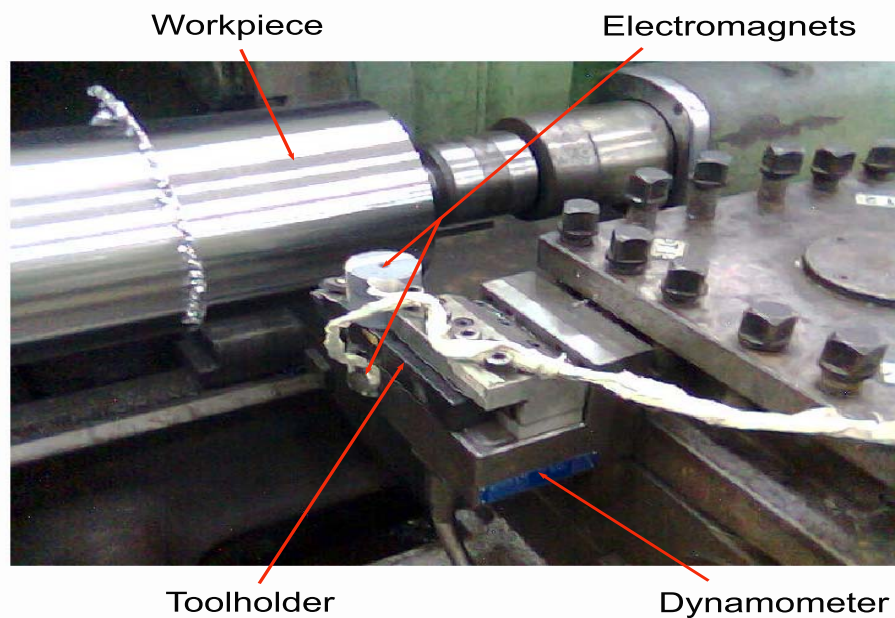


Fig. 5.2 Turning Experimental Setup including electromagnets and dynamometer

The following parameters were maintained throughout the experiments, including cutting speed, feed rate and depth of cut for the purpose of optimizing the cutting time and tool insert wear for comparability. Table 5-2 presents the workpiece properties in details. The cutting conditions are present in table 5-3 and it also contains the geometry and material of workpiece and basic information of cutting tool.

Table 5-2 Turning workpiece properties

Composition (%)	C 0.50 Fe 98.5 Si 0.30 Mn 0.70
Subcategory	Carbon steel Ferrous Metal
Yield Stress MPa	340
Tensile Strength kg/mm ²	58
Elongation at break %	20
Reduction of Area %	40
Hardness HB	210
Density kg/m ³	7.5×10^3
Modulus of Elasticity GPa	195

Table 5-3 Cutting conditions in turning case

Cutting speed	200 m/min
Feed	0.2 mm/rev
Cutting depth	1 mm
Workpiece	
Initial diameter	200 mm
Finishing diameter	160 mm
Material	ASSAB 760
Cutting tool	GC 1005
Grade	TiN-coated cemented carbide (AC 3000 series)
Composition	Co 10.2
Volume%	WC 89.3
	TaC 0.2
	NbC 0.3
Density g/cm ³	14.9
Hardness HV3	1750
Hc kA/m	22.0
Coating	TiAlN 4
Cutting time	120 mins

The introducing of magnetic field is mainly on the tool holder, of which two same electromagnets were placed on the top and bottom. The two electromagnetic are coaxial and the distance from the center to the tool insert tip at the free end of the tool holder is 50mm, as can be seen in Fig. 5.3.

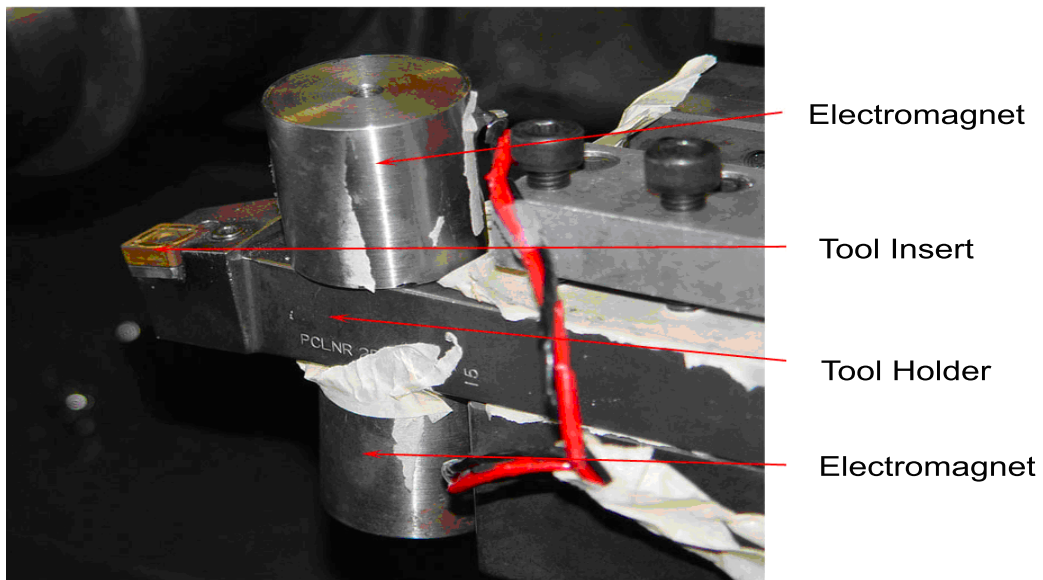


Fig. 5.3 The application of the electromagnets on the tool holder with the inserts

5.2 Experimental setup of Milling Process

Besides the series of turning machine system, another machining system was also involved to exam the performance of electromagnetic field on the cutting process. The end milling machine is shown in Fig.5.4, which is ACM 55 produced by Makino company.



Fig. 5.4 Makino Milling Machine

The cutting pair is disposable tool insert against tool steel material. There are over all 8 pieces of workpieces were milled, depending on different cutting condition with different power supply on the electromagnets. Although the tool holder can hold up to a maximum of 4 tool inserts, in order to compare the tool wear with in a reasonable cutting time and maximize the amount of tool wear, only 1 Tool Insert, Sumitomo AC 325 was used with one workpiece, as shown in Fig. 5.5 and Fig. 5.6. The properties of the tool insert are present in Table 5-4.



Figure 5.5 Fresh insert

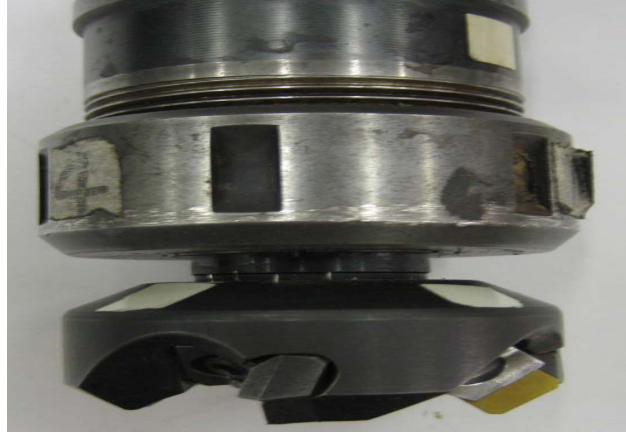


Figure 5.6 Insert attached to holder in Milling

Table 5-4 Material properties for Tool Insert

Manufacture	Sumitomo
Tool Grade	AC 325
Components	Tungsten carbide 94% Cobalt 6%
Insert Coating	Titanium Aluminum Nitride (TiAl)N
Coating Process	Physical deposition process (PVD)
Hardness	68.1 HRC
Tensile Strength	2200 N/mm ²

ASSAB 718 (tool steel) was used for the workpieces throughout the entire experiment and the material properties details are in Table 5-5. This material was chosen because of its industry relevance, as it is used in many applications in the manufacture of moulds, extrusion dies and various structural components. Its high purity and good

homogeneity results in uniform hardness of the work pieces also assist in the consistency of experimental results. To further ensure consistency, 8 blocks of ASSAB718, dimensions 210x44x106mm was ordered from the same manufacturing batch from the supplier. All the consideration is to minimize the effect of inhomogeneous, anisotropic material properties and make sure the ASSAB718 is as uniform as possible throughout the 8 blocks of material used for the experiment.

Table 5-5 Material properties for ASSAB 718

ASSAB 718	Fe 95 %
Components	C 0.33%
	Cr 1.8%
	Mn 1.4%
Density	7800 kg/m ³
Impact Strength / Toughness (Charpy Test)	11.9 Joule
Tensile Strength	1010 N/mm ²
Yield Strength	800 N/mm ²
Hardness	52 HRC
Magnetic Permeability, μ	2.5×10^{-3} H/m
Relative Permeability, μ_r	2000

The recording and measurement equipments are kind of similar to those used in turning test. Kistler Charge Amplifier 5019A was used to amplify the online voltage signal sensing through a force dynamometer and the signal was also recorded simultaneously by Sony PC 208A Instrumental Cassette Recorder. During the milling process, surface finish was measured by Surtronic 10, Taylor Hobson Surface Finish Instrumentation all around the finishing surface and averaged to get mean values after each 5 passes. Before and after the electromagnets switch on, as well as after each machining time, the magnetic field flux density was measured using Magna Gauss Meter on the top and side face of the workpiece. It is also necessary to exam the hysteresis phenomenon of the workpiece material to make sure the application of magnetic field will not affect the normal property and further function of the machining material. All the magnetic field details are essential to validate the later computer simulation of magnetic effect in milling process.

To design the experimental mill machining, not only the proper industry standard, but also the time limit as well as the wear type and attrition rate should be taken into account. The milling conditions, adjusted according to the complex situation, are listed in Table 5-6. Under these cutting conditions the dominating wear through the machining is flank wear, which we gauged by looking through a MT.16 Toolmakers Microscope.

Table 5-6 Milling Machining Conditions

Feed Rate of Machine	210.0 mm / min
Spindle speed of machine	800 rpm $w=83.78$
Depth of cut per pass	1.0 mm / pass

Different from the turning case, the electromagnet field was applied on the workpiece rather than on the tool or tool holder, because it is difficult to fix the electromagnet on the rotating tool holder. In Fig. 5.7, the electromagnets are connected to the power supply such that they can work and stick to the lateral surface base. The milling program was stopped until 35 passes has been completed for each milling conditions with the variation of magnetic field.



Figure 5.7 Electromagnets setup on workpiece in milling

5.3 Electromagnets Details

Rather than the hulky coil winding, two simple cylindrical DC electromagnets were employed and the strength of the magnetic field was controlled by the power supply. The geometry of electromagnet is listed in Table 5-7. In turning setup, these two electromagnets lay coaxially on the top and at the bottom of the tool holder, as shown below in Fig. 5.3. The low electromagnetic strength and the distance gave the extremely low magnet intensity in the vicinity of contact region, compared to the effective magnetic field strength applied by former researchers. The magnetic intensity in the vicinity of the insert tip is around 100G under 20V DC voltage supply.

Table 5-7 Electromagnet parameters

Diameter	40 mm
Height	40 mm
Power supply	10 V/ 15V/ 20V
Maximum flux density on the surface	8.92e-2 T

On the contrary, the electromagnets were attached near the base of the workpiece, rather than on the tool insert in turning case, so as to not obstruct the milling process carrying out at the top of the workpiece, because the height of the workpiece decreases gradually. The electromagnets are placed along the longitudinal ends of the workpiece to allow more even magnetic field distribution along the surface of the workpiece. To attach the electromagnets securely onto the workpiece, adhesive tape was used, as can be seen in Figure 5.7.

To get a better understanding is a base for better understanding of how the application of magnetic fields improving tool life. The diameter and height of the electromagnet are both 4 cm. The transverse cross section and surface flux densities of electromagnet under 10V, 15V and 20V voltages are shown in Fig. 1.8. The center core of the electromagnet acts as the north pole (positive) and the thin outer shell can be considered as the south pole (negative). For N-N setup, the magnetic fields radiated out of the central cores both from the left and right electromagnets, and vice versa.

5.4 Procedure of Experiments

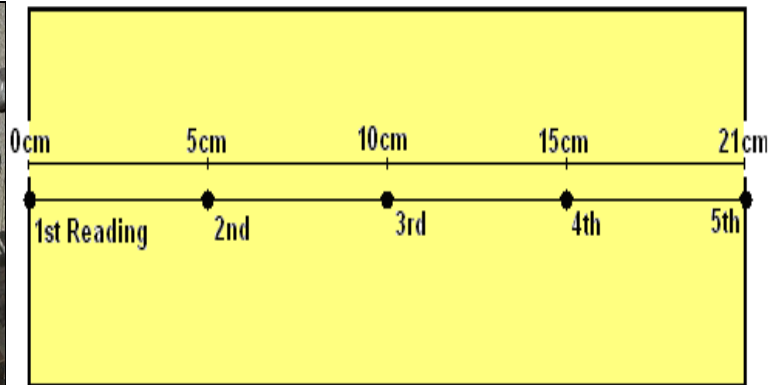
In order to examine the relationship between magnetic field and tool wear, two electromagnets were introduced into both turning and milling machining processes. In turning case, the workpiece was first cut under a defined set of cutting conditions as we mentioned in Table 5-2, without application of magnetic fields. This cutting process is then repeated with the application of magnetic field by electromagnets. In the second part of experiments, both electromagnets were set up in such a way that a north poles were generated from the core of the electromagnets. The electromagnets are then arranged in a North-North Magnetic Field Orientation, where the magnetic field is repelling against each other. In the third part of the experiments, the electromagnets are arranged in a North-South Magnetic Field Orientation. In milling, the basic steps were almost the same except for the position of the electromagnets.

5.5 Measurement of Magnetic Field

In milling case, referring to Figures 5.8 and 5.9, seven magnetic field readings were taken along the longitudinal direction. The first set of readings was taken after the workpiece is first secured onto the machine surface and the second set when the electromagnets were placed onto the workpiece and are switched on. The subsequent sets of readings were taken after every 5 milling passes where a material depth of 5mm has been removed from the workpiece. The last set of readings was taken at the completion of the milling process after the electromagnets are switched off for 30 minutes. This is to measure the presence of any residue magnetism induced onto the workpiece. And the data values are shown in Appendix B.



Figure 5.8 Top Surface



Top view of workpiece

Figure 5.9 Measured magnetic field flux density points

CHAPTER 6

EXPERIMENT ANALYSIS AND NUMERICAL SIMULATION FOR TURNING

6.1 Effect of Magnetic Field on Wear

A series of cutting experiments were performed to evaluate the tool wear reduction under different voltage applied to the electromagnets. Seven shafts (ASSAB 760) were ordered from the same stock for evaluating the tool wear for each setup, that is, one with no magnetic field applied, one for N-N configuration with 10V applied to the electromagnets, and so on. Figure 6.1 and 6.2 show the resulted tool wears measured offline. The flank wear on the clearance face was measured for every 10 minutes cutting time and the overall cutting time for each single operation was 120 minutes. These figures emphasize the effectiveness of the electromagnetic damping effect in attenuating the vibration of the flexible beam. As can be seen in these figures, the flank wear did decrease with the increase of power supply by 8% to 28%. The higher the flux density, the greater is the reduction in tool wear.

As shown in chapter one, the magnetic field is more concentrated in the center pole. We define the N-N and N-S electromagnets setup here. When the middle core of the electromagnet acts as the North pole and the thin shell can be considered as the South pole. For N-N setup, the magnetic fields radiated out of the central cores both from the top and bottom ones, and vice versa.

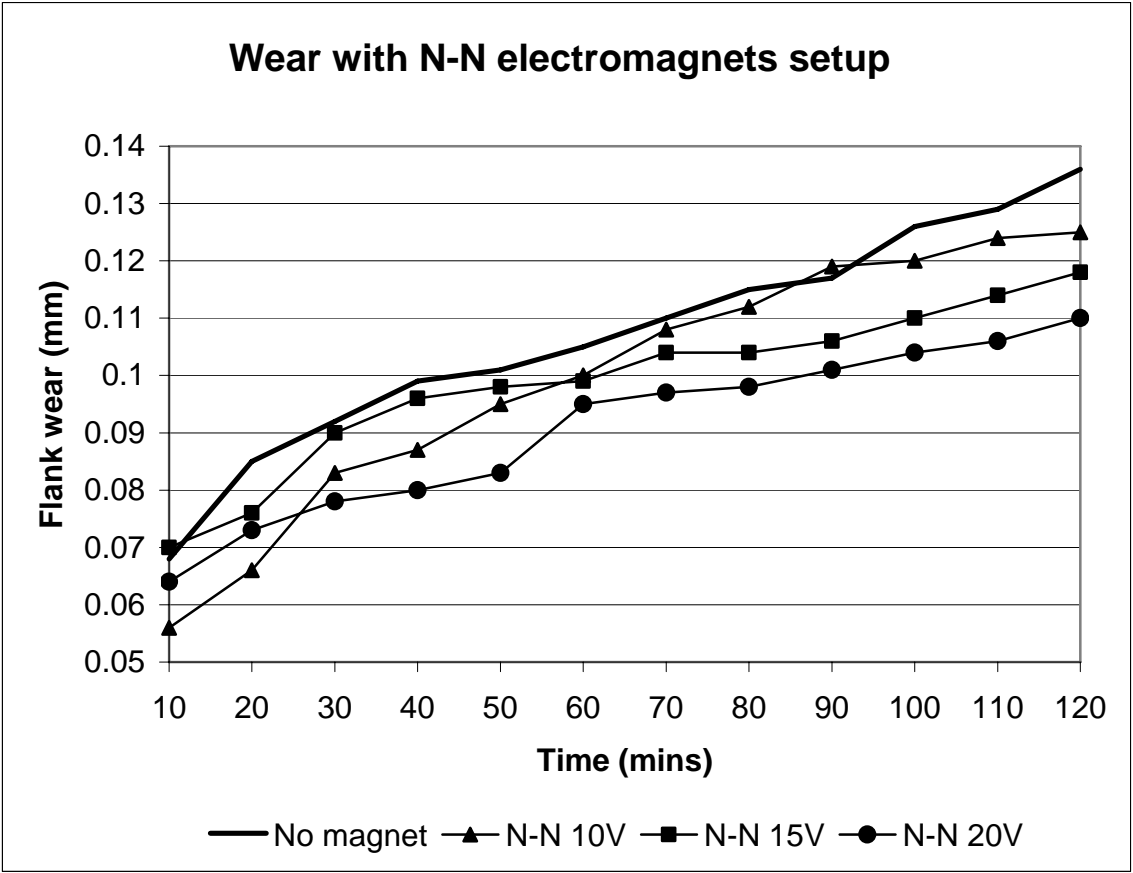


Fig. 6.1 Tool wears with and without electromagnets under the N-N setup

The presented results demonstrate clearly the effectiveness of the electromagnetic effect in damping out the structural vibrations of the tool holder. However, the N-S configuration is more effective than N-N configuration in reducing the tool wear rate. In Fig. 6.1, by changing the voltages applied on each North-centered electromagnet, the wear decreased by 8%, 13%, and 19% after 120mins machining time, respectively. Even though several deviations in the processes, the final wear decreases are proportional to the power supplies.

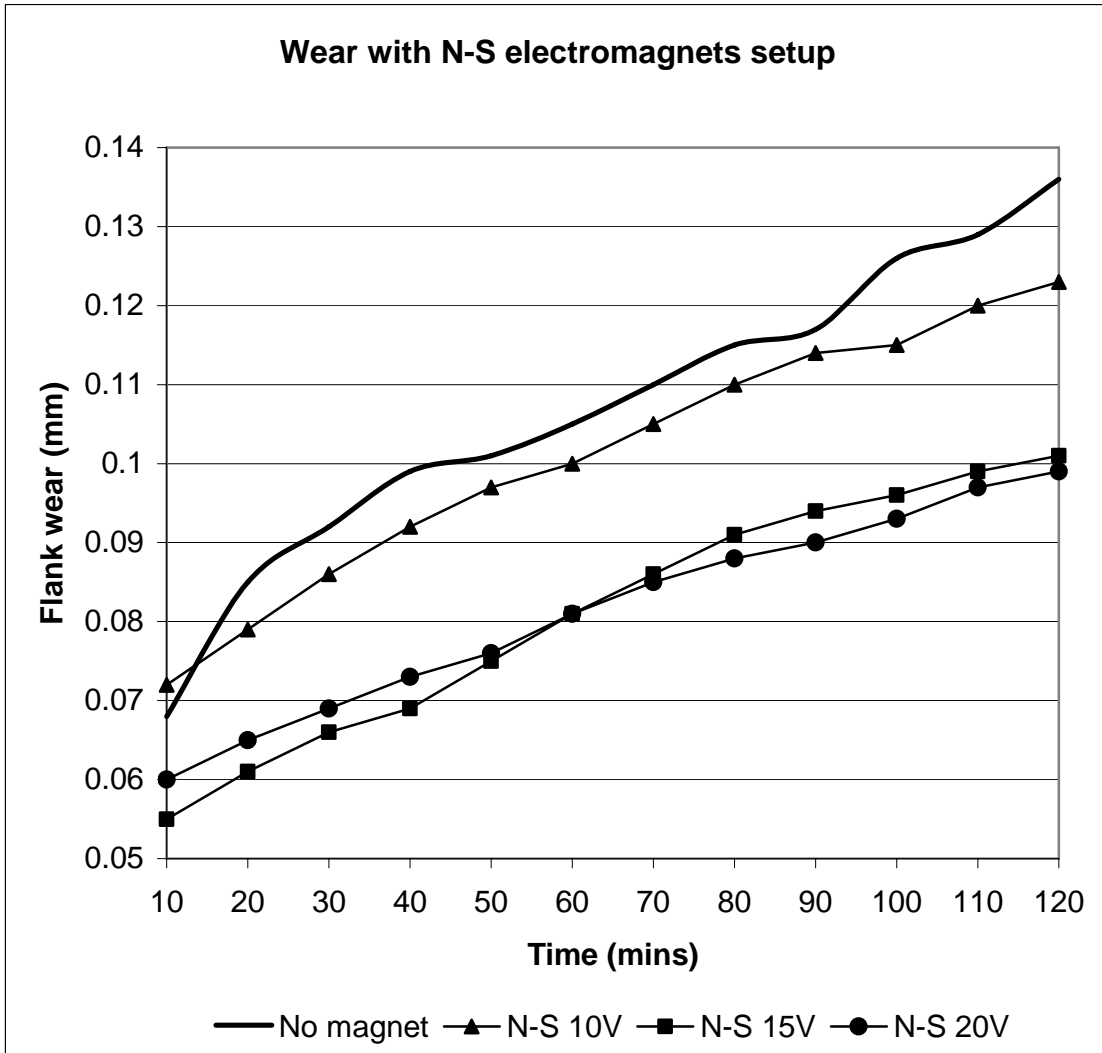


Fig. 6.2 Tool wears with and without electromagnets under the N-S setup

By contrast, the N-S setup in Fig. 6.2 indicated more effective magnetic influence on the tool wear with the reductions of 9.5%, 25.7%, and 27.2%. And as the same trend of N-N setup, the higher voltage supply corresponds to more tool wear reduction.

6.2 Variation of Force Due to Magnetization

Besides the tool wear, the cutting forces in the radial, axial and tangential directions are also recorded simultaneously. 10 second segments of the cutting data are taken for comparisons when the machining reached half the length of the shaft in order to ensure consistency and steady state values. Both radial and axial forces decreased within 100N, while the tangential forces increased up to 100N, as shown in Fig. 6.3, 6.4 and 6.5.

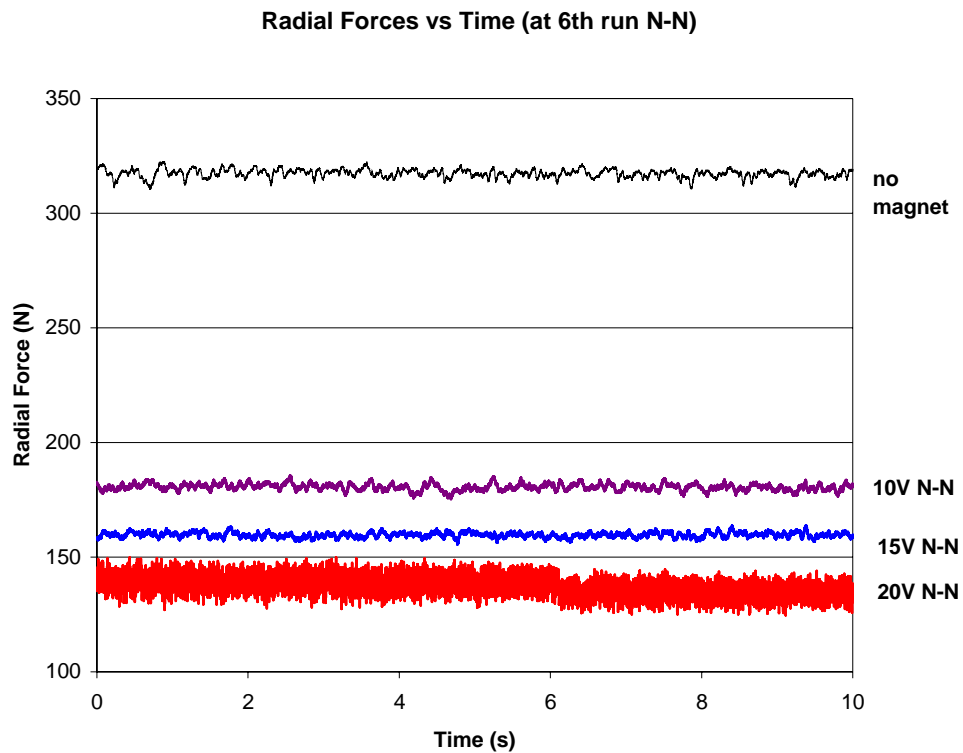


Fig. 6.3 Radial forces against time with N-N setup

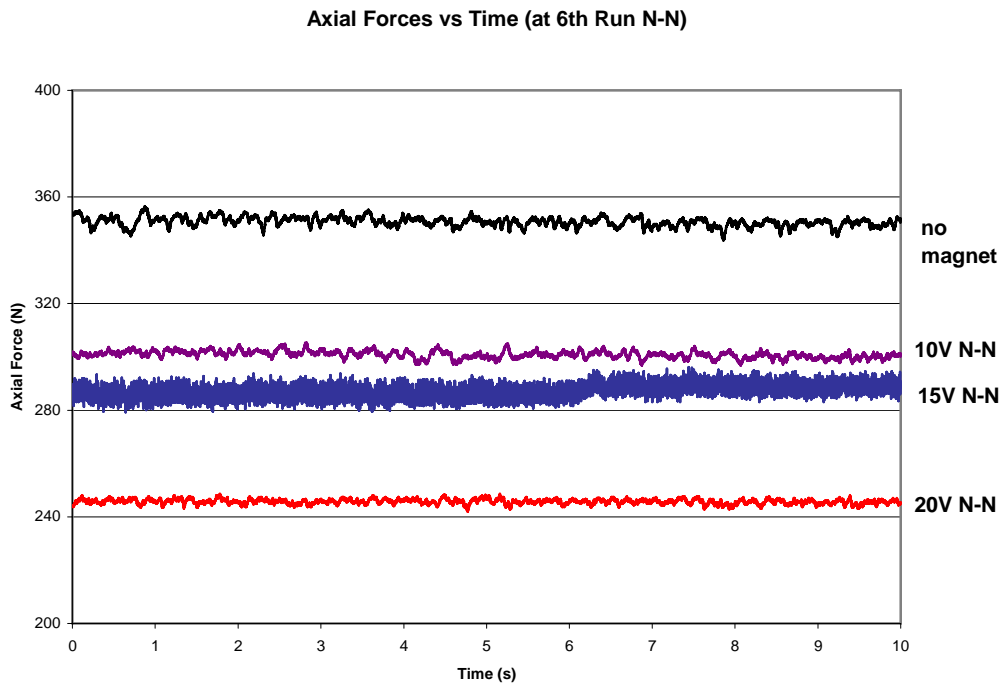


Fig. 6.4 Axial forces against time with varied power supply

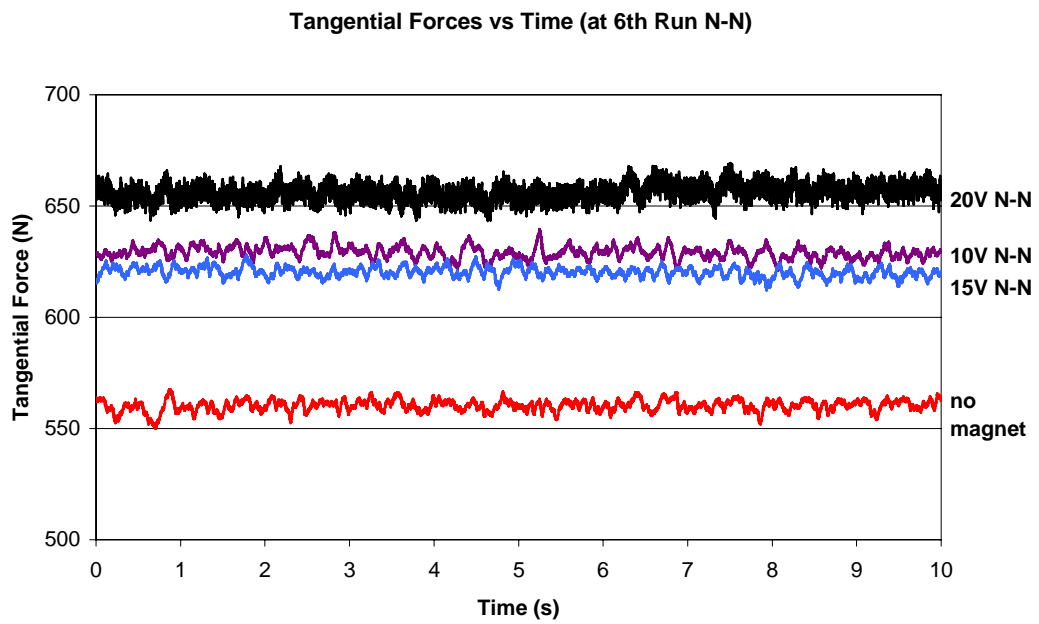


Fig. 6.5 Tangential forces against time with N-N setup

6.3 Diffusion Wear and Force

To construct the dynamic state model, the predefined factors includes feed f , cutting speed V , and depth of cut d_c are kept constant as is the typical case in turning operation. The components of the cutting force F and tool wear, which can be measured directly, act as the main analysis data. The model is represented by the following equations [33]:

$$\dot{V}_B = K_1 \sqrt{V} \exp\left(\frac{-K_2}{273 + \theta_f}\right) \quad (6.1)$$

$$F = F_0 + K_3 d_c (V_B - V_{B0}) \quad (6.2)$$

where F_0 and V_{B0} represent the initial cutting force and flank wear at the beginning of a cutting operation. Among the parameters in the flank wear model, the gradient between the force increment and flank wear development K_3 can be determined through preliminary experiments. Another attainable parameter is the activation energy of the diffusion K_2 for the given tool-workpiece combination, for example, between the cobalt atoms in a carbide tool and the iron atoms in steel workpiece.

This model describes the diffusion type of flank wear mechanism only, which is of primary concern in our cutting study with the applied cutting conditions. Under such cutting conditions shown in Table 5-2, the wear mechanism between a carbide tool and a steel workpiece is known to be dominated by the diffusion between the cobalt atoms in the tool and iron atoms in the workpiece. The abrasion mechanism accounts for the rapid flank wear development on a fresh tool during a very short initial cutting period. Therefore when such a rapid flank wear development is accounted for in such

a way, the continuing flank wear process can be appropriately represented by (6.1) and (6.2) through the end of tool insert life.

6.4 Magnetization, Lenz's law Effect on Cutting Force

In all applications a time-varying source of magnetic field induces electric currents in a nearby conducting solid. The interactions of pulsed magnetic field with the currents in the metal include the following mechanical effects:

- $\mathbf{J} \times \mathbf{B}$ body force;
- Magnetization forces;
- thermoelastic strains due to $\mathbf{J} \cdot \mathbf{J}$;
- ablation due to melting ;
- Rayleigh-Taylor instability at the solid-field interface.

And in our experiments, the variation in tool wear caused by magnetization and electromotive force depends directly on the voltage applied. So the first two forces: magnetization force and Lorentz force account for the force variation due to the presence of electromagnets.

When a conducting body is moving in a magnetic field or when the field is changing in time, an electric field \mathbf{E} and a eddy current \mathbf{J} are generated on the body. The electric field \mathbf{E} relates to the changing magnetic field \mathbf{B} through Faraday's law, while for a rigid solid with electric conductivity σ , \mathbf{J} can be expressed as $\mathbf{J} = \sigma \mathbf{E}$. For paramagnetic conductors, the effect of induced current is more pronounced than that

of induced magnetization. However, for soft ferromagnetic materials, the induced current can be omitted and magnetization plays an important role. A soft ferromagnetic material is characterized by small hysteretic losses, narrow hysteresis loop for H-M curves, and low remnant magnetization. Many nickel-iron alloys used widely as core materials for motor, generators, inductors and transformers are of this type. In calculation, the effect due to hysteresis is omitted.

Referring a body with volume V in Cartesian coordinate, the position is defined by x at time t . In the presence of an induction \mathbf{B}_0 , the total force \mathbf{F} acting on a body is

$$\mathbf{F} = \mu_0 \int_V \mathbf{M} \cdot \nabla \mathbf{H}_0 dV \quad (6.3)$$

Furthermore, by applying various vector formulas and magneto-static equations, the above integrals can be transformed into surface integrals or volume integrals with entirely different integrands. Thus on an element with volume dV and surface dS , the net forces exerted by externally applied fields and surrounding magnetized materials can not uniquely specified.

In this case, the magnetization force play the main role in modifying the cutting forces in axial, tangential and radial directions. It has been reported that the cutting force can provide an indicator of the tool wear. Although the relationship is not clear, the lower force does reflect lower wear. In turn, less force leads to less vibration of the cutting tool, which will further reduce the wear rate. And this closed loop relation can be expressed in Fig. 6.6. At the same cutting time shown in Fig. 6.1 and 6.2, the

tool wear reduced by 10% to 20%, which then in turn is reflected in smaller force values in feed and cutting depth directions.

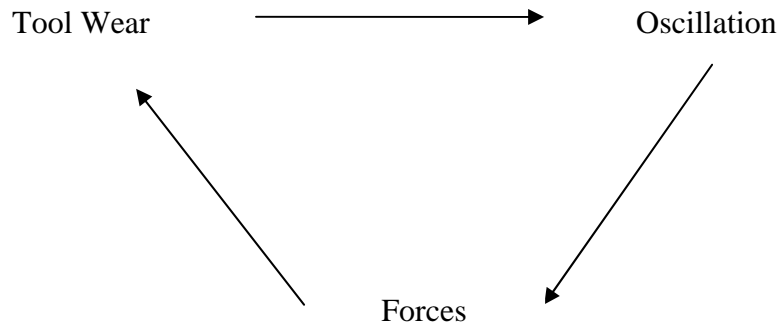


Fig. 6.6 Close loop relation

6.5 Magneto-elastic Interaction, Vibration and Tool Wear

The initial objective of introducing the magnetic field is to reduce the vibration of the tool holder and insert combination. This combination can be simplified as a cantilever beam excited by an external force which is directly related to tool wear. According to this beam model, the displacement is decided by measured forces, affected by tool wear and processing parameters. The external forces include the cutting force, thrust force, friction force, and interaction between the tool flank and workpiece. The relationship between tool wear and displacement of the tool system is developed and discussed.

A two-dimensional cantilever was established to model the dynamic displacement in feed or tangential direction. The flexural motion equilibrium including transverse deflection $w(x,t)$ and electromagnetic force $p_m(x,t)$, can be expressed as:

$$EI \frac{\partial^4 w(x,t)}{\partial x^4} + \rho A \frac{\partial^2 w(x,t)}{\partial t^2} = p_m(x,t) \quad (0 < x < l) \quad (6.4)$$

with the boundary conditions at $x=0$,

$$w(x,t)\Big|_{x=0} = 0 \quad \frac{\partial w(x,t)}{\partial x}\Big|_{x=0} = 0 \quad (6.5)$$

and at the free end, the boundary conditions are

$$\frac{d^2 w(x,t)}{dx^2}\Big|_{x=L} = 0 \quad EI \frac{d^3 w(x,t)}{dx^3}\Big|_{x=L} = F \quad (6.6)$$

where F present the net force at the free end that excites the vibration of the cantilever beam in tangential or feed direction. This interactive force is decided by the sliding asperity of flank wear on the flank surface.

The solution of the flexural deflection $w(x,t)$ can be obtained in terms of interactive force and magnetic force. At the same cutting time, the magnetic field has effectively reduced the deflection of the tool insert and this damping effect further improved the tool insert wear. In turn, the reduced tool wear was reflected on the interactive force measured. This coupling effect corresponds well with the tool wear and force in feed and cutting direction in our experiment, as shown in Fig. 6.2-6.5. The last term in the equilibrium equation p_m is the equivalent magnetic force acting on the ferromagnetic beam and the strength distribution of magnetic field. The magnetic force will

introduce negative term into deflection and can be interpreted as a damping effect which is proportional to the magnetic field intensity and material properties.

6.6 Magnetic Pole Effect on Wear

Special attention should be placed on the tool wear reduction discrepancy between the N-N setup and N-S setup. Figure 6.7 shows that north-south setup was more effective even though magnetic intensity around the rubbing area was lower under the same voltage.

The attempted explanation is in the light of energy. As explained by Su, Hung and Horng [34] the power transmitted to tool surface is the fundamental factor in determining the wear rate of tool. This indicates that a sufficient amount of energy is required for removal of a unit volume of tool material on the tool surface. Thus it is reasonable to expect that for higher material removal rate of tool, the larger the energy rate (or power) should be applied to the tool. In turning process, because of the application of electromagnets, extra energies were transmitted through the tool holder to both the tool and workpiece surface. Some of the energy is conserved in the tool holder for magnetization, while the other is transmitted to the acting area. This energy is used by the abrasion process and the wear rate of tool in the turning process is proportional to the power transmitted to tool tip.

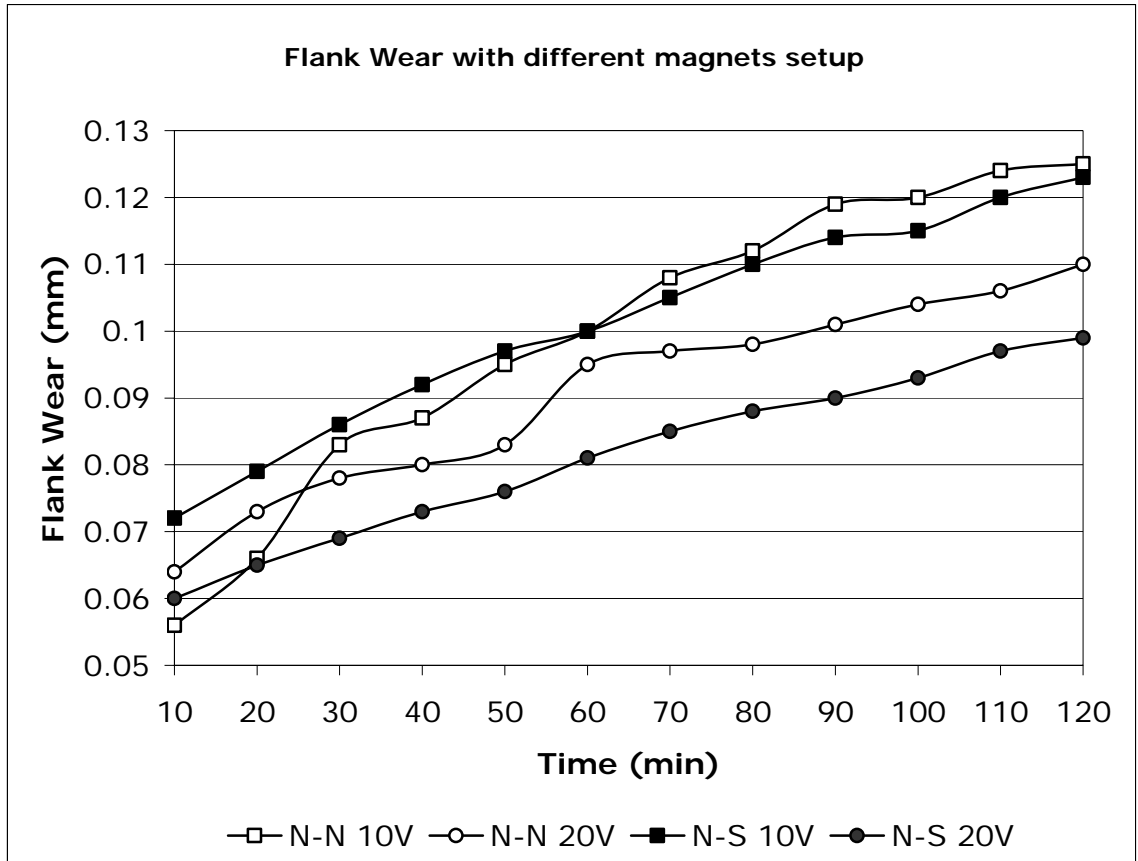


Fig. 6.7 Tool wear reduction with N-N and N-S magnetic fields

To evaluate the energy, linear approximation is convenient and sufficiently accurate as long as the ferro-material are operated below the saturation level. The energy per unit volume can be expressed as

$$U = \int_0^B \frac{B_{ave}}{\mu} dB = \frac{B_{ave}^2}{\mu} \quad (6.7)$$

Because of the fixed power supply, we may assume the same energy input. And for the N-N case, the flux density distributed inside the tool holder B is higher, in other words, more energy was conserved inside the tool holder. The tool holder consumes more energy and thus less energy is transmitted to the contacting area. Considering

the thermal effect, less energy is used to promote the formation of Aluminum oxide. As a result the aluminum oxide exert less effect in protect the tool insert. On the other hand, the N-S set up allow more energy transferring from electromagnetic energy to kinetic energy, which results in the lower wear rate for the N-S case.

6.7 Azimuthal Induction Currents and Electromagnet Model

Vector potential application model for axially symmetric structures presents current only in the angular direction. It is the azimuthal currents. A single electromagnet is formulated using the only nonzero component of the magnetic vector potential, the φ component.

For two dimensional symmetrical electromagnetic modeling, with currents having only nonzero component, the magnetic potential is used. Using the definitions of the potentials,

$$\mathbf{B} = \nabla \times \mathbf{A} \quad (6.8)$$

$$\mathbf{E} = -\nabla V - \frac{\partial \mathbf{A}}{\partial t} \quad (6.9)$$

and the constitutive relation $\mathbf{B} = \mu_0(\mathbf{H} + \mathbf{M})$, Ampere's law can be rewritten as

$$\sigma \frac{\partial \mathbf{A}}{\partial t} + \nabla \times (\mu_0^{-1} \nabla \times \mathbf{A} - \mathbf{M}) - \sigma \mathbf{v} \times (\nabla \times \mathbf{A}) + \sigma \nabla V = \mathbf{J}^e \quad (6.8)$$

The equation of continuity, which is obtained by taking the divergence of the above equation, gives us the equation

$$-\nabla \cdot \left(\sigma \frac{\partial \mathbf{A}}{\partial t} - \sigma \mathbf{v} \times (\nabla \times \mathbf{A}) + \sigma \nabla V - \mathbf{J}^e \right) = 0 \quad (6.10)$$

The Ampere's law involving the gradient of the electric potential can be written as $\nabla V = -V_{loop} / (2\pi r)$ since the electric field is present only in the azimuthal direction. V_{loop} is the potential difference for one turn around the z axis. The above equation can then, in cylindrical coordinates, be written

$$\sigma r \frac{\partial u}{\partial t} - \begin{bmatrix} \frac{\partial}{\partial r} \\ \frac{\partial}{\partial z} \end{bmatrix}^T \left(r\mu_0^{-1} \begin{bmatrix} \frac{\partial u}{\partial r} \\ \frac{\partial u}{\partial z} \end{bmatrix} + \mu_0^{-1} \begin{bmatrix} 2 \\ 0 \end{bmatrix} u - \begin{bmatrix} M_z \\ -M_r \end{bmatrix} \right) + r\sigma \left(\mathbf{v} \cdot \begin{bmatrix} \frac{\partial u}{\partial r} \\ \frac{\partial u}{\partial z} \end{bmatrix} \right) + 2\sigma v_r u = \sigma \frac{V_{loop}}{2\pi r} + J_\varphi^e \quad (6.12)$$

The dependent variable u is the nonzero component of the magnetic potential divided by the radial coordinate r, that is

$$u = \frac{A_\varphi}{r} \quad (6.13)$$

This transformation is carried out to avoid singularities at the symmetry axis. To obtain the equation for magneto-statics, the displacement is constant and dropping the first term in the equation, we get:

$$- \begin{bmatrix} \frac{\partial}{\partial r} \\ \frac{\partial}{\partial z} \end{bmatrix}^T \left(r\mu_0^{-1} \begin{bmatrix} \frac{\partial u}{\partial r} \\ \frac{\partial u}{\partial z} \end{bmatrix} + \mu_0^{-1} \begin{bmatrix} 2 \\ 0 \end{bmatrix} u - \begin{bmatrix} M_z \\ -M_r \end{bmatrix} \right) + r\sigma \left(\mathbf{v} \cdot \begin{bmatrix} \frac{\partial u}{\partial r} \\ \frac{\partial u}{\partial z} \end{bmatrix} \right) + 2\sigma v_r u = \sigma \frac{V_{loop}}{2\pi r} + J_\varphi^e \quad (6.14)$$

According to this formulation, a 2-D non-symmetric model of electromagnet was established in Fig. 6.8, which can well predict the surface distribution of magnetic flux density distribution and the area around the electromagnet. The electromagnetic

was modeled by defining the current density on the brass coils. The predicted magnetic flux density values on the magnetic surface perfectly meet the experimental measured values by Gauss Meter.

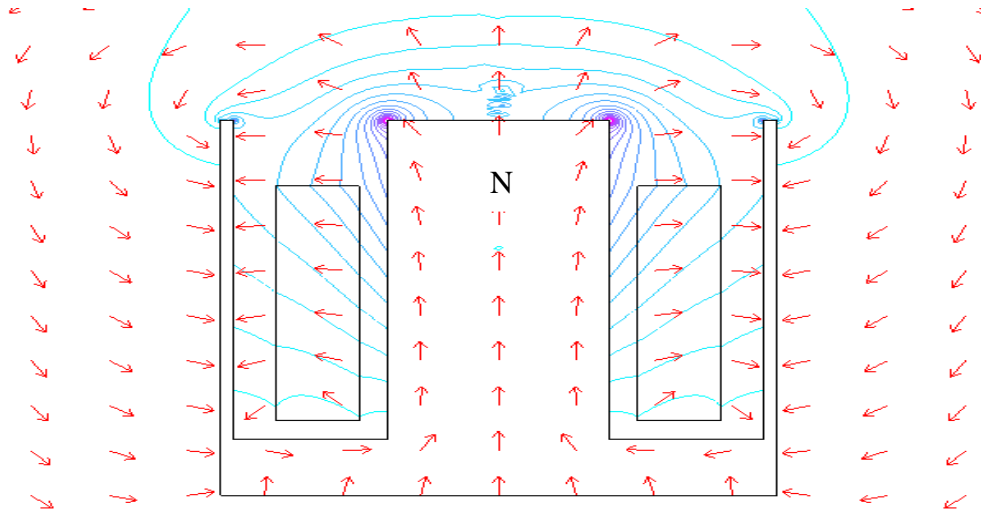


Fig. 6.8 Single cylindrical electromagnet

6.8 Computer Simulations and Discussion

To characterize the effect of magnetic field and eddy current on the tool wear, several assumptions are clarified below:

- (1) The workpiece of ASSAB 760 and the tool holder are homogeneous, isotropic and linear soft ferromagnetic material.
- (2) Only the eddy currents in effective direction are considered and the skin depth is larger than the workpiece diameter.
- (3) Because of small size of tool compared to the tool holder, the tool was assumed as part of the holder.

- (4) Under the high speed cutting condition, flank wear is predominant through the cutting process.
- (5) The magnetic flux density and the eddy currents are constant in effective volume for each single experiment condition.

On one hand, 2D non-symmetric models including the magnets setup, tool holder and workpiece facilitate the prediction of magnetic strength around the cutting area, as shown in Fig. 6.9 and Fig 6.10. The arrows in the figures indicate the magnetic field direction. On the other hand, it is shown that a linear motor model can be obtained by unrolling the workpiece and simulate the induced eddy current on the workpiece in Fig. 6.11. The mild steel workpiece rotated in front of the cutting tool, cutting the radial magnetic field. And the velocity is perpendicular to the magnetic field. To simplify the interactive mechanism, the workpiece was unrolled and considered as an endless plate piece which was similar to secondary rotor in linear induction motor.

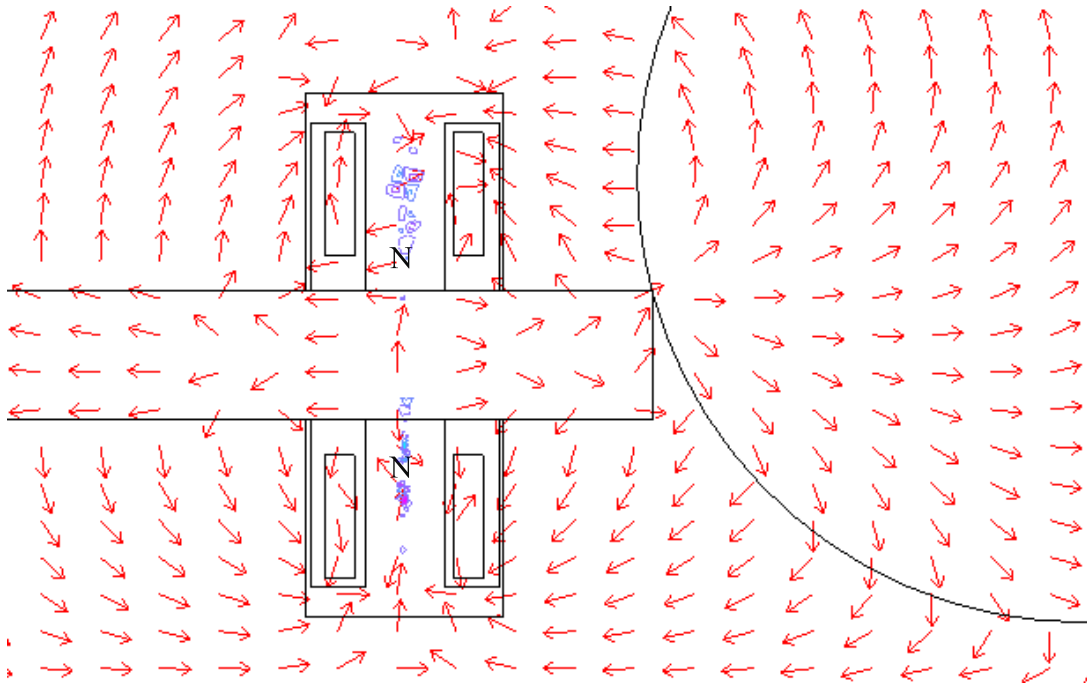


Fig. 6.9 Model of electromagnets, tool holder and workpiece (N-N)

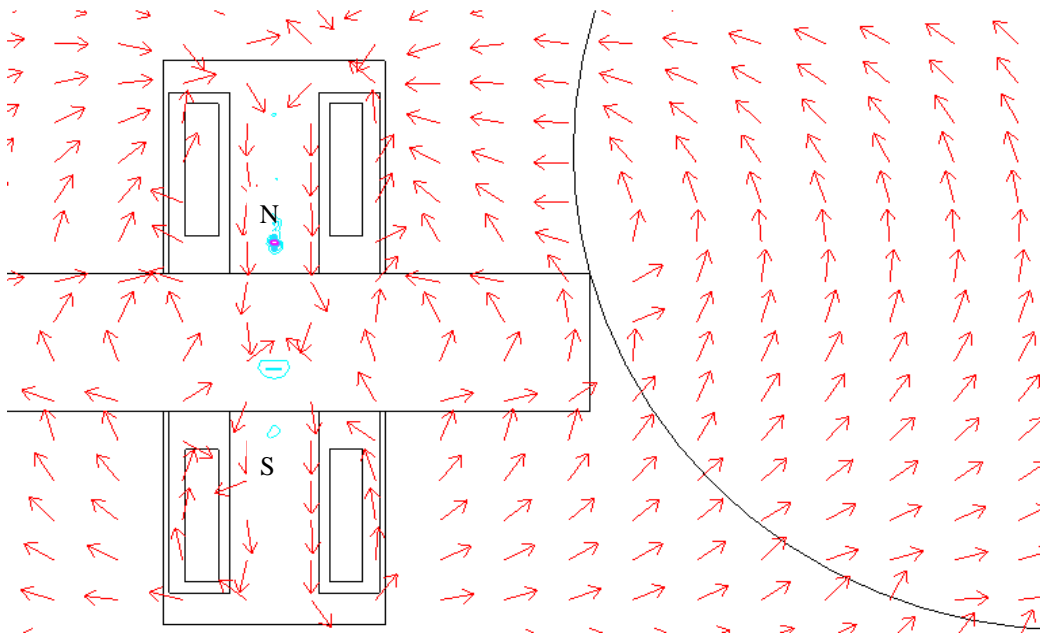


Fig. 6.10 Model of electromagnets, tool holder and workpiece (N-S)

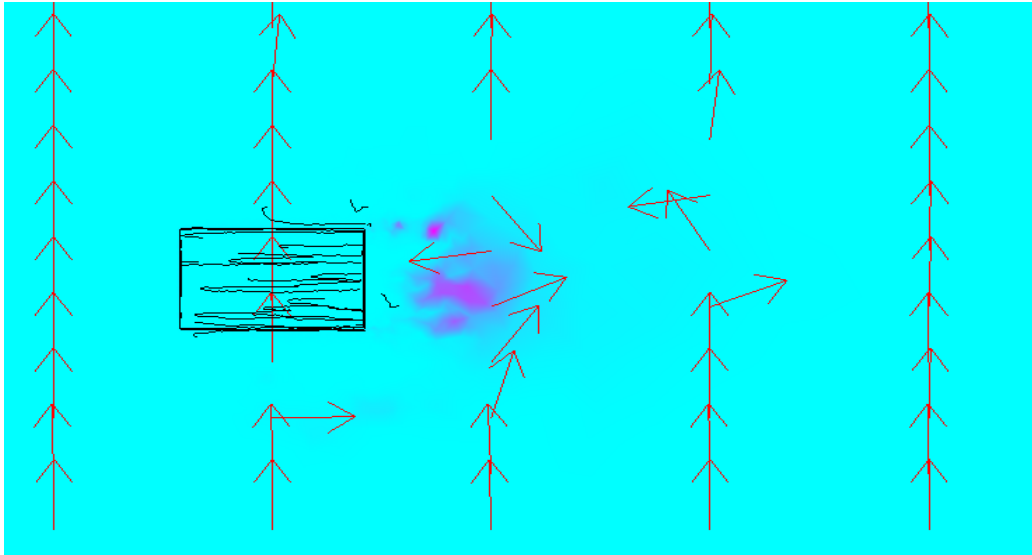


Fig. 6.11 Eddy current on the unrolled workpiece

After modeling the magnetization and induced eddy currents on the workpiece, the magnetization force and Lorentz force are compared. In terms of the ferromagnetization force, some of the calculation values at points around the contact area are listed in Table 6-1.

Table 6-1 Points values of magnetization

Coordinate	$M_r \frac{\partial}{\partial r} B_r$	$M_z \frac{\partial}{\partial z} B_z$
(0.0493, 0.0485)	-844	-7938
(0.0502, 0.0483)	-29	-8496
(0.0513, 0.0444)	1.14e4	-4e4

(0.0519, 0.0405)	-5.05e5	1.4e5
(0.0500, 0.0400)	7.18e10	-3e11
(0.0528, 0.0329)	-1.7e5	-3.8e4
(0.0534, 0.0336)	2917	5295
(0.0549, 0.0297)	700	1399
(0.0563, 0.0470)	319	-818
(0.0571, 0.0405)	-1.3e4	1635
(0.0599, 0.0338)	-4404	-118

The contact point coordinate is (0.05, 0.04), and the ferro-material workpiece suffers the force caused by magnetization $f = \int \mathbf{M} \cdot \nabla \mathbf{B} dV$. The mean value of the magnetization force density is about $4.5 \times 10^7 \text{ N/m}^2$, which is much larger than the force due to the eddy currents.

$$\mathbf{M} \cdot (\nabla \mathbf{B}) = \begin{bmatrix} M_r & M_z \end{bmatrix} \begin{bmatrix} \frac{\partial}{\partial r} B_r & \frac{\partial}{\partial r} B_z \\ \frac{\partial}{\partial z} B_r & \frac{\partial}{\partial z} B_z \end{bmatrix} = \begin{bmatrix} M_r \frac{\partial}{\partial r} B_r + M_z \frac{\partial}{\partial z} B_r & M_r \frac{\partial}{\partial r} B_z + M_z \frac{\partial}{\partial z} B_z \end{bmatrix} \quad (6.15)$$

By contrast, in terms of the eddy currents, the highest eddy current density is $8.5 \times 10^6 \text{ A/m}^2$. For conducting materials, we have $f = \int \mathbf{J} \times \mathbf{B} dV$. Even assuming the largest magnetic flux density of 0.1T inside the contacting tip, the force density can be $8.5 \times 10^5 \text{ N/m}^2$, which is two orders smaller than the magnetization force.

The two electromagnets attached near the cutting tools magnetized the ferromagnetic tool holder. Then the cutting area was surrounded by weak magnetic flux density about 100 Gauss. But the flux density at the contact point is about 800Gauss. The analysis suggests that the magnetization force density is 4.5×10^7 N/m². The effective magnetic intensity in the front face of tool holder, which was closest to the workpiece, was assumed to be constant. And including the impacting tool transverse area $12.6\text{mm} \times 4.6\text{mm}$, we may get a rough force in the range of 20N-100N. This analytical prediction is consistent with the force reduction.

CHAPTER 7

EXPERIMENT ANALYSIS AND MODELLING FOR MILLING

7.1 Effect of Magnetic Field on Wear

A series of milling experiments were performed to evaluate the tool wear reduction and force variation under different voltages supplied to the electromagnets. The resulting tool wears, defined as the mean width (V_B) responding to different magnetic field environments, were measured offline. Figure 7.1 and 7.2 show the flank wears on the clearance face for every 5 passes (one minute) through the over all 35 passes for each workpiece under one specific voltage supply to the electromagnets. The Figures emphasize the effectiveness of the extremely low electromagnetic field flux density in diminishing the tool insert flank wear.

Figure 7.1 and 7.2 record the flank wear against milling time under four different cutting conditions. The voltage supplied to the two electromagnets, which stick to the base of the workpiece side, increased from 0V to 20V. The corresponding voltages are 0V, 10V, 15V and 20V, respectively. Other cutting conditions were kept same as shown in Table 5-6. The overall cut depth is 35mm after 35 passes. And the final surface is still 31mm higher than the top of the electromagnets, which ensure the safety operation of the milling machine.

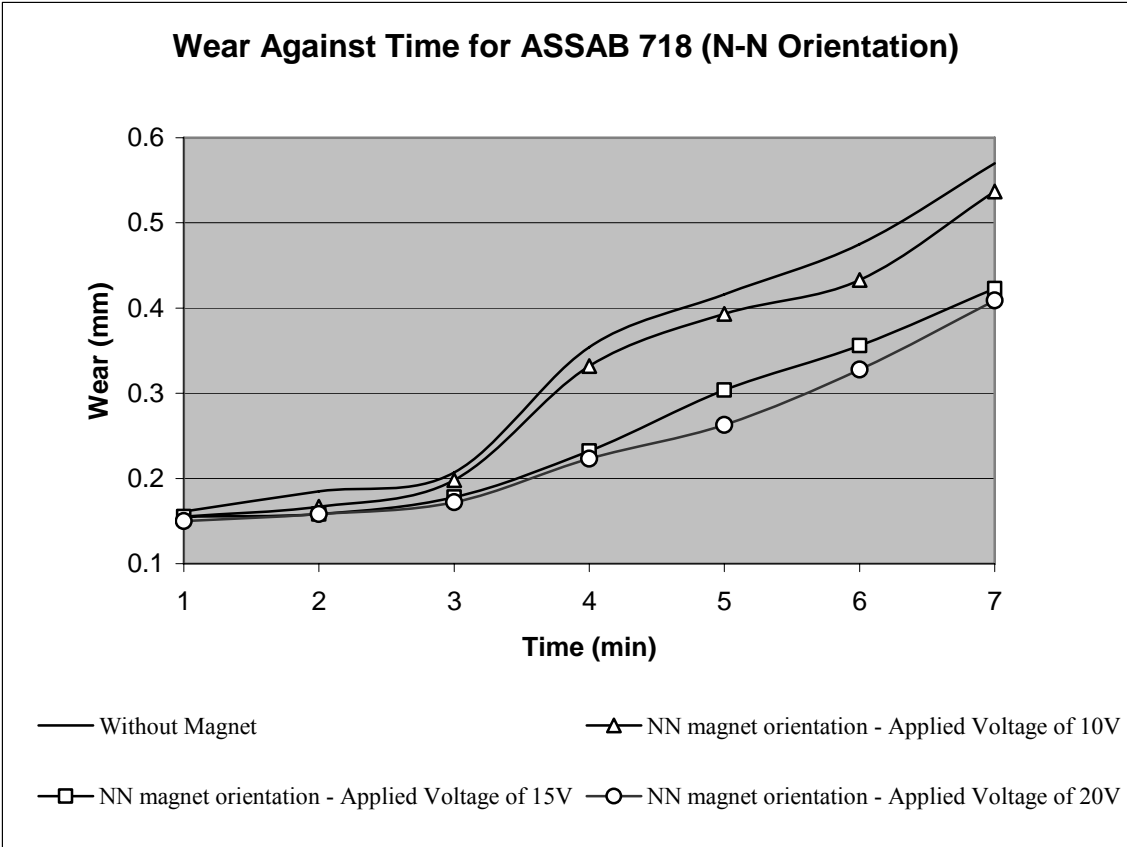


Fig. 7.1 Tool wears with and without electromagnets under the N-N setup

In Fig. 7.1, the electromagnets follow the N-N orientation. By changing the voltages applied on each north-centered electromagnet from 0V to 20V, the wear appears to differentiate apparently after 3 minutes of milling and. Similarly, the N-S orientation also shows great improvement in tool wear. And the wear reduction passes is quite consistent to the increasing trend of power supply.

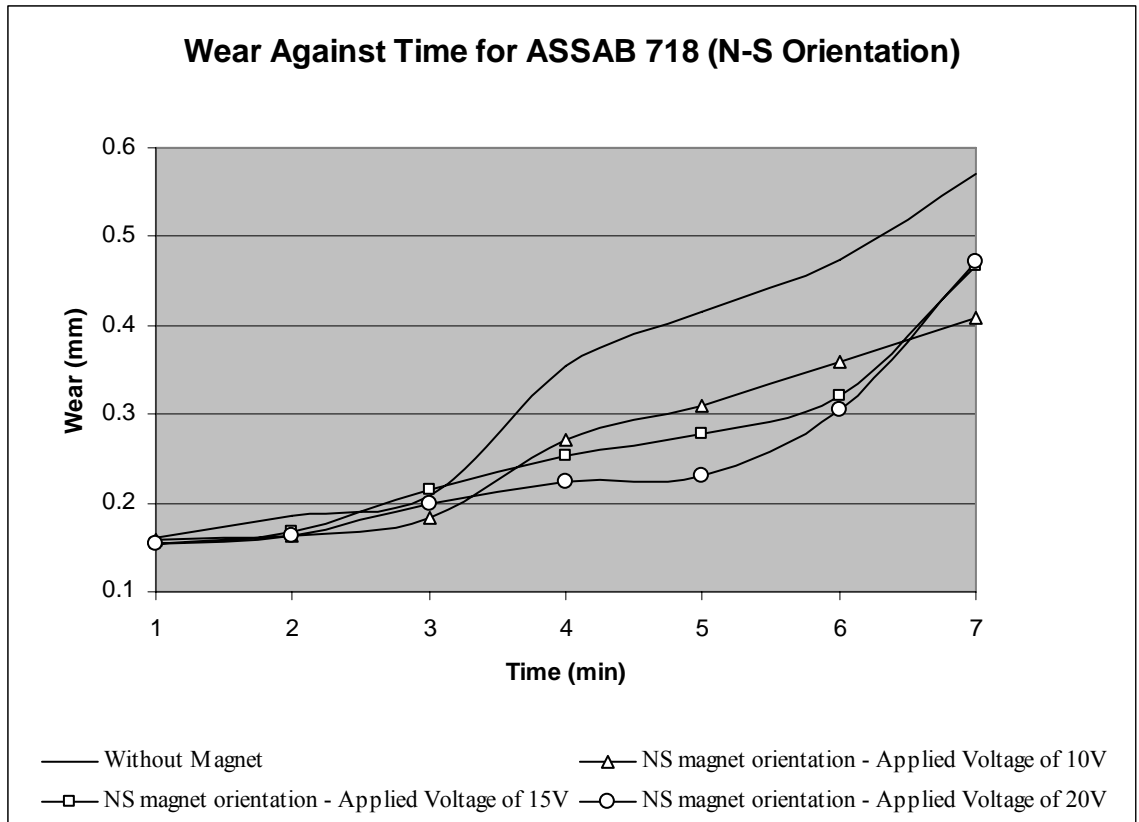


Fig. 7.2 Tool wears with and without electromagnets under the N-S setup

7.2 Variation of Force Due to Magnetization

Besides the tool wears, the maximum cutting forces in x, y and z directions are also recorded simultaneously. x is the feed direction; y is the direction in workpiece surface plane which is normal to the feed direction and z is the direction perpendicular to the surface plane. During each pass, the forces recorded are quite steady and the forces on the 21st pass are shown in Fig. 7.3 and 7.4. In end milling, only the force on the milling surface, say x and y direction are related to the tool wear on which we focus our attention. And $\sqrt{x^2+y^2}$ in the figure means the value of $\sqrt{x^2+y^2}$.

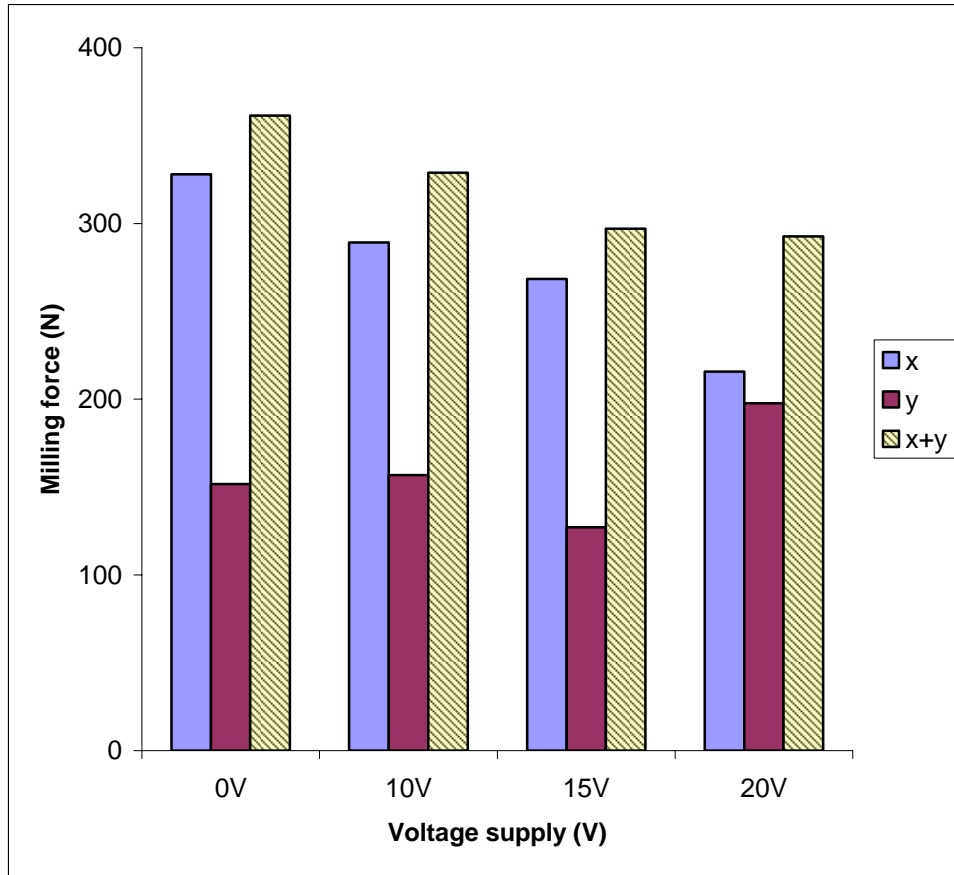


Fig. 7.3 Forces against voltage supply on the 21st pass with N-N setup

One interesting phenomenon is that for the N-N case, the combination forces of x and y directions reduce gradually as the voltage supply increases, which keep the same trend exactly with the reduction tool wear. What's more, the reducing scale is quite evenly proportional. Similarly, in N-S case, the 10V to 20V power supply result in the same reduction of combination forces, which correspond well to the small wear difference with increasing voltage supply of 10V, 15V and 20V.

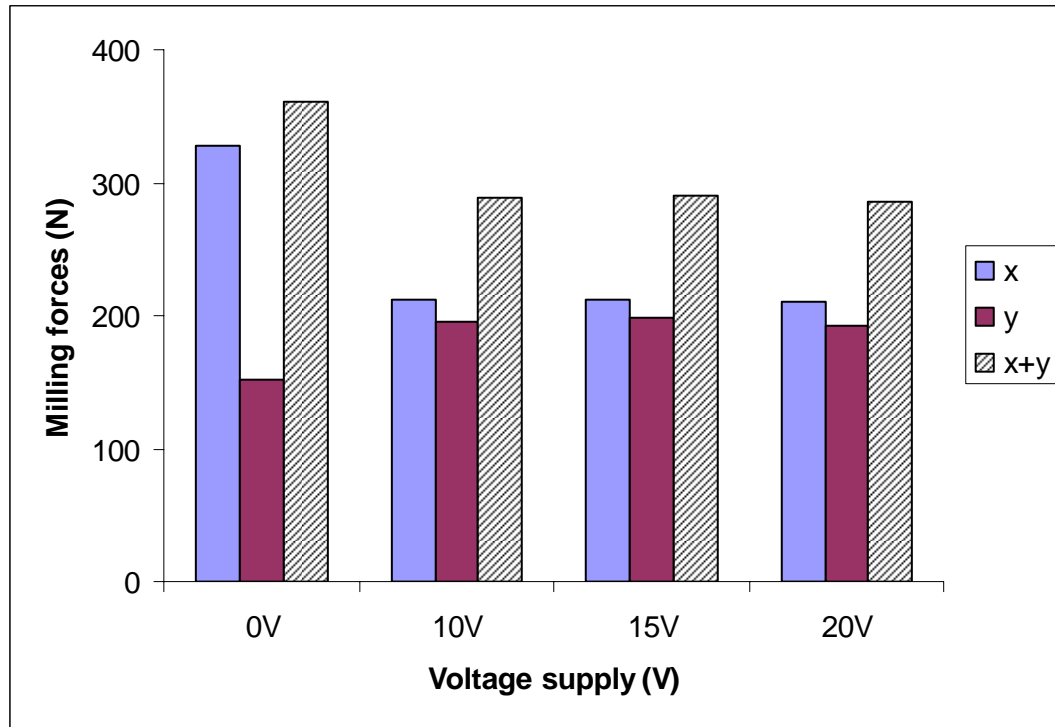


Fig. 7.4 Forces against voltage supply on the 21st pass with N-S setup

This phenomenon can be also explained in the light of a close loop relationship, which describes the interaction of tool wear and machining forces. On one hand, force or specified shear force directly determines the tool wear in machining process; on the other hand, the tool wear condition can be reflected well through the online force signal, according to which principle force have already been used as a reliable output signal to monitor the tool wear abrasion level.

Surface finish had generally showed a slight improvement under increased magnetic field conditions. Only under the cases of an applied voltage of 20V under the north-north and north-south magnet field orientation did the surface finish readings remain

constant throughout the individual experiments at $0.1\mu\text{m}$ while the others fluctuate around $0.1\mu\text{m}$ to $0.2\mu\text{m}$.

7.3 Quasi-Static and In-plane Induction Current

For conductor with conductivity σ and velocity \mathbf{v} , the Maxwell-Ampere's law can be written as

$$\mathbf{E} = \sigma^{-1} (\nabla \times \mathbf{H} - \mathbf{J}^e) - \mathbf{v} \times \mathbf{B} \quad (7.1)$$

where \mathbf{J}^e is the external current density, and σ is the electrical conductivity. Introducing Faraday's law and constitutive relation $\mathbf{B} = \mu_0 \mu_r \mathbf{H}$, the following equation is derived

$$\frac{\partial}{\partial t} (\mu_0 \mu_r \mathbf{H}) + \nabla \times (\sigma^{-1} (\nabla \times \mathbf{H} - \mathbf{J}^e) - \mu_0 \mu_r \mathbf{v} \times \mathbf{H}) = 0 \quad (7.2)$$

which is the general time-dependent formulation of quasi-static field, including permeability of vacuum μ_0 , and relative permeability μ_r .

When the currents is present only on the surface of the rotating object, the magnetic field then only has a component perpendicular to the plane. The equation is a scalar equation with z component of magnetic field H_z as the only dependent variable. This special case is formulated as

$$d \frac{\partial \mu_0 \mu_r H_z}{\partial t} - \nabla \cdot d \left(\tilde{\sigma} \nabla H_z - \mu_0 \mu_r \mathbf{v} H_z - \tilde{\sigma} \begin{bmatrix} -J_y^e \\ J_x^e \end{bmatrix} \right) = 0 \quad (7.3)$$

where d is the thickness in the z direction and

$$\tilde{\sigma} = \frac{\sigma^T}{\det(\sigma)} \quad (7.4)$$

This equation is used for transient problems. And for the constant magnetic field assumption, the first part is dropped:

$$\nabla \cdot d \left(\tilde{\sigma} \nabla H_z - \mu_0 \mu_r \nabla H_z - \tilde{\sigma} \begin{bmatrix} -J_y^e \\ J_x^e \end{bmatrix} \right) = 0 \quad (7.5)$$

7.4 Eddy Current effect on Aluminum Oxide Sliding Contact

The investigations of aluminum oxide – steel sliding contact joints carried out so far have revealed that the aluminum oxide layer and its specific tribological properties depend to a large extent on the course of friction in conditions of technically dry friction and conditions of reduced lubrication. An external electric field is one of the many factors that can affect the operating conditions of a sliding contact joint. The properties of the surface layers of joint materials, as well as their sliding contact joints as a whole, were taken into account when considering the effect of an electric field. Joints were analyzed mainly from the point of view of their electric properties whether the mating pair is conductor-conductor, conductor-dielectric or dielectric-dielectric type. Each type behaves in a different way in the electric field.

The phenomenon of tribo-electrification always accompanies the sliding mating of materials, because electric charge is generated in the friction zone and its amount and charge depend on the energetic structure of the joint materials and on the intensity of electrostatic and electro-dynamic interactions. Generally it can be stated that a specific internal electric field originates in the friction zone and after an external field

is applied, the internal field is appropriately distorted. This field distortion depends on the value and polarity of the external electric field.

During friction a potential difference occurs on the solid-solid phase boundary and its value changes with time during operation of the sliding contact joint. The variable operating conditions of a sliding contact joint result in physical and chemical phenomena such as chemisorption, thermo-emission and electrification in the friction zone.

The value of the potential at the interphase boundary depends on the properties of contact materials and on the type of friction and type of joint, i.e. conductor-conductor, conductor-dielectric or dielectric-dielectric. The existing potential difference at the interphase boundary in certain sliding contact joints can initiate, and in others can block, the interaction with the surface of a solid. An electric barrier in the form of a binary layer is generally an obstruction to the activation of the material sliding surfaces. In the case of an electric barrier of high electrochemical potential difference it can be 'removed' with an external electric field. Compensation of the binary electric layer on surfaces of metals facilitates the occurrence of electrochemical processes responsible for the creation of boundary layers.

As a result of electrochemical oxidation of aluminum alloys a Al_2O_3 layer of a defined thickness and porosity is obtained on their surface. This coating has very

good wetting properties and is included as a dielectric in especially positive adsorbents.

The polarity of the external electric field has a vital effect on changes in friction force values during mating of the joint. In the case of the sliding contact joint investigated the positive polarity of the sample (aluminum oxide) causes a fall in the friction force values. The polarity is consistent with the polarity of the internal electric field generated in the friction zone of the joint. The durability of these layers depends on, apart from the tribological properties of the joint materials, on the value of the external electric field and its polarization.

7.5 Eddy Current Effect on (TiAl)N Growth

(TiAl)N coating can usually withstand temperature as high as 800°C . One problem is that at such high temperature, oxidation is very active, which may lead to shorter tool life. However, it is found that at high temperature, a stable protective Al_2O_3 surface layer due to rapid temperature elevation during high speed machining would be formed on the outer surface in the air circumstance. Al_2O_3 itself is of steady chemical properties with low ion mobility and can act as a strong barrier for oxygen dispersion to inhibit further oxidation. This protective surface layer could enhance wear and oxidation resistance of the tool.

Certain tarnish films stop growing at the thickness s less than $1\ \mu\text{m}$, to prevent further attack by oxygen. The existence of the maximum thickness of the protecting films is

the equilibrium of energy between electrical field provision and diffusion consumption. The structure of (TiAl)N has few imperfection, which results in the obstruction when ions diffuse through them. Therefore the diffusion and the oxidation require the help of electrical field, generated between the negative oxygen ions on the external surfaces of the film and a corresponding positive charge at the film-metal interface. The Fermi level of ions decides the total required voltage, which is the product of the electric field strength and the film thickness, when the Fermi level of the ions is lifted into coincidence with the Fermi level of the metal Al. Thus the field decreases when s increases and will eventually be unable to maintain diffusion and growth when s reaches a certain s_{\max} .

When the tool rotates on the surface of workpiece, the magnetic field on the workpiece surface was cut by the rotating tool with tool holder. Thus according to Faraday's Law, voltage is induced on the moving conductor, which is also expressed as the eddy current through the rotating tool. In this case, additional electric field restores the growth of the Al_2O_3 film. It is believed that an additive field of 7×10^8 V/m or rising the temperature to about 500°C will resume the growth of the Aluminum oxide film. This effect will finally increase the thickness of Al_2O_3 film and provides extra protective wear resistance to the milling tool. If the induced eddy current is of the order of 10^6 A/m², with the extreme thin (TiAl)N coating of $1\ \mu\text{m}$, the volume current density is around 10^{12} A/m³. The order of this volume current density is of the same order compared with the necessary current density given

by $J = \sigma E$. The conductivity is 5×10^4 s/m with the expected electrical field of 10^8 order.

7.6 Thermal Effect of Eddy Current

Because the growth of the oxide necessitates that ions diffuse through the already existing film, elevated temperature promotes the diffusion by providing activation energy for the stepwise progression of diffusion.

The oxide will grow only when the energy hold by the bonds between metal and oxygen in the oxide is higher than bonds between the oxygen molecules and bonds in the metal. Metal ions migrate through the oxide and meet chemisorbed oxygen ions at the outer oxide surface, which finally leads to the film growth.

At high temperature (higher than 100°C), the rate of growth is essentially determined by the diffusion of the ions, which is proportional to the ion density gradient and the diffusion coefficient. In this case, the parabolic rate law of oxidation can approximately describe the growth rate as [35]:

$$\frac{ds}{dt} = \frac{\text{constant}}{s} \exp\left(-\frac{11600\phi}{T}\right) \quad (7.6)$$

where s is the thickness of the film, t is time, ϕ in eV is the activation energy of diffusion.

The milling machining is completed by the plastic deformation of the workpiece, accompanied with formation of chips. In the milling zone, both the milling tool and the contact point on workpiece can attain high flash temperature (several 100°C). When the tool insert rotates and mills, it cuts the magnetic field flux and eddy current is induced flowing through the small-geometry contact. This effect will further increase the contact temperature. Because Alumina film is practically insulating, the eddy current flows through the nonconductive media and a phenomenon similar to electric arc will occurs, even though the current strength is much lower than the electric arc. The contact area is so small that the temperature increased by the electric energy can reasonably account for the increasing forming rate of Aluminum film, which further decreases the wear rate under different magnetic field strength.

7.7 Polarity Effect of Induced Eddy Current

Even though the electric field is not introduced directly by voltage or current, it can also assumed that that tool part functions as the positive polar. When the eddy current induced on the tool and tool holder, it then flows to the workpiece which acts as the negative pole. According to the observation reported by Wistuba [15], the positive polarity of sample accounts for the reduction of force. In our milling force, the combination forces did decrease to some extent following the magnetic field and induced eddy current when the tool insert holds higher potential.

7.8 Computer Simulations and Discussion

Figure 7.5 and 7.6 shows the models including the magnets setup and workpiece, which help the prediction of magnetic strength around the milling area. For the N-N orientation, the magnetic field on the workpiece surface distributes evenly through the length of the workpiece. So in this case, the increase of voltage supply play an important role in the uniformly decrease of tool wear.

However, as can be seen in Fig. 7.6, the N-S setup contributes to the inhomogeneous magnetic field distribution on the workpiece surface, with different directions and strength. Accordingly, the tool wear reduction is not much proportional to the increasing voltage supply due to the non-uniform of magnetic field intensity. Neglecting the directions of the surface magnetic field, the magnetic flux density calculated from the model is gradually decreasing from 60 gauss in the edge to 10 gauss in the middle surface. The numerical calculation values are in fair agreement with the measurement data.

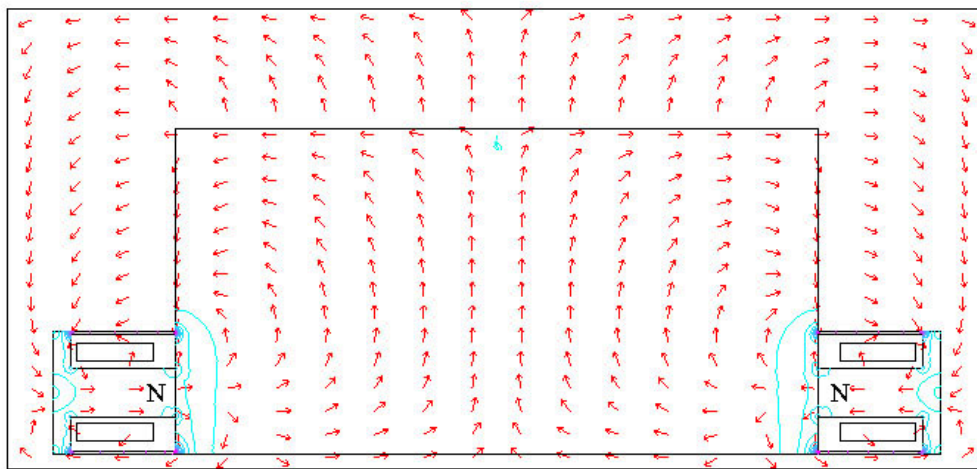


Fig. 7.5 Model of electromagnets sticking to the workpiece with N-N setup

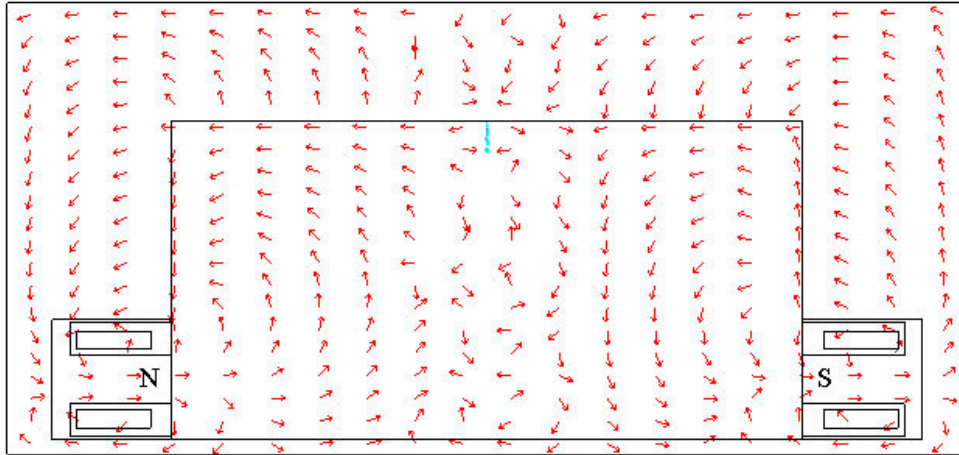


Fig. 7.6 Model of electromagnets sticking to the workpiece with N-S setup

Finally, it is shown that the motion of tool holder and tool insert can be modeled as a rotating disk and eddy current dissipates on the disk surface, as shown in Fig. 7.7.

The mild steel disk rotates on top of the workpiece, thereby cutting the magnetic flux.

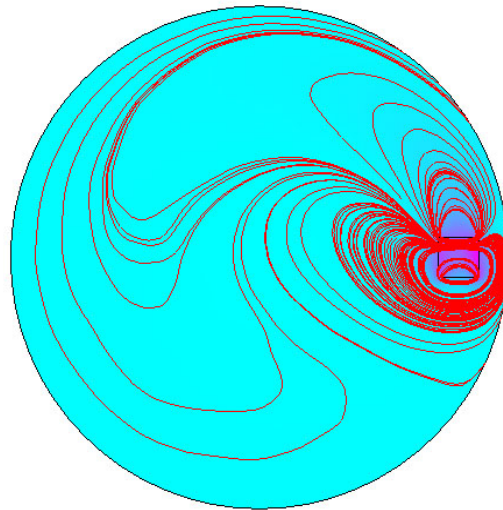


Fig. 7.7 Eddy current on the rotating disk

The model in Fig. 7.7 presents necessary information for the current density distribution. The analysis suggests that the eddy current density can reach a maximum value of $1.6 \times 10^6 \text{ A/m}^2$. With the 10^{-2} Tesla magnetic flux density, the force density can be obtained by $f = \mathbf{J} \times \mathbf{B}$. If we assume the current goes through the tool holder, the total force is evaluated to be around 5 N-30 N. This analytical prediction is consistent with the force reduction.

For the current induced on the workpiece, the current is in such a way that its own magnetic field opposes the change that produced it. Because of the current on the workpiece, there is a force loading on the workpiece and the effect of the force is impeding the change of the magnetic flux through a closed surface. This force may partially increase the interaction force between the cutting tool and workpiece since the same direction of them. The explanation in terms of Lenz's law seems correspond to the force increase in Fig. 7.3, in which higher voltage supply produced higher current density and then corresponding to higher force increasing values.

CHAPTER 8

CONCLUSION

The effect of application of magnetic field on the dynamics of cutting process is investigated. The flank wear of widely used cemented carbide tool against the ferromagnetic carbon steels decreases dramatically in the presence of magnetic field even when it is extremely weak. It has been widely studied that metal machining is such a complex process that there is no consistent trend for the formation of tool wear and the corresponding force, because of the manifold chemical and mechanical factors. Besides those investigations in terms of dislocation, material hardness and finer chip, we propose another possible factor that may contribute to the improved tool life.

In turning process, two electromagnets were setup on the top and bottom of the cutting tool holder, which provided extraordinary low magnetic intensity. The experimental examination show that the tool wear reduced 8%-28% with the applied electromagnets; correspondingly, the cutting force also decreased by 10% to 20%. It revealed that even much lower magnetic strength would lead to the longer tool life. The attempted explanation was in the light of magnetization force and forces due to induced eddy current. The dynamic cantilever model also contributes to the damping of vibration, which may explain the reduced force and wear in feed direction. On the other hand, computer simulations also indicated that the electromagnetic force may play an active role in tool wear.

Another application of electromagnets is in milling process. Rather than the magnetic field introducing into the tool insert, the electromagnets stick to the base of lateral side of the workpiece. The experimental results show that the tool wear reduced up to 44.5% with the applied electromagnets; correspondingly, the cutting force also decreased by 9% to 19%. Different from the turning case, the magnetization force can be ignored and what accounts for the force variation and tool wear reduction is the induced eddy current. The attempted explanation was in the light of induced eddy current which has effect both on mechanical force and on thermal interaction. The eddy current renders extra electrical field for the formation of Al_2O_3 film which helps to improve tool wear resistance. This effect is further promoted by the increased temperature due to the flush current. The Lorentz force is also a reasonable explanation for the milling force drop. Computer simulations also indicated that the eddy current may play an active role in improving tool wear. Nevertheless, more exploration will be necessary for the understanding of magnetic effect discrepancy in tool wear improvement.

There were also several points ignored in the analysis of the factor that may determine the tool wear rate. Our study indicates that magnetic force accounts for the variation of cutting force at axial, radial and tangential directions. However, the application of magnetic field also change the material macro hardness, increase the oxygen density around the cutting area and then facilitate the oxidation process. The further work may include the improvement of cantilever model and further exploration of the close loop relationship of the tool wear force and vibration.

It is generally assumed that the components of cutting force are linearly related to flank wear and crater wear. Crater wear is generally believed to be caused by diffusion as a result of high temperature at the tool-chip interface. Unlike the flank wear, crater wear can have a sharpening effect and can cause the force to decrease as a result of growing crater wear. The opposing effects of crater wear and flank wear on the cutting force is one of the major drawbacks in wear sensing through force measurement. The measurement of crater wear may be included in further work.

The close loop relation among force, wear and vibration is not clearly expressed by equation. Even though the magnetic force is a prospective explanation for the reduction of the tool wear, the analysis of thermal effect and magnetic pole effect deserve more exploration.

BIBLIOGRAPHY

- [1] Shaw, M.C., "Metal Cutting Principles," Clarendon Press, Oxford, 1984.
- [2] Stewart C. Black, Vic Chiles, A. J. Lissaman, and S. J. Martin, "Principles of Engineering Manufacture," Third edition, John Wiley & Sons Inc., New York-Toronto, 1996.
- [3] E. Usui, T. Shirakashi, and T. Kitagawa, "Analytical Prediction of Cutting Tool Wear," *Wear*, v100, pp.129-151, 1984.
- [4] Bobrovoskii, V. A., "Extending Tool Life by Break-in TEME Circuit," *Russ. Eng. J.*, 18, pp.70, 1966.
- [5] Kanji, M., and K. Pal, D., "Thermoelectric Compensation in Drilling," *Proceedings of the 3rd AIMTDR Conference, Bombay, 1969.*
- [6] Pal, D. K., and Gupta, N. C., "Some Experimental Studies on Drill Wear in the Presence of an Alternating Magnetic Field," *J. Inst. Eng. (India), Part AG*, v53, pp.195-200, 1973.
- [7] Muju, M. K., and Ghosh, A., "A Model of Adhesive Wear in the Presence of a Magnetic Field-I," *Wear*, v41, pp.103-116, 1977.
- [8] Muju, M. K., and Ghosh, A., "Effect of a Magnetic Field on Diffusive Wear of Cutting Tools," *Wear*, v58, pp.137-145, 1980.
- [9] D. Paulmier, H. Zaidi, R. Bedri, E. K. Kadiri, L. Pan and Q. Jiang, "Steel Surface Modifications in Magnetised Sliding Contact," *Surface & Coatings Technology*, v76-77, pp.583-588, 1995.
- [10] Mansori, M. E., Pierron, F., and Paulmier, D., "Reduction of Tool Wear in Metal Cutting Using External Electromotive Sources," *Surface & Coatings*

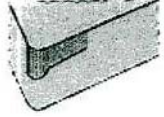
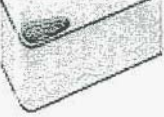
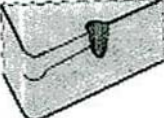
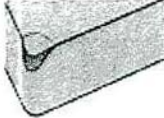
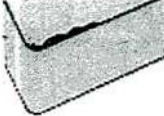
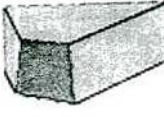
- Technology, v 163-164, pp. 472-477, 2003.
- [11] D. Paulmier, M. El Mansori, and H. Zaidi, "Study of Magnetized or Electrical Sliding Contact of a Steel XC48/graphite Couple," *Wear*, v203-204, pp. 148-154, 1997.
- [12] Yamamoto, Y., Yagi, J. , and Higaki, H., "Effect of Electric Field Externally Applied on Friction and Wear Characteristics," *Transactions of the Japan Society of Mechanical Engineers, PartC*, v57, n540, pp.2734-2739, 1991.
- [13] Yamamoto, Y., Ono, B., and Ura, A., "Effect of Applied Voltage on Friction and Wear Characteristics in Mixed Lubrication," *Lubrication Science*, v 8, n2, pp199-207, 1996.
- [14] Takeuchi, A., 1996, "In-situ Observation of Solid Contact State of Sliding Surface Using Ultrasonic Echo Technique," *Journal of Japanese Society of Tribologists*, v41, n5, pp. 381, 1996.
- [15] H. wistuba, "The Effect of an External Electric Field on the Operation of an Aluminium Oxide-cast Iron Sliding Contact Joint," *Wear*, v208, pp113-117, 1997.
- [16] A. Gangopadhyay, M. C. Paputa Peck, and S. J. Simko, "Wear Control in a Lubricated Contact Through Externally Applied Electric Current," *Tribology Transactions*, v45, n3, pp. 302-309, 2002.
- [17] Gangopadhyay, A. , Barber, G., and Han Zhao, "Tool Wear Reduction Through an Externally Applied Electric Current," *Wear*, v260, n 4-5, pp. 549-553, 2006.
- [18] Mozniker, R. A., "Effect of a Constant Magnetic field on the free Oscillations of Mechanical systems," *Izv. Acad. Nauk Ukr. SSSR*, pp.847-852, 1959.

- [19] Moon, F.C., "Problem in Magnetosolid Mechanics," Chapter V. In mechanics Today4, Nemat Nasser, Ed., Pergamon Press, New York, 1978.
- [20] Wallerstein, D. V. and Peach, M. O., "Magnetoelastic Buckling of Beams and Thin Plates of Magnetically Soft Material," J. Appl. Mech., v39, n2, pp.451-455, 1972.
- [21] Lee, J. S., Prevost, J. H., and Lee, P. C. Y., "Finite Element Analysis of Magnetically Induced Vibrations of Conductive Plates," Fusion Engineering and Design, v13, pp.125-141, 1990.
- [22] Birr, M. P. and Koryu Ishii, T., "Dynamic Stiffness of Magnetically Biased Laminated Iron Core," IEEE Transactions on Magnetics, September, pp.326-329, 1972.
- [23] Toshiya Morisue, "Analysis of a Coupled Problem: The FELIX Cantilevered Beam," IEEE Transactions on Magnetics, v26, pp.540-543, 1990.
- [24] T. Takagi, J. Tani, S. Matsuda, and S. Kawamura, "Analysis and Experiment of Dynamic Deflection of a Thin Plate with a Coupling Effect," IEEE Transactions on Magnetics., v28, pp.1259-1262, 1992.
- [25] Toshiyuki Takagi, and Junji Tani, "Dynamic Behavior Analysis of a Plate in Magnetic Field by Full Coupling and MMD Methods," IEEE Transactions on Magnetics, v 30, n5, pp.3296-3299, 1994.
- [26] Zhou, Y. H., and Zheng, X. J., "A General Expression of Magnetic Force for Soft Ferromagnetic Plates in Complex Magnetic Fields." Int. J. Eng. Sci., v35, pp.1405-1417, 1997.

- [27] Wang, X. Z., and Lee J. S., "Dynamic Stability of Ferromagnetic Beam-Plates with Magnetoelastic Interaction and Magnetic Damping in Transverse Magnetic Fields." ASME Journal of Engineering Mechanics, v132, n 4, pp.422-428, 2006.
- [28] Francis, C. Moon, "Magneto Solid Mechanics," Wiley-Interscience Publication, New York, 1984, Chapter 2,3.
- [29] R.A. McCurrie, "Ferromagnetic Materials Structure and Properties," Academic Press, London, 1994.
- [30] S. Chattopadhyay, and F. C. Moon, "Magnetoelastic Buckling and Vibration of a Rod Carrying Electric Current," Journal of Applied Mechanics, v42, pp.809-814, 1975.
- [31] Gunadhar Paria, "Advances in Applied Mechanics," Academic Press, New York, London, pp.74-76, 1967.
- [32] Pao, Y-H., and Yeh, C-S., "A linear Theory for Soft Ferromagnetic Elastic Solids," Int. J. Eng. Sci., v11, n4, pp.415, 1973.
- [33] Kannatey-Asibu, Ju., E., "A Transport-Diffusion Equation in Metal Cutting and Its Application to Analysis of the Rate of Flank Wear," ASME Journal of Engineering for Industry, v107, pp. 81-89, 1985.
- [34] Su, Y. T., Hung, T.C., and Horng, C.C., "An Experimental Study on Tool Wear of Hydrodynamic Polishing Process, Wear, v246, pp. 117-129, 2000.
- [35] R. Holm, "Electric Contacts: Theory and Application," Fourth edition, Springer-Verlag, Berlin, pp. 104, 1967.

Appendix A

Table A-1 Tool wear types

<p>Flank Wear</p> 	<p>Flank wear occurs on the clearance face of the tool and is mainly caused by the rubbing of the newly machined workpiece surface on the contact area of the tool edge. This type of wear occurs on all tools while cutting any type of work material.</p>
<p>Crater Wear</p> 	<p>Crater wear occurs on the top face of the tool. It is essentially the erosion of an area parallel to the cutting edge. This erosion process takes place as the chip being cut, rubs the top face of the tool.</p>
<p>Notch Wear</p> 	<p>Notch wear occurs locally in the area of the primary cutting edge where it contacts the workpiece surface. Caused by hard surface layers and work-hardened burrs, especially on stainless austenitic steels.</p>
<p>Nose Wear</p> 	<p>Nose wear is usually observed after a considerable cutting time, nose wear appears when the tool has already exhibited flank and/or crater wear. Wear on the nose of the cutting edge usually affects the quality of the surface finish on the workpiece.</p>
<p>Built-up Edge</p> 	<p>Edge built-up occurs on the rake face as a result of work material welding together with the cutting material. From time to time the built-up edge will break off and make damage to the cutting edge.</p>
<p>Tool Breakage</p> 	<p>Insert breakage usually means damage to tool and workpiece. Causes are varied and also depend on machine and workpiece. Often originates in notches or excessive wear.</p>

Appendix B

Change in Magnetic Field Strength during experimentation

Table B-1: Change in magnetic field along workpiece surface with depth of cut at 10V with N-N orientation

North-North Orientation					
Depth of cut (mm)	0mm	5mm	10mm	15mm	21mm
0	25	8	2	-3	-2
5	34	9	2	-5	15
10	39	10	1	-6	20
15	40	10	1	-6	20
20	41	10	1	-6	19
25	43	10	1	-7	21
30	39	7	-4	-11	22
35	36	7	-3	-11	24

Table B-2: Change in magnetic field along workpiece surface with depth of cut at 10V with N-S orientation

North-South Orientation					
Depth of cut (mm)	0mm	5mm	10mm	15mm	21mm
0	7	12	10	5	-7
5	8	20	15	5	-10
10	13	23	14	3	-11
15	13	24	13	0	-17
20	13	23	11	-1	-22
25	14	24	11	-3	-23
30	12	25	14	0	-26
35	11	27	17	6	-20

Table B-3: Change in magnetic field along workpiece surface with depth of cut at 15V with N-N orientation

North-North Orientation					
Depth of cut (mm)	0mm	5mm	10mm	15mm	21mm
0	9	-4	-2	5	21
5	17	-8	1	14	54
10	22	-6	-2	6	53
15	22	-5	0	10	56
20	22	-5	3	12	61
25	20	-6	1	10	60
30	20	-8	1	13	62
35	20	-8	1	13	62

Table B-4: Change in magnetic field along workpiece surface with depth of cut at 15V with N-S orientation

North-South Orientation					
Depth of cut (mm)	0mm	5mm	10mm	15mm	21mm
0	-6	-16	-20	-23	-7
5	-4	-14	-19	-19	-5
10	-2	-12	-15	-15	-3
15	1	-8	-13	-12	1
20	3	-5	-11	-9	5
25	1	-4	-13	-1	-7
30	-1	-6	-12	-12	5
35	-10	-10	-16	-15	6

Table B-5: Change in magnetic field along workpiece surface with depth of cut at 20V with N-N orientation

North-North Orientation					
Depth of cut (mm)	0mm	5mm	10mm	15mm	21mm
0	22	-4	-11	-17	-22
5	24	-4	-13	-20	-12
10	25	-4	-11	-21	-4
15	25	-2	-8	-16	5
20	29	-3	-11	-17	12
25	30	-8	-11	-15	15
30	30	-12	-15	-16	17
35	30	-7	-12	-11	14

Table B-6: Change in magnetic field along workpiece surface with depth of cut at 20V with N-S orientation

North-South Orientation					
Depth of cut (mm)	0mm	5mm	10mm	15mm	21mm
0	-30	-5	-6	-15	-20
5	-35	-6	1	-16	-15
10	-35	-4	5	-9	-12
15	-36	-2	9	-3	-9
0	-33	1	17	2	-9
25	-31	-2	17	0	-9
30	-31	-11	13	-4	1
35	-37	-18	-3	-12	6